CRYSTALLIZATION AND MELTING BEHAVIOR OF (e-CAPROLACTONE)-BASED HOMOPOLYMER AND TRIBLOCK COPOLYMER

by

LISA ARNOLD

Dissertation submitted to the faculty of
the Virginia Polytechnic Institute & State University
in partial fulfillment of the requirements for the degree of

DOCTOR OF PHILOSOPHY IN CHEMISTRY

APPROVED:

Hervé Marand, Chairman

Harry W. Gibson

Thomas C. Ward

James P. Wightman

Garth L. Wilkes

August, 1995

Blacksburg, Virginia

Key Words: Crystallization, Melting, Poly(e-caprolactone), Poly(propylene oxide), Block Copolymer

CRYSTALLIZATION AND MELTING BEHAVIOR OF (ε–CAPROLACTONE)-BASED HOMOPOLYMER AND TRIBLOCK COPOLYMER

by

LISA ARNOLD

Dr. H. Marand, Chairman
Department of Chemistry

(ABSTRACT)

The goal of this work is to examine the applicability of the Lauritzen-Hoffman (LH) surface nucleation theory to the crystallization kinetics of poly(ε-caprolactone), PCL. This theory has successfully predicted a number of experimental observations such as the temperature dependence of spherulitic growth rates and the inverse relation between undercooling and the lamellar thickness. Claims have appeared in the literature that analysis of growth rate data using the LH theory does not yield physically meaningful parameters. This work will show that the lateral and fold interfacial free energy parameters, σ and σ_e, found by analysis with the LH theory are related to the chemical structure of the polymer chain in the case of PCL. The fold interfacial free energy is related to the chain stiffness, and a recent proposal[1] relates σ to the characteristic ratio, C_∞. This work will examine the validity of the proposed relationship for the case of PCL. The effect of polymer chain architecture on the crystallization behavior was also

investigated. The crystallization behavior of poly(ε-caprolactone) was compared and contrasted to that of a triblock copolymer containing (ε-caprolactone) blocks.

In order to test the proposed inverse relationship between the lateral interfacial free energy, σ, and the characteristic ratio, an experimental value of σ was determined. The temperature dependence of growth rate data was analyzed using the LH theory, and the Gibbs-Thomson-Tammann analysis was carried out to determine $\sigma\sigma_e$ and σ_e, respectively. These analyses yielded values of 10.3 ± 3.1 erg/cm^2 for the lateral interfacial free energy, σ, and 64 ± 6 erg/cm^2 for the fold interfacial free energy, σ_e. The calculated value of σ was then used to determine a value of 4.5 ± 1.3 for the characteristic ratio, C_∞. This value is within a 20% margin of error of published literature values of the characteristic ratio which suggests the LH theory and σ-C_∞ relationship are qualitatively consistent with one another.

The isothermal crystallization and melting behavior of poly(ε-caprolactone) and poly(ε-caprolactone-*b*-propylene oxide-*b*-ε-caprolactone) were compared utilizing differential scanning calorimetry, polarized optical microscopy, and small angle x-ray scattering. Results show that the triblock copolymer crystallizes in a similar fashion as the homopolymer, and the poly(propylene oxide) midblock acts as a non-crystallizable defect. The circumstances under which double endothermic behavior is seen in the homopolymer and three distinct endotherms are observed in the triblock copolymer are discussed.

[1] J.D. Hoffman, R.L. Miller, H. Marand, and D. Roitman, Mcaromolecules, 1992, **25**, 2221.

Acknowledgements

I would like to express my most sincere thanks to my advisor, professor Herve Marand, for his guidance and support. I would also like to thank professors Gibson, Ward, Wightman, and Wilkes for serving as my committee members. Appreciation is extended to my colleagues; Pak-Meng Cham, Dawn Reinhard, Chad Snyder, Jiang Huang, Darrell Iler, Felix Gandara-Guzman, and other members of the group for their friendship and help.

My special thanks goes to my husband, Robert Arnold, whose never-ending love, patience, and encouragement that have made the completion of this dissertation possible.

Table of Contents

List of Figures

List of Tables

Chapter 1. Introduction

Crystallinity can significantly change the bulk properties of a polymeric material. For this reason, a fundamental understanding of the manner in which polymer crystallization occurs is needed. This work will examine how well the theories proposed for the kinetics of crystallization can analyze growth rate data to determine physically significant parameters. The effect of chain topology on crystallization is investigated by comparing the crystallization and melting behavior of poly(ε-caprolactone) to a triblock copolymer, poly(ε-caprolactone-*b*-propylene oxide-*b*- ε-caprolactone).

The Lauritzen-Hoffman (LH) surface nucleation theory has been shown in many cases to model the temperature dependence of the crystal growth rate, G, and crystal lamellar thickness of several polymers. The LH growth rate theory predicts that spherulitic growth will exhibit contributions from segmental diffusion and secondary nucleation. [7]

$$G = G_o \exp\left[\frac{-U^*}{R(T_x - T_\infty)}\right]\exp\left[\frac{-K_g}{T_x \Delta f}\right] \qquad (1)$$

where U* is the activation energy for the transport of crystallizable segments across the melt-crystal interface, R is the gas constant, $T_\infty \cong T_g - 30$, Δf is the free energy of fusion, and K_g is the nucleation constant which varies for each regime.

$$K_g = \frac{j b_0 \sigma \sigma_e}{k} \qquad (2)$$

The lateral and fold interfacial free energies are σ and σ_e, respectively, k is the Boltzmann constant, and b_0 is the layer thickness. The factor, j, accounts for the crystallization regime; j = 4 for Regimes I and III, while j = 2 for Regime II.

A recent proposal provides a molecular meaning for the lateral surface free energy of a melt-crystallized polymer. This is done through an inverse relation between σ and the characteristic ratio, C_∞,[1]

$$\sigma_{theor} \cong \Delta h_f \left(\frac{a_0}{2}\right)\left(\frac{l_b}{l_u}\right)\left(\frac{1}{C_\infty}\right) \qquad (3)$$

where l_b is the bond length, l_u is the projected bond length in the chain direction in the crystalline state, Δh_f is the heat of fusion, and a_0 is the width of the molecule along the growth front.

The validity of this proposed equation was investigated for the case of poly(ε-caprolactone). Poly(ε-caprolactone) (PCL) is a low melting polyester and has the following chemical structure;

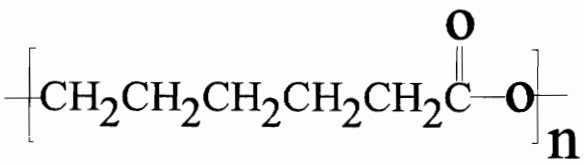

In order to examine this proposed relation (equation 3), a careful determination of the equilibrium melting temperature of poly(ε-caprolactone) was made to analyze growth rate data with the Lauritzen-Hoffman surface nucleation theory. Analysis gave a value for

the product of the surface energies, $\sigma\sigma_e$, which was combined with an independent value for the fold surface free energy, σ_e, found using the Gibbs-Thomson-Tammann analysis. This gave a value for σ which was used to test the proposed relation.

An additional focus in this work was to determine how the crystallization and melting behavior of a crystallizable polymer changes due to the chain architecture. The morphology, melting, and crystallization behavior of an (ε-caprolactone)-based homopolymer and triblock copolymer, poly (ε-caprolactone-*b*- propylene oxide-*b*- ε-caprolactone), was compared and contrasted. This was then considered in light of theories on block copolymer crystallization.

Chapter 2 of this thesis will provide an introduction to the lamellar and spherulitic morphology of semi-crystalline polymers. It will be followed by a discussion of growth rate theories. The Lauritzen-Hoffman surface nucleation growth rate theory will be emphasized as this is the model which was used to analyze the data. An important quantity in any growth rate theory is the equilibrium melting temperature. The methods used to determine this quantity will be reviewed. Additional factors become important when a block copolymer is crystallized from a micro-phase separated melt. These are discussed and followed with a review of the properties of poly(ε-caprolactone).

The experimental procedures and theory behind data analysis are reported in Chapter 3. Chapter 4 will discuss the crystallization behavior of poly(ε-caprolactone). This section will emphasize the careful determination of the equilibrium melting temperature and fold surface free energy with respect to how these quantities are needed to test the proposed σ - C_∞ relation.

Chapter 5 will discuss the melting behavior of (ε-caprolactone) in the homopolymer and triblock copolymer. The origins and conditions where multiple endothermic behavior is observed will be brought out.

The final results and discussion chapter is Chapter 6, which will examine the crystallization behavior of the triblock copolymer. The morphology and growth rate behavior will be considered in light of the behavior of the homopolymer. Chapter 7 summarizes the conclusions of this work, and chapter 8 describes the future directions that this work suggests.

Chapter 2. Literature Review

2.1 Semi-Crystalline Model of Polymers

This review will focus on the case of crystallization for linear, flexible polymer chains under quiescent conditions from the melt state. Crystallization under external fields or for rigid macromolecules will be outside the scope of this review.

2.1.1 Lamellar Morphology

Solution grown polymer single crystals were found to have a thin platelet morphology which is large in two dimensions and where the 'thin' dimension is on the order of magnitude of tens of nanometers. Electron diffraction patterns revealed that the polymer chain is oriented more or less parallel to the thin dimension of the crystal.[61] Due to the fact that the length of polymer chains range from ten to one hundred times that of the thickness of the lamellae, Keller[62] and Storkes[68] proposed that the polymer chains must fold many times in a regular fashion to form the thin lamellae.

The thickness of the lamellae can be determined with electron microscopy, small-angle x-ray scattering (SAXS), or low-frequency Raman spectroscopy (LAM). Measurements with these techniques have shown that the lamellar thickness of a semi-crystalline polymer is defined for a given crystallization temperature, or more specifically, by the undercooling, ΔT , (where $\Delta T = T_m - T_x$ or $T_m - T_d$; T_m is the equilibrium melting, and T_d is the dissolution temperature).[64] The lamellar thickness found by solution crystallization measurements in different solvents have shown it to be inversely proportional to the undercooling, ΔT.

2.1.2 Spherulitic Development and Structure

Spherulites develop as a result of two fundamental processes: primary nucleation and crystal growth.[7] The primary nucleation process is caused by fluctuations in chain conformations, density, and ordering when the melt is in the temperature range between the glass transition temperature and the equilibrium melting temperature. These fluctuations cause a small amount of crystalline material to form the primary nuclei. The number and size of the primary nuclei depends on the crystallization temperature.

The growth process begins once the primary nuclei are formed, and continues until impingement between spherulites. As the polymer crystal grows, the lamellae progressively splay out in all directions (Figure 1).[8] Small angle branching causes these structures to go through sheaflike forms (Figure 1d) and to eventually become spherulitic (Figure 1e). Spherulites have diameters in the range of 0.5 to a few hundred micrometers and form birefringent structures with spherical symmetry which are generally characterized by a Maltese cross optical extinction pattern when viewed under cross polarization conditions. X-ray investigations have shown that the polymer chain axis in the lamellae is usually approximately perpendicular to the radius of the spherulite (Figure 2).[5]

The spherulitic radius will increase linearly with crystallization time during isothermal crystallization. This growth rate is constant at a given crystallization temperature and can be experimentally determined by polarized optical microscopy (Figure 3).

An examination of the temperature dependence of the growth rate (Figure 4) shows it to be a bell-shaped curve with boundaries at the glass transition and equilibrium melting temperature. The bell-shaped curve is a result of two competing factors controlling polymer crystallization: diffusion of the polymer chain to the melt-crystal

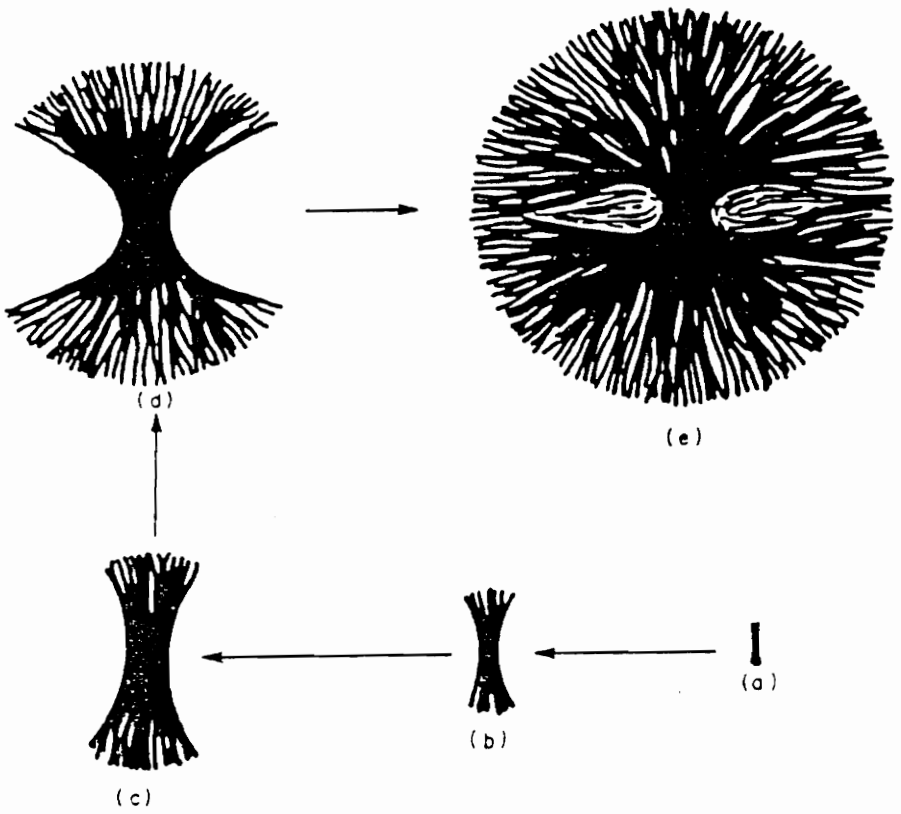

Figure 1. Development of Spherulitic Structure (reference 8).

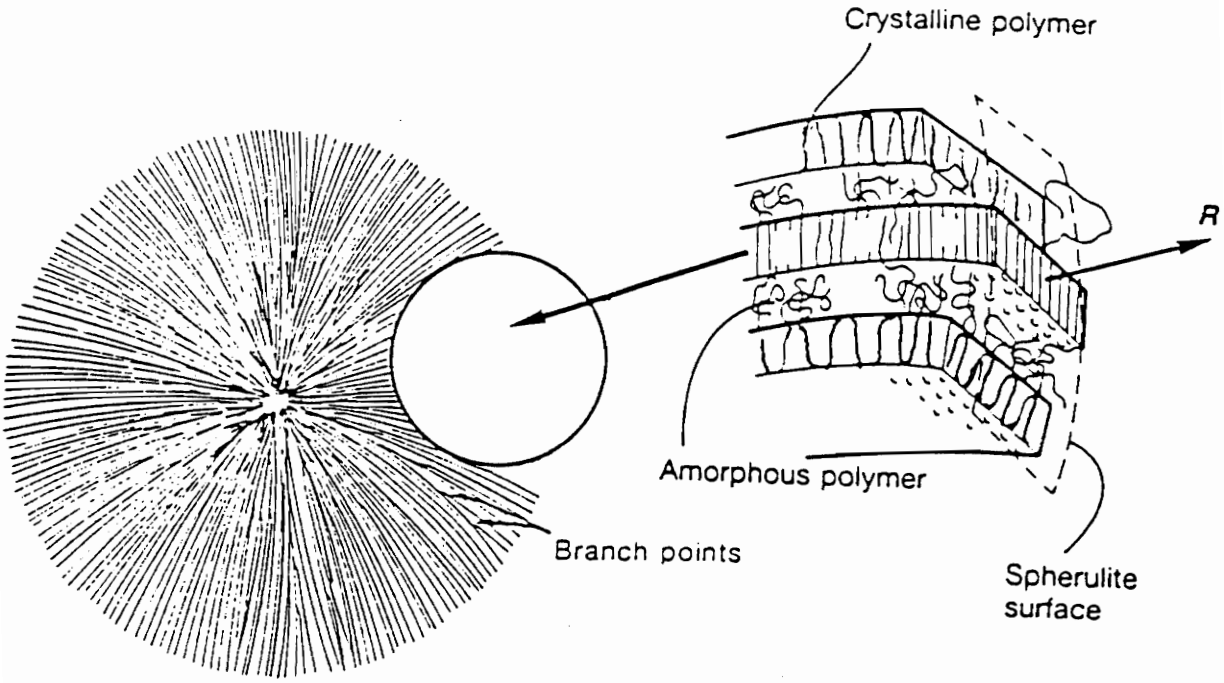

Figure 2. Schematic Diagram of a Spherulite (from reference 4)

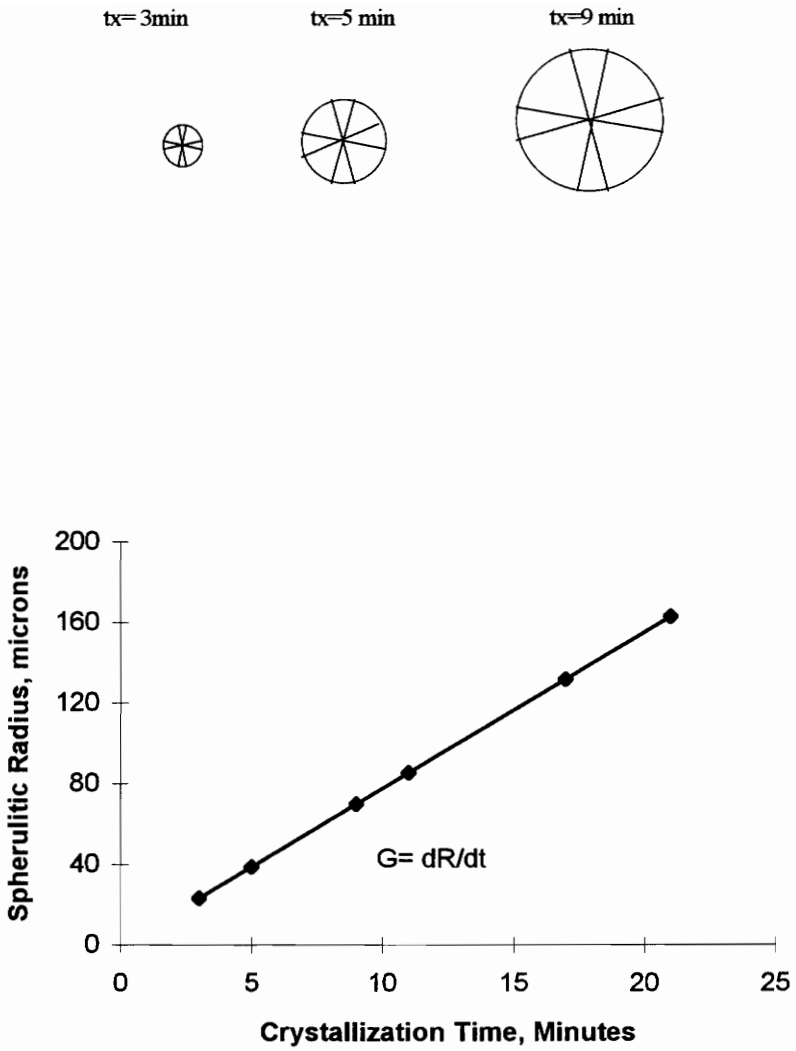

Figure 3. Experimentally Determined Growth Rate.

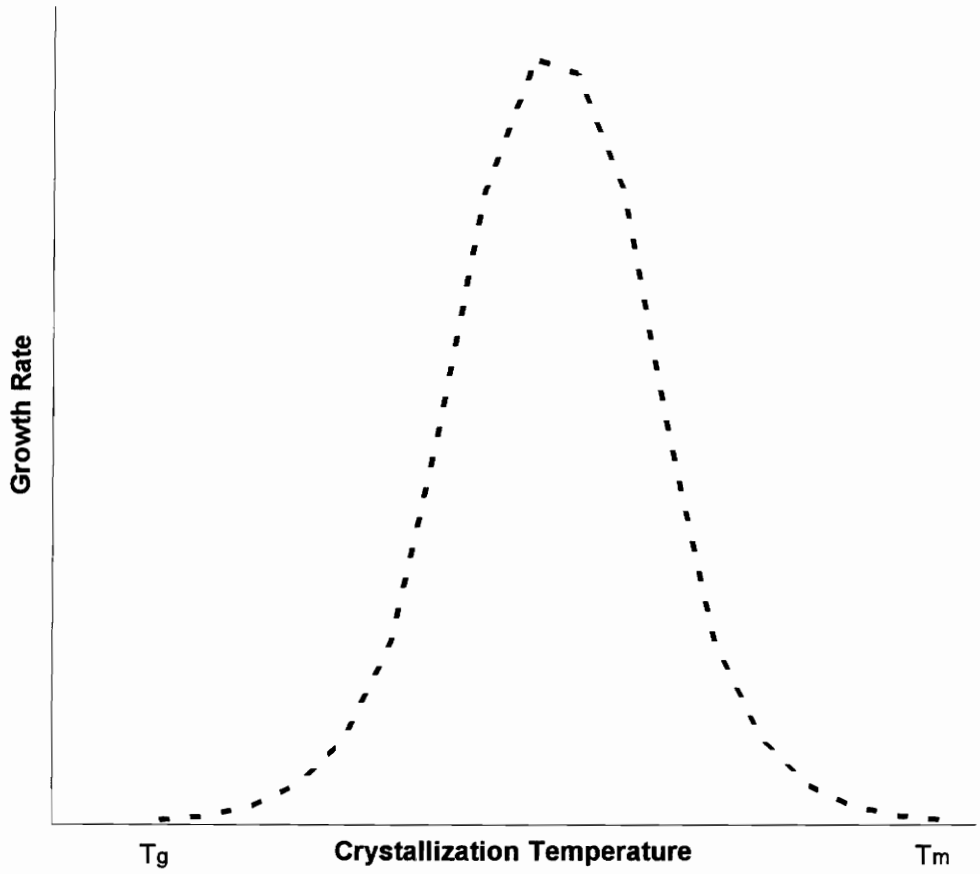

Figure 4. Temperature Dependence of the Crystal Growth Rate

interface, and secondary nucleation.

Crystallization will not occur below the T_g because the polymer will not be able to diffuse to the crystal-melt interface. As the temperature is increased, the polymer melt is less viscous, and the rate of diffusion of chains to the growing crystal will increase. The influence of diffusion is particularly significant when the polymer is crystallized at or below the maximum of the growth rate curve.

The second controlling factor in the growth rate is the secondary nucleation process. The secondary nucleation rate increases with decreasing temperature. This factor is the most important in the crystallization behavior of poly(ε-caprolactone) because the temperature range where the growth rate data can be obtained is beyond the maximum of the growth rate curve, and is significantly above the glass transition temperature.

2.2 Kinetic Growth Rate Theories

2.2.1 Driving Force for Crystallization

The basis of all growth rate theories is the driving force for crystallization. This driving force can be evaluated by determining the difference in Gibbs free energy between the solid and liquid states, $\Delta\Phi_{crystal}$. This is found from the bulk free energy of crystallization (Δf_c), and the free energy needed to create the lateral (σ) and fold surfaces (σ_e) (Figure 5),[7]

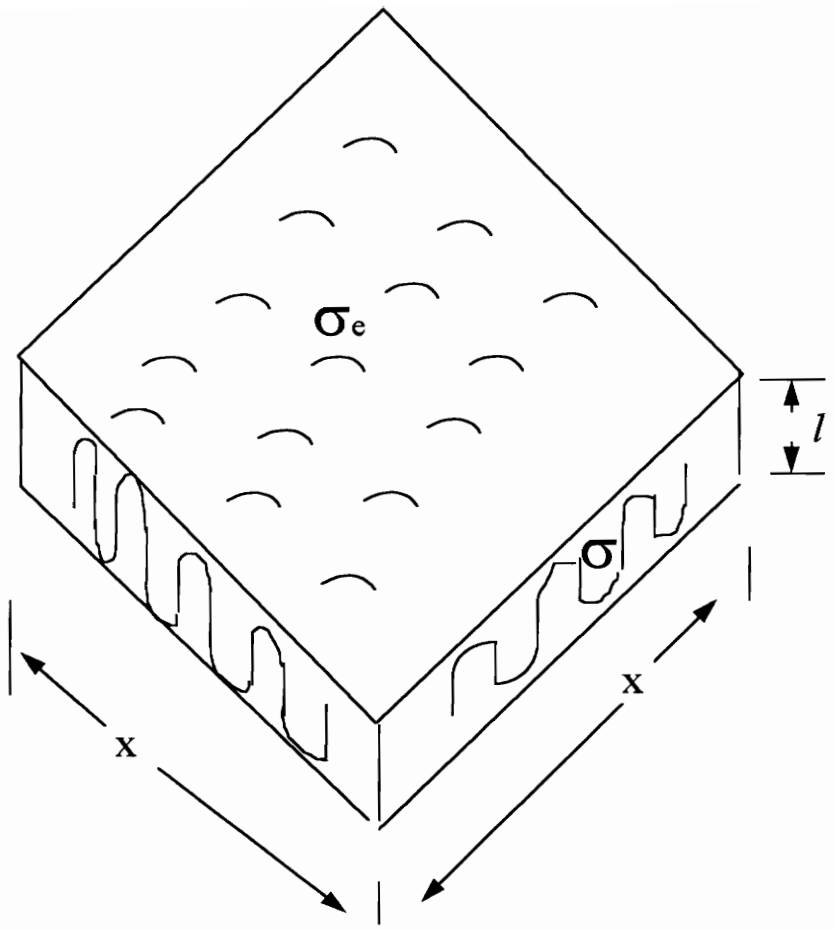

Figure 5. Schematic of a Chain-Folded Polymeric Lamellar Crystal

$$\Delta\Phi_{crystal} = 4xl\sigma + 2x^2\sigma_e + x^2 l(\Delta f_c) \tag{4}$$

where the bulk free energy of crystallization can be expressed by the following.

$$-\Delta f_c = \Delta h_f - T\Delta s_f = \Delta h_f - \frac{T\Delta h_f}{T_m} = \frac{\Delta h_f \Delta T}{T_m} \tag{5}$$

In order to form a crystal that is stable with respect to the liquid, $\Delta\Phi_{crystal}$ must be negative. For polymer lamellae in which the thin platelike approximation is valid (x >> l), this implies that the lamellar thickness must be larger than the minimum lamellar thickness, l_{min}, given by

$$l_{\min} = \frac{-2\sigma_e}{\Delta f_c} \tag{6}$$

The minimum lamellar thickness for low undercoolings, ΔT, is greater than for higher ΔT. An increase in ΔT will cause the free energy of formation of a single chain-folded crystal to become more negative. This will increase the driving force for crystallization.

Concurrently, as the lamellae become thicker the driving force levels off due to a smaller effect of surface energy as the surface to volume ratio decreases (Figure 6). If this driving force were the sole contributor to the growth rate and the observed lamellar thickness of the polymer crystal, an infinitely thick crystal would be predicted.[62]

A "barrier" term is introduced which increases exponentially with thickness to account for the experimentally observed finite thickness of the polymer crystal. The

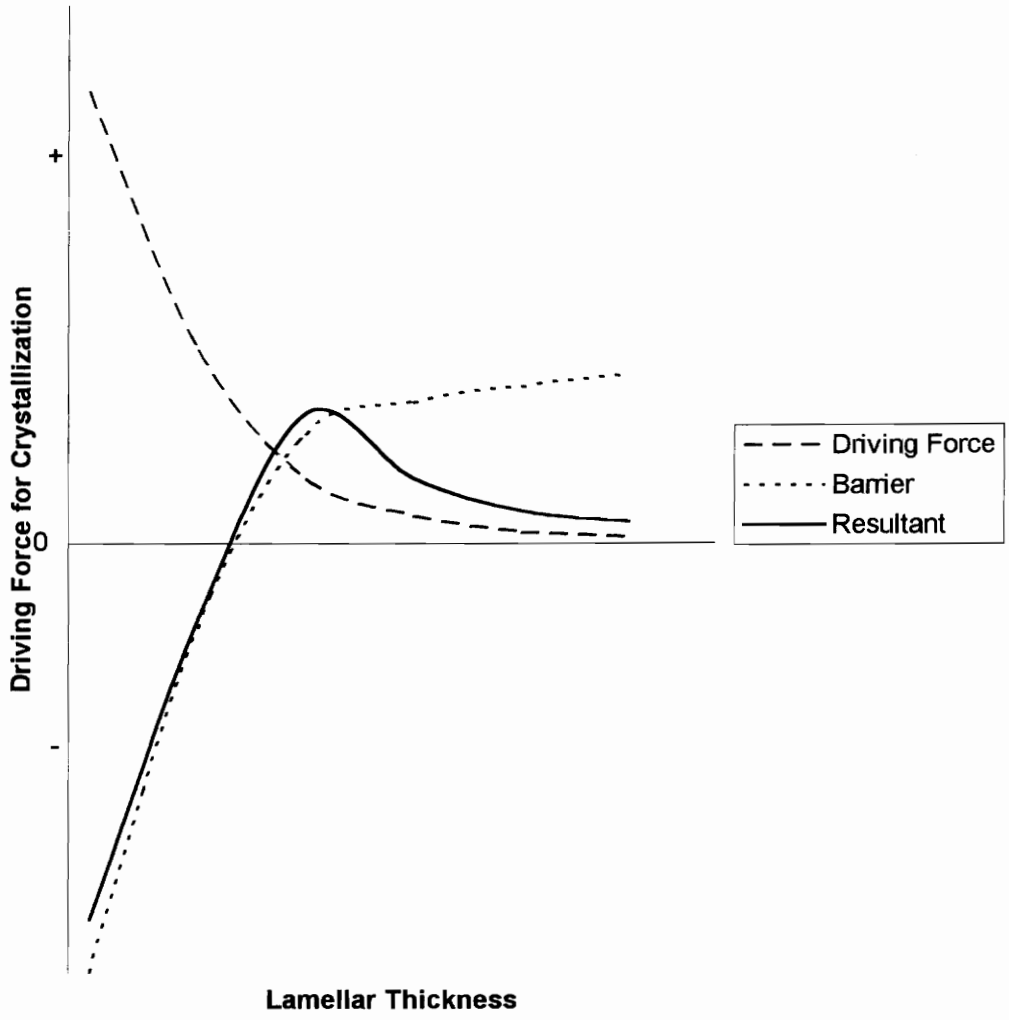

Figure 6. Driving Force and Barrier to Crystallization (from reference 61).

barrier for the nucleation process is overcome by random fluctuations in the melt. There is consensus among those working in the field of crystallization that polymer crystal growth at low undercoolings is controlled by a nucleation process. The debate centers on the nature of this barrier. Lauritzen and Hoffman believe the nature of the barrier is surface enthalpic, while Sadler and Goldbeck-Wood consider the barrier to be entropic. In entropic barrier theories, the polymer molecule is allowed only a few of many possible paths for crystallization. Surface nucleation barrier theories have an energy barrier that must be overcome.[62] The details of this theory will be given in the following section.

The combined effect of the barrier term and driving force produce a most probable lamellar thickness of the polymer crystal. This thickness is slightly above the minimum thickness.

2.2 Surface Nucleation Theory

The basic model for surface nucleation theories is that a single stem of thickness, l, nucleates on a flat crystal surface (Figure 7). The deposition of the first stem (ν=1) incurs a high free energy cost, $2b_o l\sigma$, (Figure 8) due to the formation of two new lateral surfaces that are created. This free energy barrier to crystallization is called the nucleation barrier. A decrease in free energy due to crystallization is also associated with this process. The most probable position for the deposition of the second stem is adjacent to the first stem, because an additional nucleation barrier will not be incurred from the creation of new lateral surfaces. Each additional stem involves a cost to form the folds ($2a_o b_o \sigma_e$) and a free energy reduction due to crystallization. As the number of stems increases, the cost of free energy to form the new fold surfaces overwhelmed by the decrease in free energy due to crystallization (Figure 8).

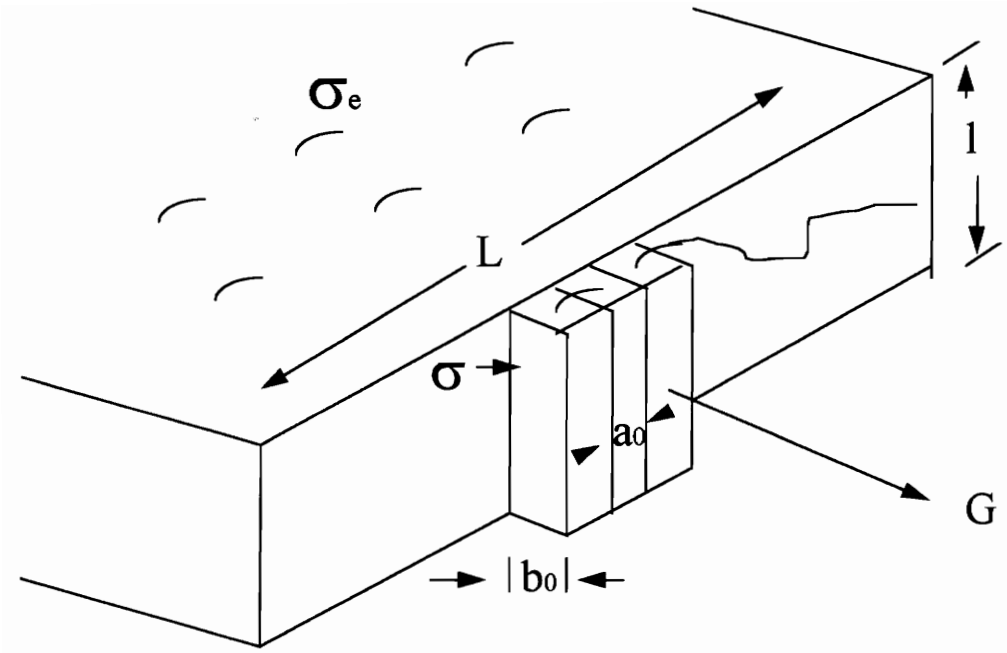

Figure 7. Illustration of the Kinetics of Lamellar Growth (from reference 33).

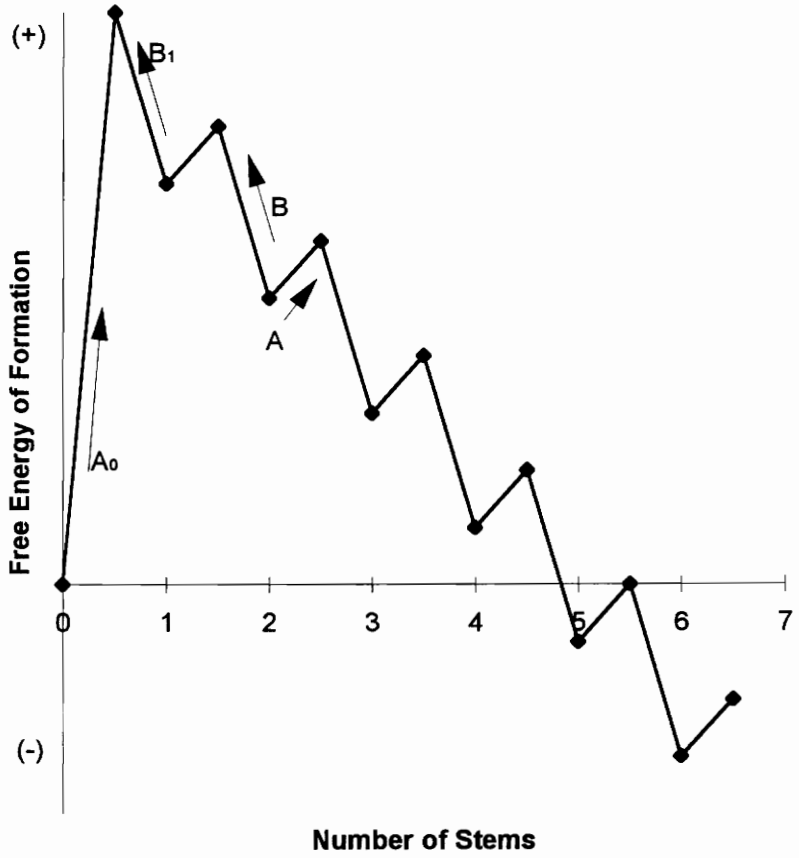

Figure 8. Free Energy of Formation of a Chain Folded Surface Nucleus (from reference 7)

The deposition of the first stem and the lateral spread by the addition of subsequent stems are characterized by the secondary nucleation rate, i, and the spreading rate, g. The relative magnitude of these two rates with respect to one another is the basis of crystallization regimes.

For high crystallization temperatures (Regime I), secondary nucleation is the rate determining step for lamellar growth (Figure 9a). Once a surface nucleus is formed, the layer is completed before another nucleus is formed. This is because the substrate completion rate is greater than the surface nucleation rate. The growth rate is proportional to i,[7]

$$G = b_o i L_p \qquad \text{(Regime I)} \qquad (7)$$

where b_0 is the layer thickness (Figure 7), and L_p is the substrate length. The average substrate length is the distance between imperfections on the crystal surface. This implies there can be multiple substrate lengths, L_p, on a crystal facet of length, L.

Regime II occurs at lower crystallization temperatures. Multiple nucleation occurs on the substrate in this regime (Figure 9b). In this case, the rate of substrate completion and nucleation are of the same order of magnitude, and the growth rate is proportional to the square root of the surface nucleation rate.[7]

$$G = b_o (ig)^{1/2} \qquad (8)$$

Regime III occurs at even lower crystallization temperatures. In this regime, the surface nucleation rate is so much greater than the substrate completion rate that no

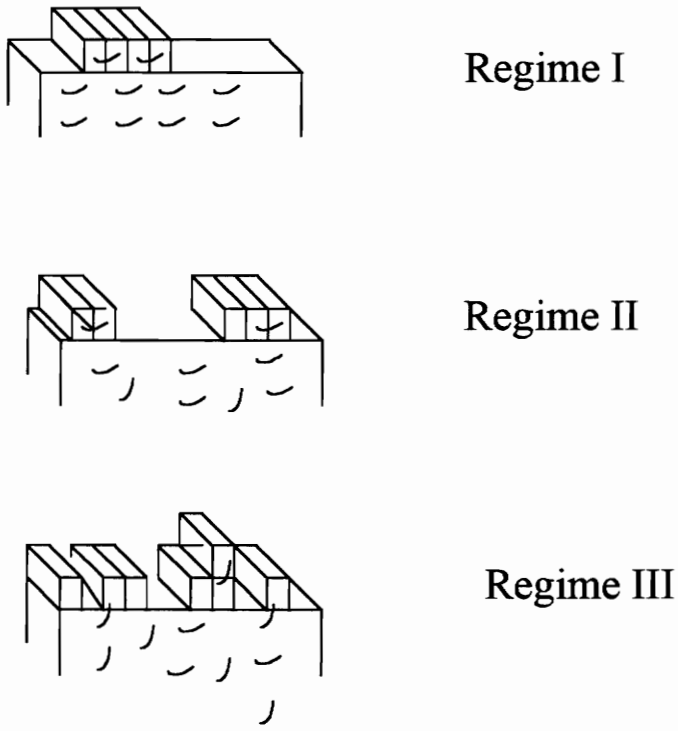

Figure 9. The Relative Magnitude of the Secondary Nucleation Rate, *i*, to the Substrate Completion Rate, g, is the Basis of Crystallization Regimes (from reference 33).

substrate completion is expected in this regime. Thus, the growth rate is again proportional to the secondary nucleation rate.[7]

$$G = b_o i L_{III} \qquad \text{(Regime III)} \tag{9}$$

2.2.2.1 Lauritzen-Hoffman Model

The Lauritzen-Hoffman model derives specific expressions for the surface nucleation and spreading rate. These are derived from a model which calculates rate constants to describe the probability for the rate of removal or addition of stems. The rate determining step for adding the first stem on a substrate is described by the rate A_0, A is the rate constant to add a stem next to an existing stem. The rate constants for stem removal are given by B_0 and B_1; B_0 is the rate constant for the removal of an isolated stem, and B_1 is the rate constant to remove a stem next to an additional stem.

$$A_0 = \beta \exp\left[-\left(2b_0 l\sigma - \psi a_0 b_0 l\Delta f\right)/kT\right] \tag{10}$$

$$A = \beta \exp\left[-\left(2a_0 b_0 \sigma_e - \psi a_0 b_0 l\Delta f\right)/kT\right] \tag{11}$$

$$B_0 = B_1 = \beta \exp\left[-\left((1-\psi) a_0 b_0 l\Delta f\right)/kT\right] \tag{12}$$

The factor β is a retardation factor accounting for the temperature dependence of segmental motions involved in the transport of the polymer segments to the crystallization site. At high undercoolings it is extremely temperature dependent. The factor Ψ represents the fraction of the free energy of crystallization incurred during the stem deposition process, and Δf is the free energy of fusion.

A general steady state expression to describe the flux, S, over the nucleation barrier into the stable region was derived. The equation for the steady state of the formation of nuclei of thickness, l, has been found to be the following,[7]

$$S(l) = \frac{N_0 A_0 (A - B)}{A - B + B_1} \tag{13}$$

where N_0 represents the number of participating species. Assuming that the rates of backward reaction are the same for all stems (B_0=B_1), the following expression is obtained.

$$S(l) = \beta N_0 \exp\left[\frac{-2b_0 l\sigma + \psi a_0 b_0 l\Delta f}{kT}\right] \cdot \left[1 - \exp\left[\frac{-a_0 b_0 l\Delta f + 2a_0 b_0 \sigma_e}{kT}\right]\right] \tag{14}$$

where

$$\beta = \frac{\kappa}{n}\left(\frac{kT}{h}\right) \exp\left[\frac{-U^*}{R(T_x - T_\infty)}\right] \tag{15}$$

The frequency factor, (kT/h), is in events per second, and κ is found from the following,

$$\kappa = h \exp\left(\frac{U^*}{R(T_0 - T_\infty)}\right) \exp\left(\frac{q}{kT}\right) \frac{1}{\zeta_0 l_g^{*2}} \tag{16}$$

where q is the work of chain folding, l^*_g is the initial lamellar thickness, and ζ_0 is the monomeric friction coefficient. The total flow, S_T, is found by summing equation (14) over all possible values of l. Note that the lower limit of integration corresponds to the minimum lamellar thickness (see Equation 6).

$$S_T = \left(\frac{1}{l_u}\right)\int_{2\sigma_e/\Delta f}^{\infty} S(l)dl = N_0\left(\frac{\beta}{l_u}\right)P\exp\left[\frac{2a_0b_0\sigma_e\psi}{kT}\right]\cdot\exp\left[\frac{-4b_0\sigma\sigma_e}{\Delta fkT}\right] \quad (17)$$

where P is the following

$$P = \frac{kT}{2b_0\sigma - a_0b_0\Delta f\,\psi} - \frac{kT}{2b_0\sigma + (1-\psi)a_0b_0\Delta f} \quad (18)$$

At low undercoolings, the principal variation in S_T will be from the last exponential in equation (17). This exponential represents the effect of temperature on the secondary nucleation rate. At high undercoolings, the factor β becomes important.

These equations allow important quantities such as the spreading rate, secondary nucleation rate, average lamellar thickness, and growth rate to be determined.

The spreading rate, g, is found by the following,

$$g = a_0(A - B_1) \quad (19)$$

$$g = a_0\beta\exp[-q/kT]\cdot\left[1-\exp\left(-a_0b_0\delta l(\Delta f)/kT\right)\right] \quad (20)$$

where δl is the given in equation (24).

The secondary surface nucleation rate is the total flux per available sites,

$$i = \frac{S_T}{N_{L_p}a_o} \quad (21)$$

where N_{L_p} is the number of sites per persistence length, and a_0 is the 'length' of one site.

The average lamellar thickness, $\langle l\rangle_{ave}$, is found from the flux.

$$< l >_{ave} = \frac{\int_{2\sigma_e/\Delta f}^{\infty} lS(l)dl}{\int_{2\sigma_e/\Delta f}^{\infty} S(l)dl} \tag{22}$$

$$= \frac{2\sigma_e}{\Delta f} + \delta l \tag{23}$$

where

$$\delta l = \frac{kT}{2b_0\sigma} \cdot \frac{2 + (1-2\psi)(a_0\Delta f \ / 2\sigma)}{\left[1 - \frac{a_0\Delta f\psi}{2\sigma}\right]\left[1 + \frac{a_0\Delta f(1-\psi)}{2\sigma}\right]} \tag{24}$$

Recalling that the approximation for the free energy of crystallization, Δf, is $\Delta h_f(\Delta T)/T_m$; it is seen that the Lauritzen-Hoffman nucleation theory predicts the experimentally observed fact that the lamellar thickness is inversely proportional to the undercooling.

The growth rate equations for Regimes I and II can be found using equations (7) and (8). Typically, the factors that are not strongly temperature dependent are grouped in a pre-exponential factor, G_0. The expressions for G_0 are dependent on the crystallization regime.

Traditionally, the growth rate equation applicable to all growth rate regimes is the following;

$$G = G_o \exp\left[\frac{-U^*}{R(T_x - T_\infty)}\right] \exp\left[\frac{-K_g}{T_x \Delta f}\right] \tag{25}$$

where U* is the activation energy for the transport of crystallizable segments across the melt-crystal interface, R is the gas constant, $T_\infty = T_g - 30$, Δf is the free energy of fusion, and K_g is the nucleation constant which varies for each regime.

$$K_g = \frac{jb_0\sigma\sigma_e}{k} \tag{26}$$

The lateral surface free energy is σ, σ_e is the fold surface free energy, k is the Boltzmann constant, and b_0 is the layer thickness (Figure 7). The factor, j, accounts for the crystallization regime; j = 4 for Regimes I and III, while j = 2 for Regime II.

Frequently, the free energy of fusion is approximated by the following empirical relation, where f is a factor which empirically accounts for the temperature dependence of the free energy of fusion.

$$\Delta f = \frac{\Delta h_f \Delta T}{T_m} \cdot \frac{2T_x}{T_m + T_x} = \frac{\Delta h_f \Delta T}{T_m} \cdot f \tag{27}$$

In this case, the following growth rate equation is used.

$$G = G_O \exp\left[\frac{-U^*}{R(T_x - T_\infty)}\right] \exp\left[\frac{-K_g'}{T_x \Delta T f}\right] \tag{28}$$

where

$$K_g' = \frac{jb_0\sigma\sigma_e T_m}{k\Delta h_f} \tag{29}$$

A plot of $\ln G + U^*/R(T_x-T_\infty)$ vs. $1/T_x\Delta Tf$ is used to determine a value for the nucleation constant.

The basis of the above equations is that the factors in the pre-exponential factor are not temperature dependent. However, an examination of the factor β shows there are two temperature dependent terms; $\exp(-U^*/R(T_x-T_\infty))$ and $\exp(q/kT)$. For this reason, the traditional Lauritzen-Hoffmann growth rate equation was modified to the following,

$$G = G_o^{'} \exp\left[\frac{-U^*}{R(T_x - T_\infty)}\right]\exp\left[\frac{-K_g}{T_x \Delta f}\right]\exp\left[\frac{jq}{4kT}\right] \qquad (30)$$

where j is regime dependent; j=4 for Regime I and III, and j=2 for Regime II.

The factors in the nucleation constant can be related to the chemical structure of the crystallizing chain. The value of the fold surface free energy is a measure of how easily the polymer chain can fold back on itself to form the chain-folded lamellae. This is related to the stiffness of the polymer chain. The work of chain folding, q, is directly proportional to the fold surface free energy.

$$q = 2a_o b_o \sigma_e \qquad (31)$$

A new relation has been proposed to give a molecular meaning to the lateral surface free energy, σ. This postulates that the lateral surface free energy of a melt crystallized polymer is inversely proportional to the characteristic ratio as determined by solution measurements, and suggests that the first step in the secondary nucleation process is entropic in nature. The characteristic ratio, C_∞, is a quantity which describes the

perturbation due to fixed valence angles between chain atoms and steric repulsions to bond rotation on the mean square end-to-end distance of a random walk chain, $\langle r^2 \rangle_0$ for flexible polymers.

$$C_\infty \equiv \frac{\langle r^2 \rangle_0}{n l_b^2} = \left(\frac{1-\cos\theta}{1+\cos\theta}\right)\left(\frac{1+<\cos\varphi>}{1-<\cos\varphi>}\right) \tag{32}$$

The number of carbon atoms in the chain is n, l_b is the C-C bond length, θ is the valence angle, and φ is the bond rotation angle (Figure 10).

The proposed relation is obtained by equating the free energy for the polymer chain to go from state i (the random coil melt) --> ii (the 'localized' activated complex) with the free energy to attain the rate-determining activated state of the first stem in the 'low Ψ' formulation of nucleation theory (Figure 11). The entropy change for the above process is postulated to be[17]

$$\Delta S_{i \to ii} = \frac{-\Delta S_f}{C_\infty} \tag{33}$$

where ΔS_f is the entropy of fusion. The entropy of fusion is given by $\Delta h_f / T_m$.

Due to the fact that state ii involves little or no heat of fusion,

$$\Delta G_{i \to ii} = -T\Delta S_{i \to ii} = T\left(\frac{\Delta h_f}{T_m}\right) a_0 b_0 l_b n C_\infty^{-1} \tag{34}$$

where l_b is the bond length and a_0 is the width of the molecule.

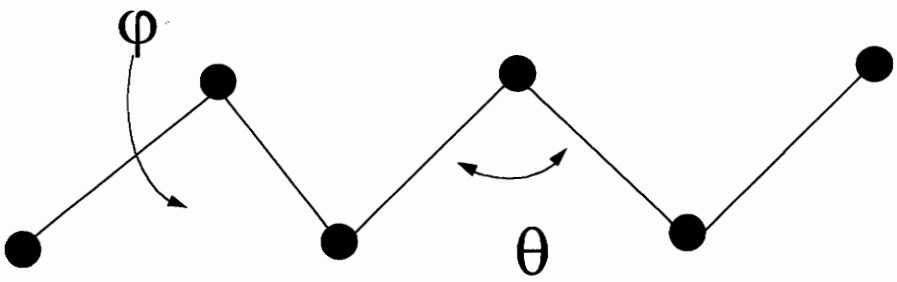

Figure 10. Angles Used in the Determination of the Characteristic Ratio of a Flexible Polymer Chain (from reference 55)

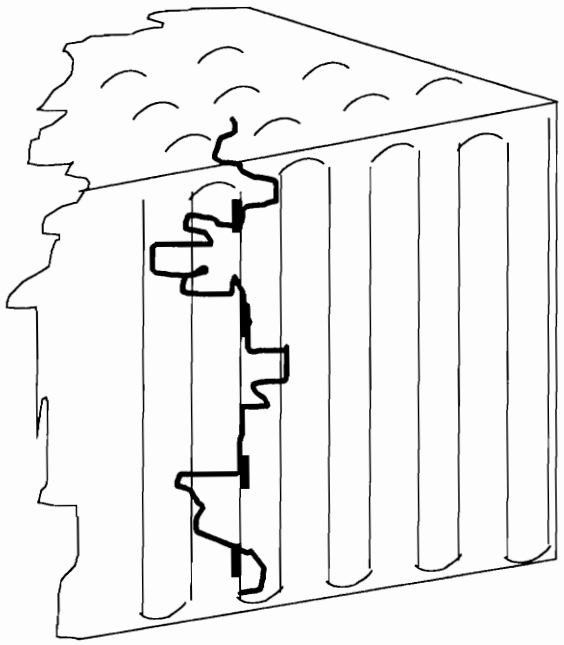

Figure 11. Localized Activated Complex of the Polymer Chain (from reference 7).

The free energy to attain the activated state in nucleation is the following,[17]

$$\Delta G^{*}_{i \rightarrow ii} = 2b_0 \sigma l_u n^{*} \tag{35}$$

where $l_u n^*$ is the initial lamellar thickness, l_g^*. Equating the two free energies will lead to the proposed relation:

$$\sigma_{theor} = T\left(\frac{\Delta h_f}{T_m}\right)\left(\frac{a_0}{2}\right)\left(\frac{l_b}{l_u}\right)\left(\frac{1}{C_\infty}\right) \tag{36}$$

or

$$\cong \Delta h_f \left(\frac{a_0}{2}\right)\left(\frac{l_b}{l_u}\right)\left(\frac{1}{C_\infty}\right) \tag{37}$$

It is important to note that the above derivation is based on the assumption that the polymer is in the melt state in the unperturbed, or theta condition.

Certain polymers, such as some polypeptides and high melting polyesters have a relatively rigid unit, l_{unit}. This unit consists of a number of backbone atoms which are treated collectively as a 'virtual bond.' In this case, the characteristic ratio is defined as;[1]

$$C_\infty \equiv \frac{< R^2 >_0}{x l^2_{unit}} \tag{38}$$

where x is the number of units in the polymer chain.

When virtual bonds are present, the free energy to attain the activated state in the nucleation process is given by $2b_0\sigma x^* l_{unit}$. The free energy to go from state *i* to *ii* becomes $T(\Delta h_f/T_m)a_0b_0x^*l_{unit}$. Thus, the equation for the theoretical value of the lateral surface energy becomes the following.[1]

$$\sigma_{theor} = T\left(\frac{\Delta h_f}{T_m}\right)\frac{a_0}{2}\left(\frac{1}{C_\infty}\right) \cong \Delta h_f\left(\frac{a_0}{2}\right)\left(\frac{1}{C_\infty}\right) \tag{39}$$

An examination of the two extreme values for the characteristic ratio can lead to a better understanding of what this relation states. For the case of the 'freely jointed' model, the value of the characteristic ratio is one. As this is a small value for C_∞, the calculated value for σ will be large. This indicates a large amount of conformational entropy is lost when a freely jointed chain in the melt becomes physically adsorbed on the crystal growth front. This makes sense because the chain needs to give up degrees of freedom to assume the more constrained state in the crystal.[17]

The other extreme is the near-rigid rod. In this case, C_∞ --> n. Thus, the value of σ will be very small. This is because a very small entropy change is needed to attain the 'confined' condition in the crystal.

Experimental data was available for polyethylene, isotactic polystyrene, and poly (L-lactic acid) to test the proposed relation.[1] The values of C_∞ calculated from melt crystallized growth rate data agreed with that determined by solution measurements in each case. This thesis will report on the experimental data and calculations for the case of the low melting polyester, poly(ε-caprolactone).

The Lauritzen-Hoffman surface nucleation theory has been able to account for the temperature dependence of the growth rate of many polymers. However, several criticisms of the model have been voiced.

An examination of equations (22,24) shows that when $\psi \neq 0$ there exists a certain undercooling at which the lamellar thickness is predicted to diverge. This has been called the δl catastrophe, but has never been experimentally determined. If $\psi = 0$, the δl catastrophe is not predicted. A further critique is that the parameter ψ is not physically meaningful and can be adjusted during data analysis to get a better fit of the data. In a recent revision of the nucleation theory, the lamellar thickness dependence of β has been taken into account.[65] This changes the expressions for the surface nucleation rate, *i,* so there is no longer a dependence on ψ for the rate. Thus, the δl catastrophe is no longer predicted.

Other criticisms include the use of an 'artificial' substrate length, L_p, to determine the growth rate in Regime I. The persistence length is less than the substrate length and is used because the 'radial' growth rate of a single crystal is independent of crystal size. The persistence length is the average distance between imperfections. Another comment is that crystals in Regime I and II are expected to have flat facets. However, polyethylene has exhibited a curved growth front at high temperatures.[62]

Additionally, the fact that regime transitions are accompanied by morphological or crystallographic changes has been brought out. These changes could alter lattice and fold surface parameters. Their values should be known in order to analyze the growth rate data correctly.[62]

Criticisms of the LH nucleation barrier model have brought about alternative proposals. The Lauritzen-Hoffman nucleation theory only allows folding of chains when they reach a certain lamellar thickness. Point has developed a model in which the chain is

allowed to fold at any point during stem formation. The stem will attain its thermodynamically and kinetically preferred length by folding and unfolding. This fact changes the simple nucleation barrier proposed in the LH model. Mathematically, the determination of a steady-state expression becomes more difficult due to an additional rate constant for the forward rate of folding, C_i. Estimations made by choosing any value of C_i show that its inclusion will prevent the δl catastrophe from occurring, and it prevents the lamellar thickness from increasing with undercooling. However, in order to predict the experimentally observed decrease in lamellar thickness with increasing undercooling, a specific choice in rate constants is needed.[62]

Another proposal believes the barrier is due to an entropic nature. This model suggests the barrier to crystallization is not from nucleation but from the many ways in which the polymer chain can attach itself to the growth face. The addition and removal of small stems have been mathematically simulated. Sadler and Gilmer have developed models which assume the growth front is rough and there is an entropic barrier to crystallization. Their computer simulations have been able to predict crystal thickness and growth rate behavior qualitatively.[62]

The proposed σ-C_∞ relation adds an entropic nature to the barrier. The random coil chain in the melt will lose configurations (i.e. reduce entropy) when it closely approaches a surface. A short section of the molecule will be semi-confined but not crystallographically attached. The formation of the 'aligned' state is thought to be the rate-determining step in putting down the first stem.

2.3 Equilibrium Melting Temperature

In order to analyze growth rate data, it is necessary to determine an accurate value of the equilibrium melting temperature of the polymer. The equilibrium melting temperature, T_m is defined as the temperature at which a perfect, infinitely large crystal of the polymer of finite molecular weight crystallizes and melts at the same temperature. The equilibrium melting temperature of an inifinite molecular weight polymer is T_m°. Three methods will be used to determine T_m: Gibbs-Thomson-Tammann, Hoffman-Weeks, and an analysis using the Hoffman growth rate theory.

2.3.1 Gibbs-Thomson-Tammann Method

The Gibbs-Thomson-Tammann (GTT) method to determine the equilibrium melting temperature is based on a thermodynamic approach. It is based on the same equation by which the driving force for crystallization was derived (equations 4,5). At the melting point of the crystal, $\Delta\Phi_{crystal} = 0$. Using this information and the thin platelike crystal approximation which says $x >> l$; one obtains the following relationship between the observed and equilibrium melting temperature.

$$T_m' = T_m\left[1 - \frac{2\sigma_e}{\Delta h_f l}\right] \tag{40}$$

The equilibrium melting temperature can be determined from the intercept of a plot of T_m' vs. $1/l$. This equation is valid if the observed melting temperature is measured where one is reasonably certain of the lamellar thickness. In order to ensure this, heating rates large enough to prohibit extensive lamellar thickening must be used. However, high heating rates can introduce the problem of thermal lag. Samples cut to identical shape and weight should be used so the amount of thermal lag will only depend on heating rate.

2.3.2 Hoffman-Weeks Method

This method assumes that the crystal lamellar thickness, l, in the spherulite is proportional to the kinetically controlled initial lamellar thickness, l^*_g.

$$l = \gamma l_g^* \tag{41}$$

The thickening coefficient is γ, and

$$l_g^* = \frac{2\sigma_e T_m^0}{\Delta h_f \Delta T} + \delta l \tag{42}$$

The undercooling is ΔT which is equal to $T_m - T_x$, where T_x is the crystallization temperature. The heat of fusion is Δh_f, and σ_e is the fold surface free energy, and δl is the additional thickness needed to allow the surface nucleus to enter the region of stability.

Assuming that δl is small with respect to $2\sigma_e/\Delta f$, and that γ is constant, the following equation is obtained by inserting equation (42) into equation (40)

$$T_m' = T_m\left[1-\frac{1}{\gamma}\right]+\frac{T_x}{\gamma} \tag{43}$$

The equilibrium melting temperature is then found from the intersection of the linear least squares fit of T_m' vs. T_x with $T_m' = T_x$. A generalized Hoffman-Weeks plot is shown in Figure 12.

The above treatment assumes the thickening coefficient, γ, does not depend on crystallization temperature or time. However, it is well known that polymeric crystals may thicken at a given crystallization temperature. In order to try to minimize thickening effects, samples are crystallized to only 10% crystallinity.

2.4 Crystallization of Block Copolymers

Block copolymers have long sequences (blocks) of one type of repeat unit joined at one or both ends to blocks of a chemically different repeat unit. Combination of two chemically different repeat units into one molecule can produce a molecule which possesses different surface and bulk properties from the corresponding homopolymers. The different properties result from the chemical nature of the blocks, the block lengths, and architecture (i.e., diblock, triblock, or multiblock).

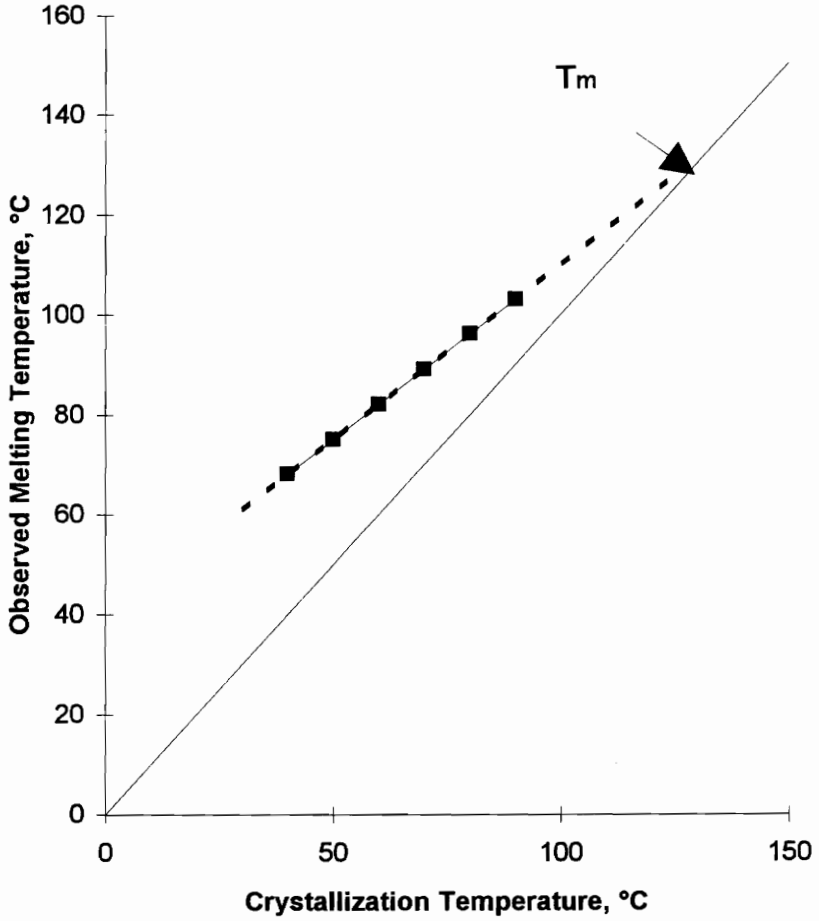

Figure 12. Example of a Hoffman-Weeks Plot

Theoretical predictions have been made for the crystallization of diblock copolymers from a micro-phase separated melt where one block is amorphous.[21,22] These predictions can be modified for the case of triblock copolymers where the center block is crystalline or amorphous. The main difference between the homopolymer and diblock copolymer crystallized from a phase separated melt is due to the differences in the driving forces of crystallization. The crystallization of the homopolymer is kinetically controlled, while the block copolymer crystallization is thermodynamically controlled.[20] In a homopolymer, the lamellar thickness is a function of the undercooling, the lateral and fold surface free energies, and the heat of fusion.[21]

$$l = \frac{2\sigma_e T_m}{\Delta h_f^0 \Delta T} + \delta l \qquad (44)$$

A homopolymer will reduce the number of chain folds to become an extended chain crystal in the limit of infinite annealing times. In contrast, the diblock and triblock copolymers will anneal to a finite equilibrium thickness.[21] An extended chain crystal would not be in equilibrium for the block copolymer because the amorphous chain would also need to be fully extended. The fully extended chain is not the most favorable for the amorphous chains because of the entropy gain that can be achieved in the random coil state.[23] The amorphous block wishes to increase the minimum separation between cilia tie points, λ, (Figure 13), while there is an opposing tendency from the crystalline block which wishes to decrease λ. This results in an equilibrium value of λ.

Molecular weight is not a prominent factor in determining the lamellar thickness for the homopolymer. In contrast, it has been found that the solution crystallization of block copolymers is a function of molecular weight due to the minimization of free energies to determine the lamellar thickness.[20] Both the theoretical crystalline lamellar

thickness, l_c, and the thickness of the amorphous region, l_a, have been calculated for diblock copolymers.[21]

$$l_a = \frac{r_a^{2/3}\left(\sigma + \sigma_e \rho_c\right)^{1/3}}{\left(3kT\rho_a\right)^{1/3}} \tag{45}$$

$$l_c = \frac{r_c \rho_a^{2/3}\left(\sigma + \sigma_e \rho_c\right)^{1/3}}{\rho_c r_a^{1/3}\left(3kT\right)^{1/3}} \tag{46}$$

Both thicknesses depend on molecular weight. The molecular weight of the amorphous and crystalline forming portions are given by r_a and r_c.

2.4.1 Block Copolymers Containing Poly (ε-Caprolactone)

Diblock copolymers containing an amorphous block of polystyrene or polybutadiene, and a crystallizable block of poly(ethylene oxide) or poly(ε-caprolactone) have been studied by Gallot *et al.*[29,30] They have examined the morphology of the diblock copolymers with and without a solvent that was preferential to the amorphous block. Measurements of chain folding and lamellar thicknesses were made. The effect of molecular weight, solvent concentrations, and crystallization temperatures on the lamellar crystalline structure have been made. No mention was made of whether these polymers were microphase separated in the melt.

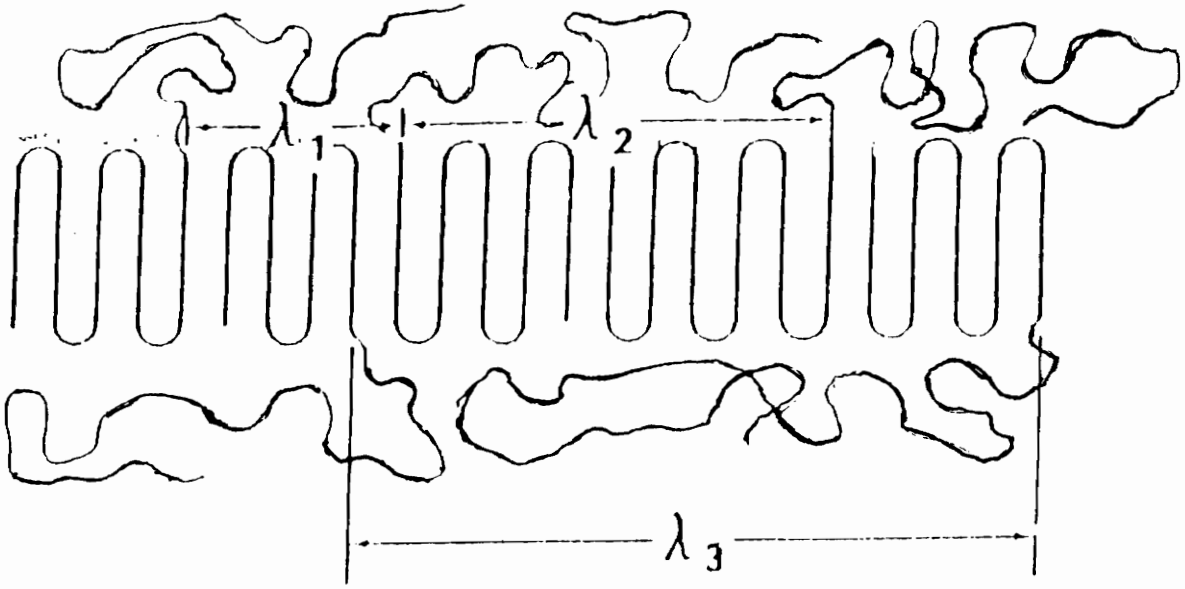

Figure 13. Schematic Diagram of the Minimum Separation Between Cilia Tie Points When a Block Copolymer Crystallizes. (from reference 21).

A series of poly(ε-caprolactone-*b*-ethylene glycol-*b*-ε-caprolactone) triblock copolymers were studied by Nojima *et al.*[28] In this case, both chemical repeat units are crystallizable. The effects of different molecular weights of the poly(ε-caprolactone) end-block on the long spacing and WAXD diffractograms were shown. The WAXD results showed that the crystals of PEG and PCL crystallized independently. SAXS measurements showed a decrease in long spacing when short poly(ε-caprolactone) end-blocks were used, and an increase in long spacing with increasing block length for longer blocks. The results for the block copolymers were then compared to studies on a blend of poly(ε-caprolactone)\poly(ethylene glycol) oligomers. In the blend, it was found that the long spacing was not influenced by the second component. These authors did not comment on whether there was phase separation of the block copolymer in the melt.

Triblock copolymers containing poly(ε-caprolactone-*b*-dimethyl siloxane-*b*-ε-caprolactone) were examined by Lovinger *et al.*[32] The triblock copolymers differed in the length of the poly(ε-caprolactone) end-blocks. The molecular structure, crystallization, solid state morphology, thermal properties, and phase behavior of the two copolymers and homopolymer were reported. It was found that the copolymers have the same crystal structure and a reduced growth rate as compared to the homopolymer. A theoretical discussion of the influence of molecular weight of the crystallizable block on chain folding was also given. Again, no comment was given as to whether the block copolymer was microphase separated in the melt.

A SAXS study of an ε-caprolactone-butadiene diblock copolymer was carried out by Nojima *et al.*[28] They observed the process of morphology formation by time-resolved SAXS and interpreted their data in light of the equilibrium theory of block copolymer

crystallization. They concluded a kinetic factor still intervenes. This was due to the fact that the time dependence of the maximum intensity of the SAXS curve followed the familiar sigmoidal curve found in the crystallization of homopolymers.

The triblock copolymer that was examined in this thesis is poly (ε-caprolactone-*b*-propylene oxide-*b*- poly (ε-caprolactone). This triblock copolymer was synthesized for use as a fracture toughness modifier for styrene-acrylonitrile resins. The poly (propylene oxide) midblock would be a rubber toughening agent for the resin, while the poly (ε-caprolactone) end-blocks would anchor the block copolymer into the styrene-acrylonitrile resin.[57]

2.5 Properties of Poly(ε-caprolactone)

An attractive property of PCL is that it is miscible with a diverse group of polymers [40, 50-54]. This group includes poly (vinyl chloride), styrene/acrylonitrile copolymers, nitrocellulose, cellulose propionate, cellulose butyrate, polyhydroxyether, and polyepichlorohydrin.

Crystal structure analysis of the poly (ε-caprolactone) has shown that the chains pack in a nonplanar structure.[36,37] The chain conformation of PCL is almost planar zigzag, but deviates from the fully extended form. This is because the CH_2 sequences are planar, but the plane of atoms of the ester group tilts slightly to the fiber axis.[36]

The unit cell is orthorhombic, and the unit cell parameters obtained from electron diffraction patterns are the following at room temperature.

a = 7.48 Å
b= 4.98 Å
c= 17.26 Å

These parameters give a calculated crystalline density for poly (ε-caprolactone) of 1.20 g/cm^3.[36]

There is a close similarity in the a and b unit cell dimensions of PCL and polyethylene. The unit cell dimensions for polyethylene are the following.

a = 7.496 Å
b=4.93 Å
c= 2.534 Å

The amorphous density for poly(ε-caprolactone) has been determined by dilatometric methods to be 1.095 g/cm^3.[38] The heat of fusion was calculated using the diluent method and found to be 32.4 cal/gm.[24] The glass transition temperature was determined by DSC to be -63°C. [49] Numerous values have been reported for the equilibrium melting temperature of poly(ε-caprolactone).[13, 24, 40-42, 44, 46] The range of these values is from 58-74 °C. (Table 1).

Several studies of the crystallization behavior of poly(ε-caprolactone) have been carried out. There have been studies of the homopolymer, [18,19,14] and blends of PCL with poly(vinylchloride)[16, 39, 43, 64], polycarbonate[42, 54], poly(hydroxyether of bisphenol A)[42], poly(chloromethymethacrylate)[41], poly(2-chloro ethyl methacrylate)[41], and poly(styreneco-acrylonitrile)[15, 16,64]. Ternary blend systems of poly(ε-caprolactone)-poly(vinyl chloride)-styrene-co-acrylonitrile copolymer[18], as well as blends with random copolymers have been examined.[16]

Most of the work done on PCL blends focused on determining blend interaction parameters from melting point depression studies. The papers which analyzed growth rate data with the Lauritzen-Hoffman growth rate equation to determine the fold and lateral interfacial free energies (σ_e, and σ) used the Thomas-Staveley empirical relationship to estimate σ.

$$\sigma = \alpha(a_o b_o)^{1/2} \Delta h_f \qquad (47)$$

A value of $\alpha \cong 0.1$ was assumed in the referenced work to give a calculated value of 6.7 erg/cm^2 for σ. This value was then combined with $\sigma\sigma_e$ found from growth rate analysis to determine a value of σ_e. A wide range of values for this parameter have been reported in the literature ranging from 27 erg/cm^2 by Ong and Price[64] to 112 erg/cm^2 by Goulet and Prud'homme[46]. Intermediate values of σ_e = 85.7 and 87.1 erg/cm^2 have also been found.[19,45] Reasons for the wide disparity in values include the use of different equilibrium melting temperatures and crystallization regimes. One motivation for this work is to determine an accurate value of the equilibrium melting temperature and value for σ_e so the growth rate data for poly(ε-caprolactone) can be rigourously analyzed. An experimental value of σ can then be compared to the value obtained using the empirical Thomas-Staveley relationship.

Examination of the melting behavior of PCL in blends of poly(ε-caprolactone) with poly(styrene-co-acrylonitrile), SAN, show double endothermic behavior. The relative magnitude of the lower endotherm increased with SAN concentration for melt-crystallized samples.[15] This behavior was not seen with samples which were crystallized from solution. Heating rate studies led the authors to suggest that the reason behind the double endothermic behavior was melting and recrystallizaiton during the DSC heating rate scan. Another author studied the effect of annealing temperature on the double endothermic behavior in PCL/SAN blends. It was found that as the annealing temperature increased, the shape of the lower endotherm changed from a broad shoulder to a clearly defined endothermic peak.[51] This author suggested the origin of the lower endothermic peak was due to crystallization during quenching.

Table 1. Reported Values of the Equilibrium Melting Temperature for poly(ε-caprolactone).

<Mw>, kg/mol	Tm, °Celsius	Reference
7	68	19
15	69	19
17.6	59	45
20	58	43
40	70	19
40	71	46
47	66	41
48	74	44
49	63	39

Blends of PCL with a random copolymer of vinylidene chloride with vinyl chloride, (PCL/P(VCl_2-VC)) exhibit double endothermic behavior for PCL concentrations below 70%.[16] These authors excluded the formation of a second crystalline structure with a different unit cell and the concept of melting and recrystallization during the heating rate scan as reasons for this behavior. They suggest the formation of a different morphological phase with the same unit cell but double -peak lamellar thickness distribution as the origins of the double melting behavior.

Ong and Price found that the melting behavior of PCL changed in a series of PCL/PVC blends of different concentrations.[64] The pure poly(ε-caprolactone) had a shoulder prior to the melting endotherm. Increasing the concentration of poly(vinyl chloride) broadens the melting peak and enlarges the low temperature endotherm prior to the melting endotherm. These authors ascribed this behavior to the slow crystallization rate of PCL in the viscous matrix of the blends.

Chapter 3. Experimental

3.1 Materials

The materials used in this study were poly(ε-caprolactone) and a triblock containing poly(ε-caprolactone). The triblock copolymer used was poly(ε-caprolactone-*b*-propylene oxide-*b*-ε-caprolactone).

The poly(ε-caprolactone) homopolymer was purchased from Scientific Polymers, Inc (Lot Number 03). The $<M_n>$ and $<M_w>$ were found to be 15 kg/mol and 26.5 kg/mol by gel permeation chromatography. The polydispersity of the homopolymer is 1.7. Samples were dissolved in chloroform and polystyrene standards were used for calibration in the GPC analysis. A ^{1}H-NMR spectrum was taken of the polymer to confirm the identity of the polymer (Figure 14). NMR samples were run at room temperature, dissolved in d-chloroform, and run on a Bruker NMR.

The triblock copolymer, poly(ε-caprolactone-*b*-propylene oxide-*b*-ε-caprolactone), was synthesized by A. Brink in this university. Poly(ε-caprolactone) was polymerized by a ring opening polymerization off both ends of a known molecular weight of poly(propylene oxide), PPO, (<Mw> =14 kg/mol and <Mn> =10.5 kg/mol). Confirmation of the structure was done by NMR (Figures 15,16) as stated above. Knowledge of the molecular weight of the PPO block allowed the molecular weight of the two PCL blocks to be determined. This corresponded to the copolymer containing 80 weight % PCL. Assuming that the two PCL blocks are of equal length, a number average molecular weight value of 21 kg/mol was calculated for each PCL block. This gives a

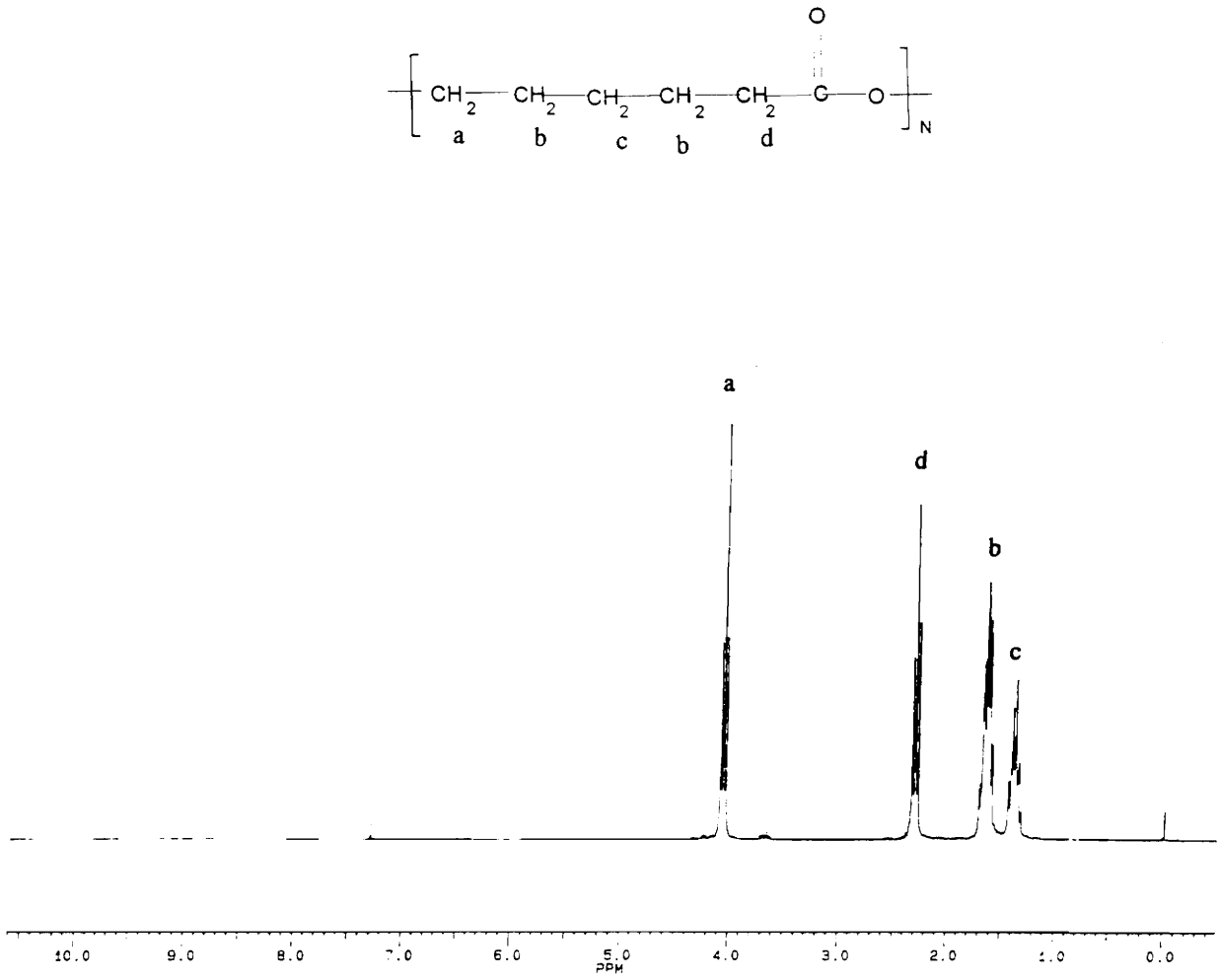

Figure 14. NMR Spectrum of Poly(ε–caprolactone).

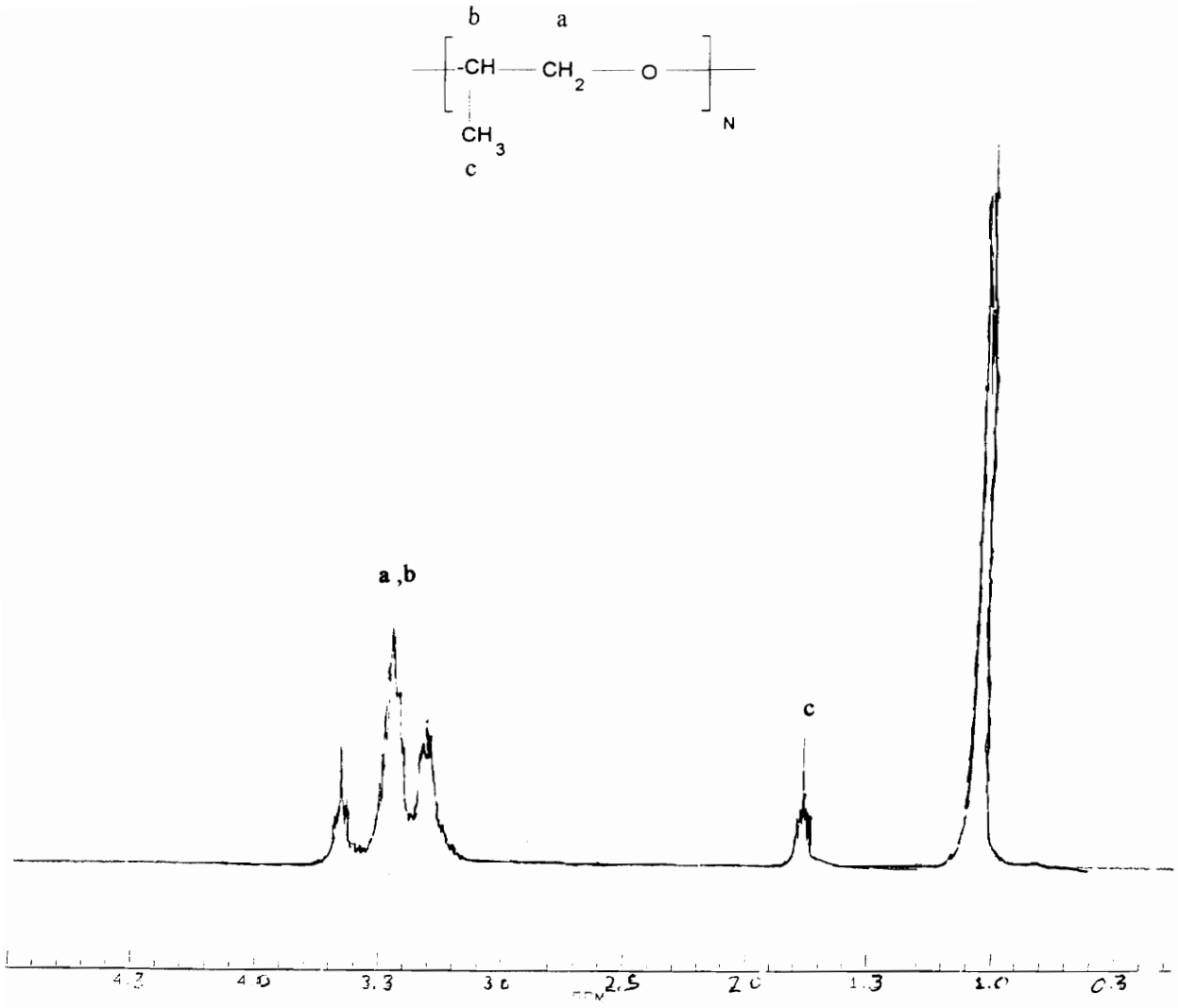

Figure 16. NMR Spectrum of Poly(propylene oxide).

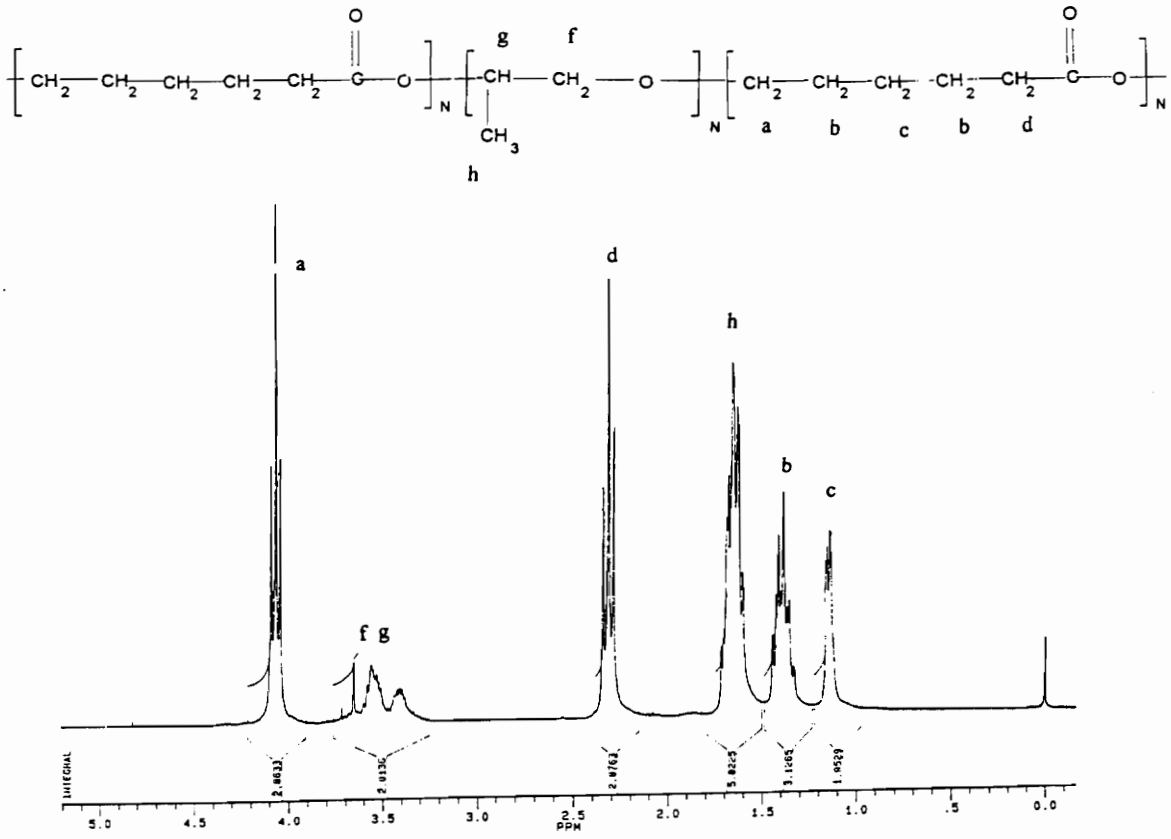

Figure 16. NMR Spectrum of Poly(ε–caprolactone-*b*-propylene oxide-*b*-ε–caprolactone).

total number average molecular weight of 52.5 kg/mol for the triblock copolymer. The GPC analysis was done using a universal calibration on samples that were dissolved in chloroform. Elemental analysis for carbon and hydrogen was done by Atlantic Microlab, Inc. Results show the copolymer to be 62.9 % carbon and 9.0 % hydrogen, which corresponds to a triblock copolymer containing 80 weight % PCL and 20 weight % poly (propylene oxide). The polydispersity was found to be 1.6.

3.2 Differential Scanning Calorimetry

The observed melting temperature and weight percent crystallinity were determined by DSC. In the determination of the equilibrium melting temperature by the Hoffman-Weeks method, the weight (3.0 +/- 0.1 mg) and shape of the samples were kept constant. Samples were crystallized to 10 +/- 5 % crystallinity in order to minimize lamellar thickening. The observed melting temperature was taken as the maximum of the endotherm. Calibration of the temperature and heat of fusion was done with indium.

For the Gibbs-Thomson-Tammann analysis, the observed melting temperature was found on samples cut to identical shape and weight (3.0 +/- 0.1 mg). The heating scan was run on a Perkin-Elmer DSC-2 under nitrogen flow at rates of 10, 20, 40, and 80°C/min, and the observed melting temperature was taken as the maximum of the melting endotherm. The temperature was calibrated with an indium standard run at a heating rate of 0.31°C/min.

The volume percent crystallinity can be calculated from the weight percent crystallinity. The weight percent crystallinity is determined by integrating the area under

the melting endotherm. Knowledge of the crystalline and amorphous densities of PCL allow the conversion of this value to volume percent crystallinity.

3.3 Small Angle X-ray Scattering

3.3.1 Determination of Long Spacing

The lamellar thickness was calculated from the long spacing which was determined by small angle x-ray scattering (SAXS). The samples used to determine the long spacing were melted at 100°C for five minutes and then transferred to an oil bath at the desired crystallization temperature. The samples were crystallized for long periods of time (at least 3-4 times the half time of crystallization) to insure the samples were as crystalline as possible.

The small angle x-ray scattering curves were recorded with a Kratky Compact Small Angle System using Cu Kα X-ray radiation (λ=1.542 Angstroms) equipped with a Braun position sensitive detector. Scattering profiles from the sample as well as parasitic scattering curves were recorded for each sample. Data processing included successive subtraction of the parasitic scattering, smoothing, desmearing, and Lorentzian correction. The long spacing was taken as the maximum of the scattering peak after the data had been analyzed.

Correction for parasitic scattering is needed for any scattering that is present when the sample is absent. The parasitic scattering is primarily from the edges of the collimating

system. The parasitic scattering is recorded when the sample is placed between the x-ray source and the first collimator. The detector will not see any scattering from the sample when it is in this position. Additionally, the main beam will still be attenuated or absorbed by the sample. Thus, the transmission correction factor on the intensity is also carried out in this process.[9] Once the parasitic scattering has been obtained it can be subtracted from the scattering data. The background-subtracted scattering data is then smoothed. This is necessary because desmearing can magnify spurious effects and the smoothed data will serve as the first approximation in the desmearing routine.

Desmearing the data is necessary because the data was taken using a slit collimated geometry. This geometry 'smears' the data, and in order to get the intensity data a pin-hole collimated system would have recorded, the data must be desmeared. The 'smearing' of the data occurs because of the slit length. The slit smeared intensity, $\tilde{I}(q)$, is related to the intensity, I(q), obtained under a pinhole collimation by the following relation.

$$\tilde{I}(q) = \int_{-\infty}^{\infty} w(t) \cdot I\left(t^2 + q^2\right)^{1/2} dt \qquad (48)$$

The slit-length weighting function of the primary beam reaching through the collimating system at the detector is w(t).[2] The effect of the slit-width may be included in this expression, however this correction is usually neglibile. The slit-length weighting function is determined experimentally by turning the detector 90° and recording the beam profile.

During desmearing , equation 48 is inverted by a numerical method. The method that was used in this work is Glatter's iterative process[14]. This technique makes successive approximations until the difference between the approximations becomes very small.

After desmearing, the channel numbers are converted to the scattering vector, q, by calibration with a lead stearate standard. The desmeared data is then Lorentz corrected. This correction is needed because the position-sensitive detector only detects a 'slice' of the diffraction cone. The areas of the diffraction cone will increase with increasing radius. This fact is taken into account by multiplying the intensity by q^2.

The desmeared-Lorentz corrected data is then considered in light of the model for semi-crystalline polymers. This model states that chain-folded lamellar crystals are in regular stacks separated by amorphous interlayers. A characteristic quantity of this model is the long spacing (Figure 17). The long spacing, L, is an average quantity over the sample and corresponds to the sum of the crystalline lamellar thickness, l_c, and the amorphous layer thickness, l_a, in the semi-crystalline polymer.

The long spacing can be estimated from the SAXS data by employing a form of the Bragg relation

$$L = \frac{2\pi}{q_{max}} \tag{49}$$

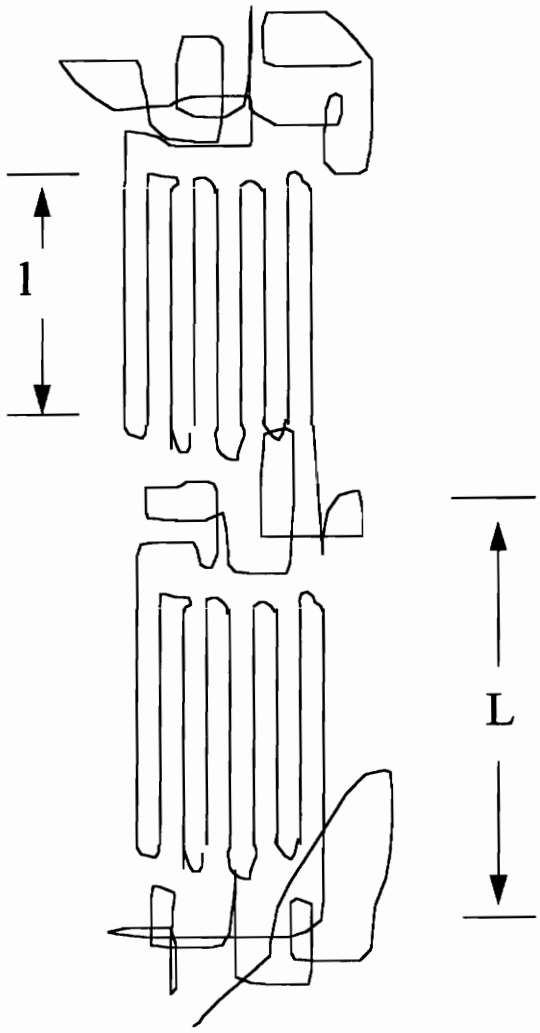

Figure 17. Long Spacing and Crystalline Lamellar Thickness.

where q_{max} is the scattering vector at the Bragg maximum.

For samples in which the lamellar stacks are volume filling, or the amorphous content is only located in the interlamellar region, the lamellar thickness, *l*, can be determined if the volume percent crystallinity, ϕ_{cv}, is known.

$$l = L\varphi_{cv} \tag{50}$$

3.3.2 Isothermal Crystallization Studies

The isothermal crystallization behavior was monitored as a function of time with SAXS using an in-house built hot stage whose temperature was controlled by an Omega temperature controller (± 0.4 °C) under nitrogen flow. Temperature calibration was done with lead stearate. The SAXS data was taken for two minutes. The integrated intensity was taken as the area under the raw data curve. After the channel number was converted to scattering vector using lead stearate as a standard, the relative invariant, Q', was taken as the area under the curve of Iq^2 vs. q. Due to the fact that it was the change in the invariant that was of interest; normalization with respect to the intensity of the primary beam, and the scattering power of a single electron was not performed. The volume of the sample was kept constant, so normalization for the volume was not needed.

The relative invariant represents the scattering power of the sample in the small angle region.

$$Q' = 4\pi \int_0^\infty q^2 I(q) dq \tag{51}$$

In the interpretation of the relative invariant, it is assumed that the crystalline and amorphous volume fractions in the lamellar stacks are φ_{cl} and (1- φ_{cl}), respectively. The fraction of material that forms lamellar stacks is φ_L, while the fraction of material formed by the larger amorphous regions outside the lamellar stack is (1-φ_L). The volume fraction filled with spherulites is φ_s,

$$Q = \varphi_s \varphi_L \varphi_{cL} (1 - \varphi_{cL}) (\Delta\rho)^2 \tag{52}$$

where $\Delta\rho$ is the difference in the electron density between the two phases. If the sample is completely filled by spherulites, and the spherulites are completely filled with lamellar stacks; φ_s, =φ_L =1.

The invariant depends only on $\Delta\rho$ and the relative volume fraction in each of the phases. It does not depend on structural details like the shape or dimensions of the phases. [2] For a semi-crystalline polymer with less than 50% local crystallinity, an increase in the invariant will correspond to an increase in crystallinity. The kinetics of crystallization can be observed by recording the change in the invariant with crystallization time, because the volume fraction of each phase will change with percent crystallinity. Kinetic data can be obtained before and after the sample is completely filled with spherulites. This allows the rates of primary and secondary crystallization to be determined.

For the isothermal crystallization studies, the parasitic scattering was recorded at room temperature. An analysis of the effect of temperature on the parasitic scattering

found that temperature did not significantly affect the parasitic scattering. The experiments were run only 30°C above room temperature. Data analysis for the long spacing was the same as stated above.

Samples were prepared for isothermal crystallization by placing the polymer in a sample holder between two layers of Kapton film (0.33 mil thickness). The sample was then melted on a hot plate at 100°C for five minutes and transferred to the hot stage which was already at the appropriate crystallization temperature.

3.4 Polarized Optical Microscopy

Growth rate measurements were obtained by measuring the change in the spherulitic radius with time during the isothermal crystallization process. The samples were melt pressed between two glass slides. Measurements of the growth rate were done by melting the samples at 100 °C for 5 minutes, and then cooling to the crystallization temperature. An Olympus BS-2 polarized optical microscope equipped with a Linkham THM 600 hot stage operated under dry nitrogen purge, Linkham TC91 temperature controller (± 0.1 °C), Ikegami ITC510 b/w video camera, and Hitachi VT-f445a VHS video cassette recorder were utilized. Data analysis was performed using an Olympus Corp Cue Micro-300 video caliper. Reported growth rates are an average of 3-6 spherulitic growth rate determinations. Temperature calibration was carried out with benzophenone (T_m= 48.1 °C).

Chapter 4. Crystallization Behavior of Poly(ε-caprolactone)

This section will discuss the crystallization behavior of poly(ε-caprolactone). The chapter will begin with the determination of the equilibrium melting temperature. Once this value has been obtained the growth rate data is analyzed to find a value for the product of the surface energies, $\sigma\sigma_e$. This value is combined with an independent determination of the fold surface free energy, σ_e, to determine a value for the lateral surface free energy, σ. The value of σ is then used in the proposed σ-C_∞ relation to check its validity for the case of poly(ε-caprolactone).

4.1 Determination of the Equilibrium Melting Temperature

In order to analyze the growth rate data, an accurate value of the equilibrium melting temperature is needed. Three methods were used to determine the T_m for the pure homopolymer of PCL; Hoffman-Weeks, the Gibbs-Thomson-Tammann treatment, and an analysis using the Lauritzen-Hoffman growth rate theory.

4.1.1. Hoffman-Weeks Method

In the Hoffman-Weeks method, the observed melting temperature is measured for samples crystallized at a variety of crystallization temperatures.[7] The equilibrium melting temperature is determined by extrapolating the line from the plot of the observed melting temperature, T_m', vs. the crystallization temperature, T_x, to the interception of the line where $T_m' = T_x$. This extrapolation is based on the following equation

$$T_m' = T_m\left(1-\frac{1}{\gamma}\right)+\frac{T_x}{\gamma} \qquad (53)$$

where γ is the thickening coefficient. A linear plot will be observed if the thickening coefficient is constant.

An examination of the Hoffman-Weeks plot for PCL (Figure 18, Table 2) shows it to be non-linear. This suggests the thickening coefficient is not constant. As the crystallization temperature is increased, the polymer crystals should thicken faster, leading to a subsequent increase in the thickening coefficient. This behavior accounts for the upswing in the plot at higher crystallization temperatures.

If the extrapolation to determine T_m is made where the thickening coefficient is constant (lower crystallization temperatures), a value of 65° Celsius is found. This value is in the range of other reported values of T_m .[16,18,19,39,41,43]

The equilibrium melting temperature of a polymer is the temperature at which an extended polymer chain will melt and crystallize. Using this definition, the Hoffman-Weeks value of T_m for PCL can be shown to be too low. A sample crystallized at 58°C for 2 months had an observed melting temperature of 68 °C. This observed melting temperature is greater than the equilibrium melting temperature predicted by the Hoffman-Weeks method, while the crystallization temperature is lower. This indicates the true T_m is higher than that determined by the Hoffman-Weeks method. Additionally, other experimental results (Gibbs-Thomson-Tammann method and growth rate measurements) indicate the value of the equilibrium melting temperature is higher.

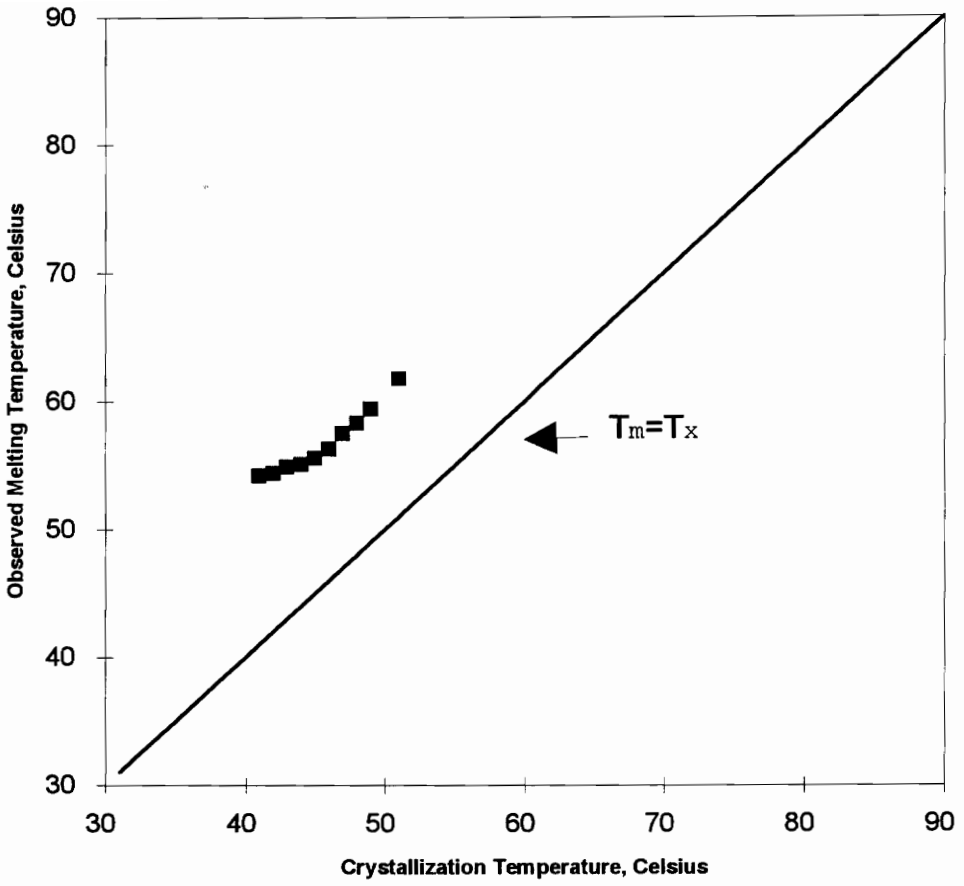

Figure 18. Hoffman-Weeks Analysis of Poly(ε–caprolactone).

Table 2. Hoffman-Weeks Data for Poly(ε–caprolactone).

Crystallization Temperature, Celsius	Crystallization time	Observed Melting Temperature, Celsius	Weight Percent Crystallinity
41	4 min	54.2	9.7
42	5 min	54.4	5.2
43	9 min	54.9	7.2
44	16.5 min	55.1	10.2
45	26.25 min	55.6	10
46	47.5 min	56.3	5.8
47	1.5 hr	57.5	15.5
48	3 hr	58.3	8.6
49	5 hr 23 min	59.4	14.3
51	21.75 hr	61.7	15.9

4.1.2 Gibbs-Thomson-Tammann Method

The Gibbs-Thomson-Tammann treatment was used to determine a value for the equilibrium melting temperature and the fold surface free energy, σ_e, of PCL. The experimental procedures were based on those used to determine the T_m and σ_e of poly(pivalolactone).[22] This method is based on the following equation

$$T_m' = T_m\left(1-\frac{2\sigma_e}{\Delta h_f l}\right) \qquad (54)$$

where the l is the lamellar thickness of the crystal. A plot of T_m' vs. $1/l$ will have a slope proportional to σ_e and an intercept equal to the value of the equilibrium melting temperature.

This equation is valid if the lamellar thickness is much greater than its width and if the observed melting temperature is measured under conditions where one is reasonably certain of the lamellar thickness. In order to ensure that the second condition is valid, heating rates large enough to prohibit extensive thickening were used. However, high heating rates can introduce the problem of thermal lag. In order to account for this, samples of identical shape and weight were used.

Small angle x-ray scattering (SAXS) was used to determine the lamellar thickness of polymer samples. The small angle x-ray scattering arises from the electron density fluctuations between the crystalline lamellae and interlamellar amorphous regions in semicrystalline polymers. If the stacking of lamellae upon each other is periodic, then Bragg's Law can be used to determine the long period from the scattering maximum.

The data from SAXS shows the expected increase in lamellar thickness with increasing crystallization temperature (Table 3). Analysis was done using the Bragg equation to find the long spacing (where $q = 4\pi\sin\theta/\lambda$)

$$L = \frac{2\pi}{q_{firstorder}} \tag{55}$$

If the amorphous content is located between the lamellae, the lamellar thickness can be found by knowing the volume percent crystallinity, φ_{cv} ,

$$l = \varphi_{cv} L \tag{56}$$

The SAXS profile of poly(ε-caprolactone) indicates the lamellar stacking is periodic due to the sharpness of the scattering peak and the presence of a second order peak located at approximately twice the scattering angle (Figure 19). This combined with the fact that the crystallinity of PCL is very high (about 70 %) makes the presence of pockets of amorphous material outside of the lamellar stacks unlikely.

The volume percent crystallinity is found using the weight fraction crystallinity (from DSC data) and the amorphous and crystalline densities (ρ_c, ρ_a). The values used were ρ_c = 1.195 g/cm^3 [23], ρ_a = 1.095 g/cm^3 [23], and Δh_f = 32.4 cal/g.[24]

$$\varphi_{c,v} = \frac{\left(\frac{\Delta h_f}{\Delta h_f^0}\right)\left(\frac{\rho_a}{\rho_c}\right)}{\left[1-\left(1-\left(\frac{\rho_a}{\rho_c}\right)\right)\left(\frac{\Delta h_f}{\Delta h_f^0}\right)\right]} \tag{57}$$

Table 3. Data for PCL samples crystallized at different crystallization temperatures.

Crystallization Temperature (°C)	**Crystallization Time** (Days)	**Long Spacing** (nm)	**Heat of Fusion** (Cal/g)	**Volume Percent Crystallinity**	**Lamellar Thickness** (nm)
30	4	11.7	23.5	70.8	8.3
34	3	12.0	23.8	71.6	8.6
42	5	12.8	22.9	69.5	8.9
44	4	13.1	23.5	71.3	9.3
46	4	13.3	23.4	69.2	9.2
48	4	13.9	23.1	69.4	9.7
50	6	14.1	23.3	70.2	9.9

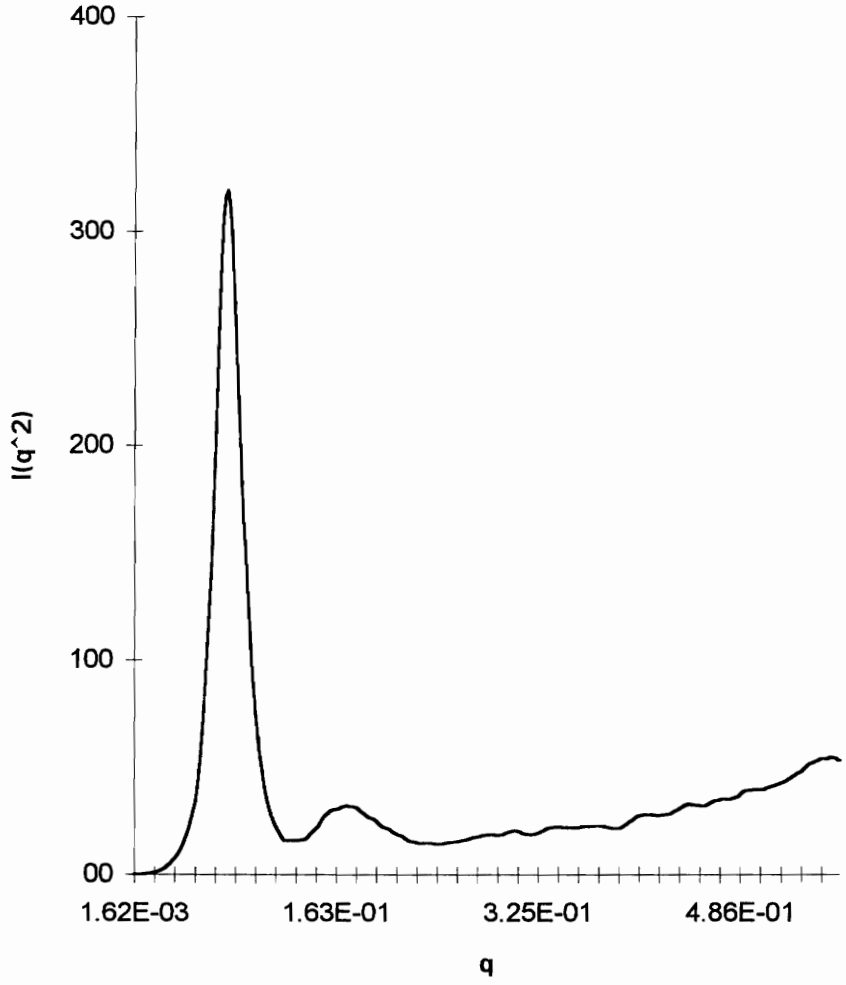

Figure 19. Small Angle X-ray Scattering Profile of Poly(ε–caprolactone); T_c =46°C.

A plot of T_m' vs. $1/l$ was made (Figure 20, Table 4) for each of the heating rates used to determine the observed melting temperature by DSC. The value of the apparent equilibrium melting temperature, T_m^{app}, was found for each heating rate by extrapolating to $1/l = 0$.

The effect of thermal lag is more pronounced for higher heating rates. Due to the poor thermal conductivity of polymers, there is not enough time for the heat to be transmitted from the heating elements of the DSC cell to the sample. This leads to higher observed melting points for increasing heating rates. The samples in this study were cut to identical size, weight, and shape. For this reason, the observed melting temperatures at different heating rates were not corrected for thermal lag because these effects should be the same for all samples and only depend on heating rate.

The effect of different heating rates is taken into account by plotting the apparent equilibrium melting temperature vs. heating rate (Figure 21, Table 5). The true equilibrium melting temperature is found by extrapolating this graph to a heating rate of 0°C/min. The extrapolation procedure gave a value of 85 ± 4 °C for the equilibrium melting temperature. The uncertainty in this value is from experimental measurements and the extrapolation procedures.

4.1.3 Lauritzen-Hoffman Growth Rate Equation

Another method used to estimate the equilibrium melting temperature is to analyze growth rate data using the modified Lauritzen-Hoffman growth rate equation.

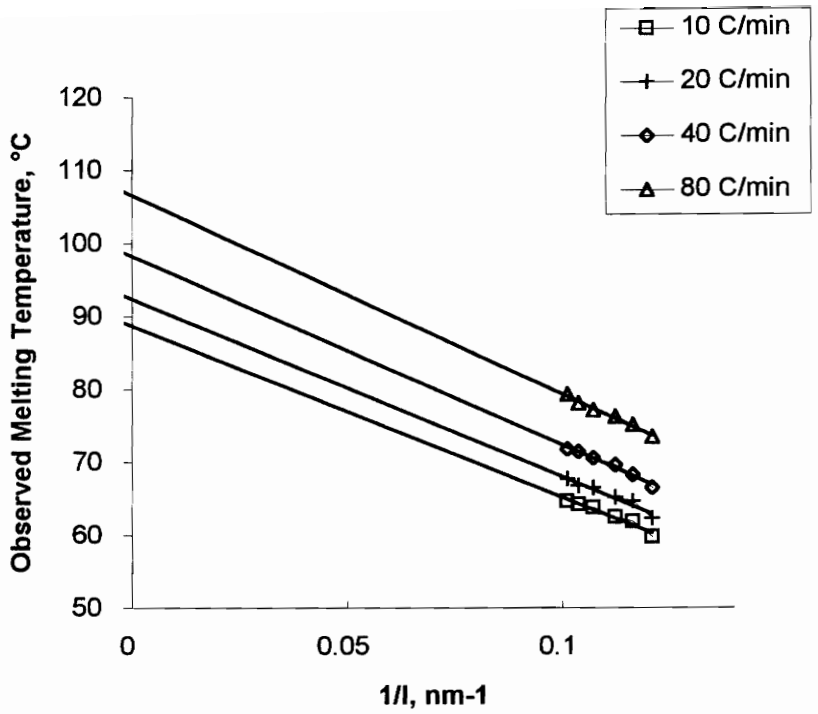

Figure 20. Gibbs-Thomson-Tammann Analysis; T_m' vs. $1/l$.

Table 4. Gibbs-Thomson-Tammann Analysis Data for poly(ε-caprolactone).

1/(*l*)	Observed Melting Temperature, °C Heating Rate, °C/min			
(nm $^{-1}$)	10	20	40	80
0.121	59.7	62.3	66.5	73.4
0.116	61.8	64.6	68.2	75.1
0.112	62.4	65.2	69.5	76.2
0.107	63.8	66.5	70.5	77.1
0.104	64.2	66.7	71.4	78.0
0.101	64.6	67.7	71.7	79.3

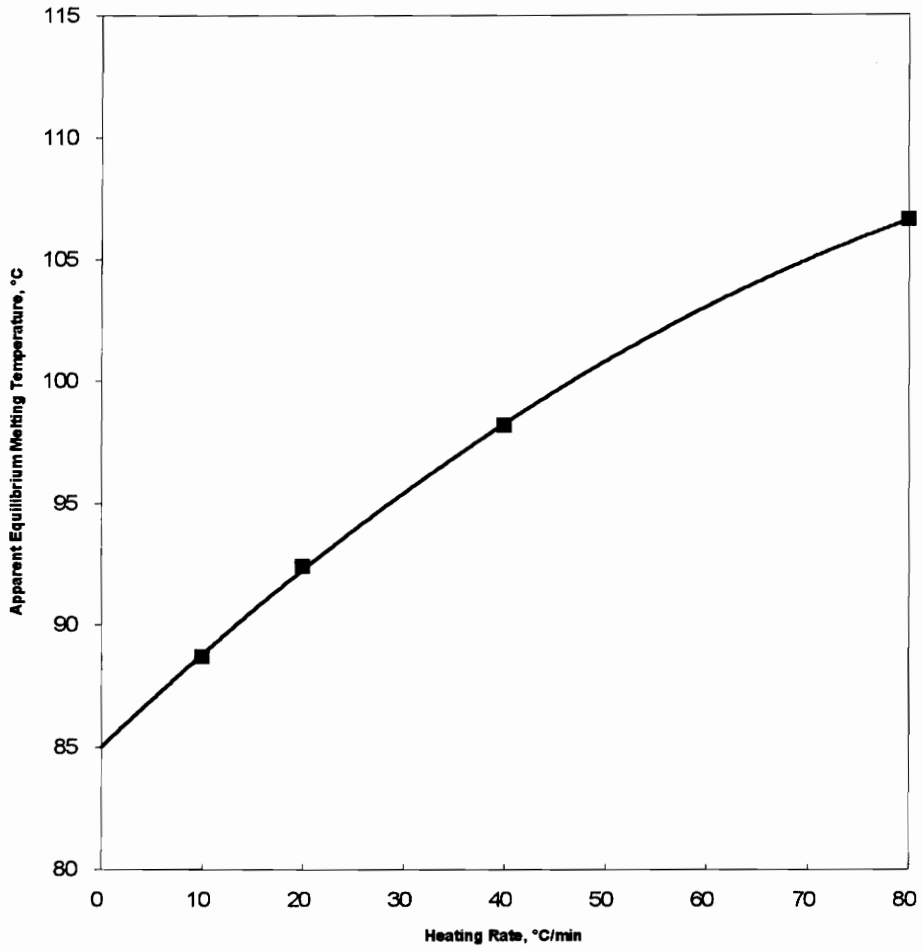

Figure 21. Gibbs-Thomson-Tammann Analysis; T_m^{app} vs. Heating Rate.

Table 5. Effect of Heating Rate on the Equilibrium Melting Temperature.

Heating Rate, °C/min	T_m^{app}, °C
10	88.7
20	92.4
40	98.2
80	106.6

$$G = G_0 \exp\left(\frac{jq}{4kT}\right) \exp\left(\frac{-U^*}{R(T_x - T_\infty)}\right) \exp\left(\frac{-K_g}{T_x \Delta f}\right) \quad (58)$$

where,

$$K_g = \frac{jb_0 \sigma \sigma_e}{k} \quad (59)$$

and G is the growth rate, U* is the activation energy for which a value of 1500 cal/mol is used, T_∞ is (T_g-30), k is the Boltzmann constant, Δf is the free energy of fusion at the crystallization temperature, and j depends on the regime in which the polymer is crystallizing.

An estimate of the equilibrium temperature is obtained by non-linear analysis of the above equation. This was done with Table Curve 2D software which solves the equation in an iterative fashion. A value of 82 ± 12 °C was found using this method.

Use of the traditional Lauritzen-Hoffman growth rate equation yields a similar value for the equilibrium melting temperature.

$$G = G_0 \exp\left(\frac{-U^*}{R(T_x - T_\infty)}\right) \exp\left(\frac{-K_g'}{T(\Delta T) f}\right) \quad (60)$$

$$K_g' = \frac{jb_0 \sigma \sigma_e T_m}{\Delta h_f k} \quad (61)$$

A value for the equilibrium melting temperature can be obtained by linearizing the above equation. This is done by finding the value of R^2 (which is a statistical measure of

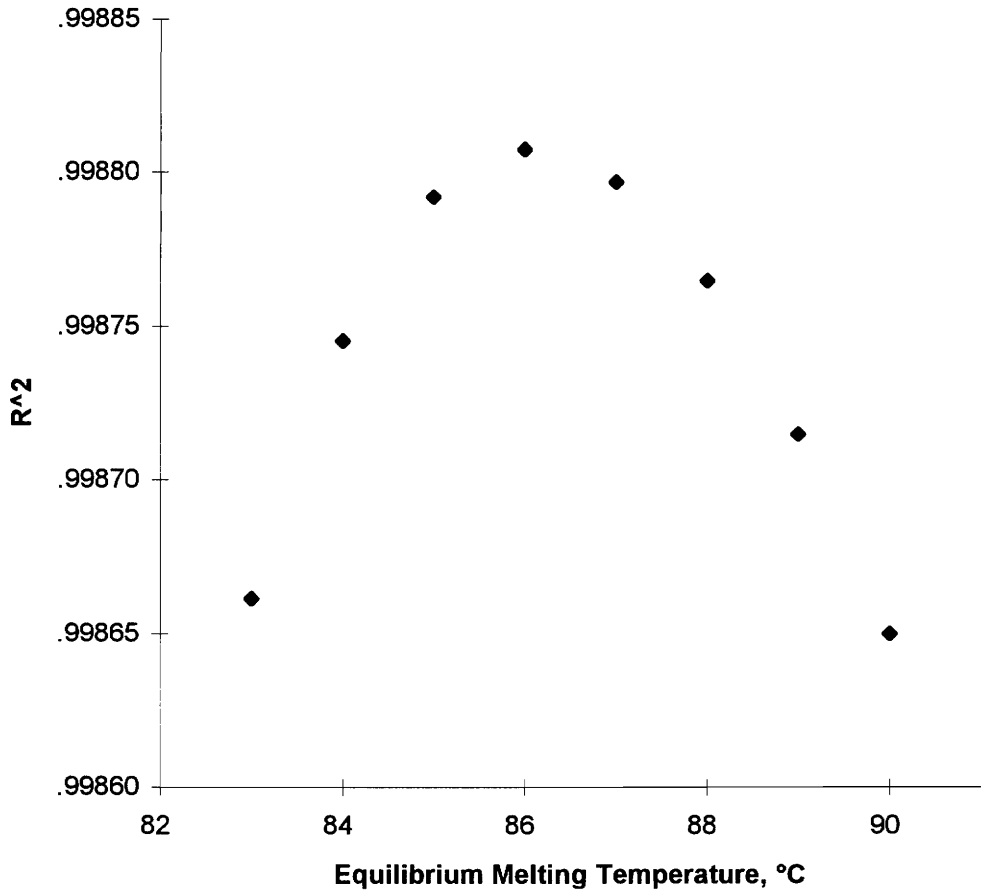

Figure 22. Determination of the Equilibrium Melting Temperature by Linear Least Squares Analysis Fit of Experimental Data by the Lauritzen-Hoffman Growth Rate Equation.

how straight a line the data points make) for a variety of values of T_m (Figure 22). The T_m which gives the maximum value of R^2 is where the line is the most linear, and is taken as the true equilibrium melting temperature. This type of analysis is mainly dependent on the two endpoints, so it was carried out for a variety of ranges of the data. Use of this method yields a value of 86° C for the equilibrium melting temperature.

The value for the equilibrium melting temperature from the GTT analysis produces a value approximately 10-15°C higher than reported values of T_m. Estimation of the equilibrium melting temperature by growth rate data analysis confirms that this value is in the correct range. Additional evidence which confirms this equilibrium melting temperature comes from the Hoffman-Weeks plot for the triblock copolymer with (ε-caprolactone) endblocks which predicts a T_m of 85 °C (See Section 6.2). Previous determinations of the T_m of poly(ε-caprolactone) used the Hoffman-Weeks and diluent methods. The Hoffman-Weeks method has been shown to underestimate the value of T_m for certain polymers[66], and neither method addresses the problems of thermal lag and thickening during the DSC heating scan. Both methods used in this paper suggest the true T_m of PCL is higher than previously reported.

4.2 Determination of the Fold Surface Free Energy, σ_e

The fold surface free energy, σ_e, is proportional to the slope of the plot of T_m' vs. $1/l$. Thermal lag should be constant for each data set because the samples were cut to identical shape and weight. Thus, thickening should be the only variable affecting the slope of the line. At slow heating rates, the polymer crystal may undergo thickening during the

heating scan required to measure the observed melting temperature. For this reason, only the highest heating rates were used in the extrapolation of σ_e vs. 1/(heating rate) to infinite heating rates (Figure 23, Table 6). The calculated value for the fold surface free energy (using T_m= 85°C) is 64 ± 6 erg/cm^2.

The work of chain folding, q, can be found once a value for the fold surface free energy has been determined,

$$q = 2A_0\sigma_e \tag{62}$$

where A_0 is the cross sectional area of the stem. Calculations give a value of 3.4 kcal/mole for poly(ε–caprolactone) for the work of chain folding. This value is less than that of polyethylene (q=4.9 kcal/mole) which has close similarities in the a and b unit cell dimensions. This decrease in the work of chain folding may be expected because the flexible ester group of poly(ε–caprolactone) is incorporated in the fold and could ecrease the value of the fold surface free energy of the polymer crystal.

4.3 Growth Rate Data Analysis

Once a value for the equilibrium melting temperature is known, the growth rate data (Figure 24, Table 7) can be analyzed to determine a value for the product of the surface energies, $\sigma\sigma_e$. The first step in the growth rate data analysis is to determine in which regime the polymer is crystallizing.

The difference between crystallization regimes is due to the relative magnitude of the secondary nucleation rate, *i*, with respect to the substrate completion rate, *g*. If the

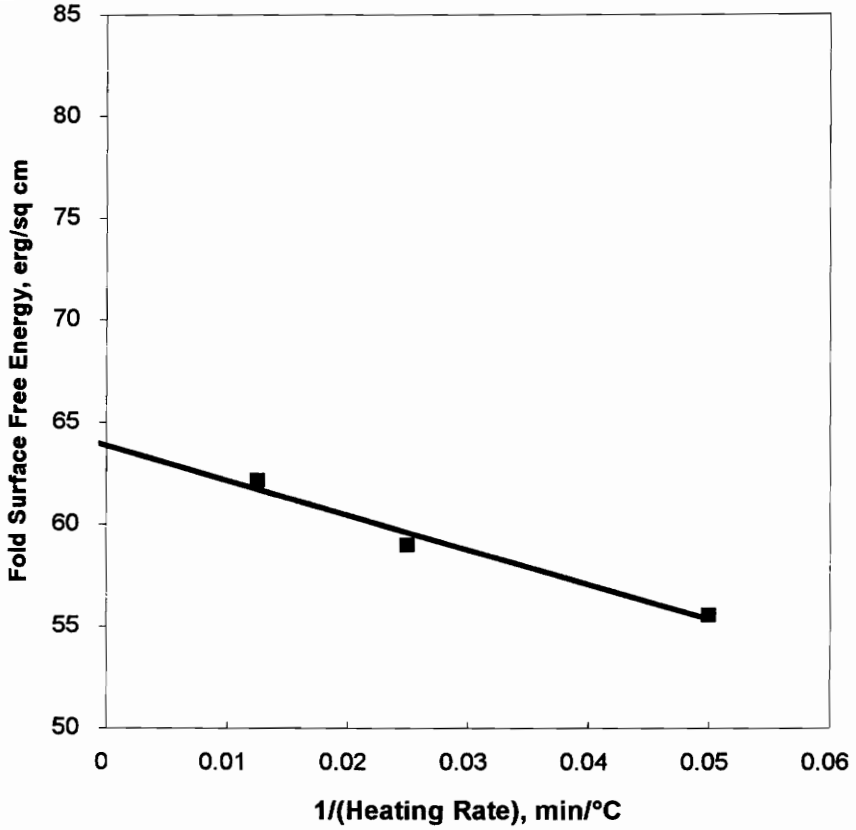

Figure 23. Determination of the Fold Surface Free Energy of PCL.

Table 6. Data for the Determination of the Fold Surface Free Energy of PCL.

Heating Rate; °C/min	Slope, nm°C	Fold Surface Free Energy, erg/cm^2
10	-235.7	53.5
20	-244.6	55.5
40	-259.3	59.0
80	-273.0	62.0

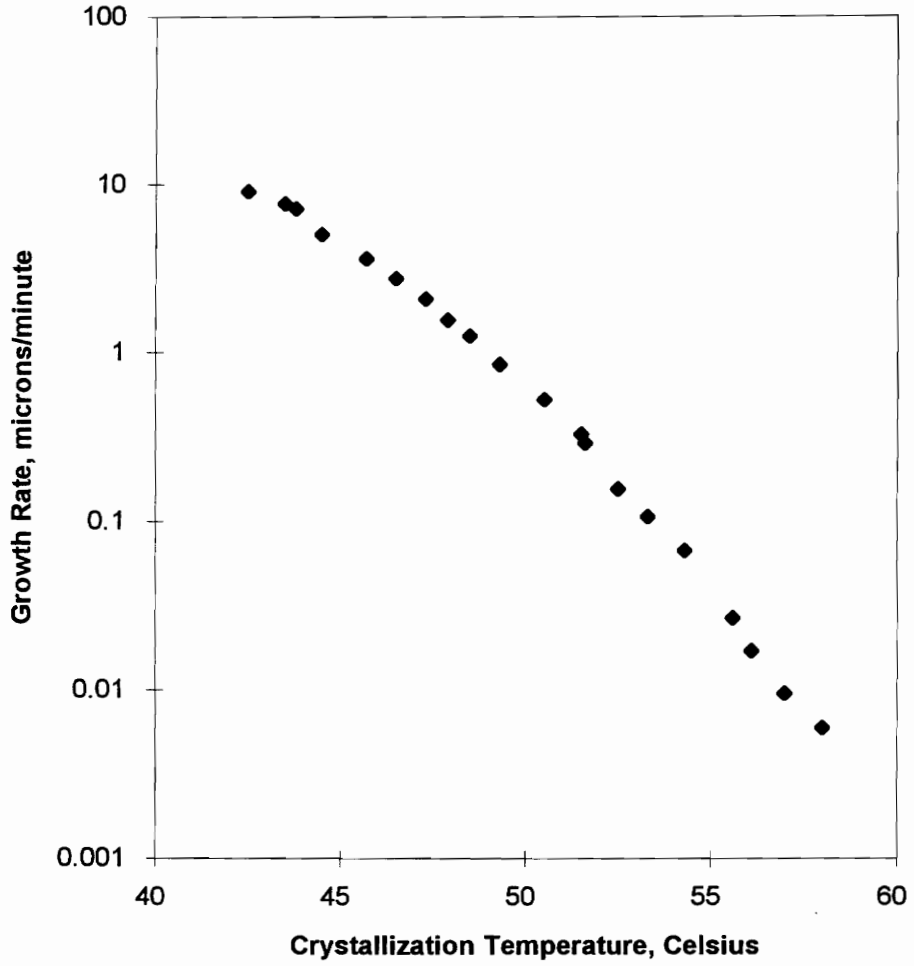

Figure 24. Growth Rate Data of pure PCL.

Table 7. Growth Rate Data for pure PCL.

Crystallization Temperature, °C	Growth Rate, μm/min	Standard Deviation, μm/min
41.3	12.37	0.42
42.5	9.06	0.24
43.5	7.72	1.05
43.8	7.16	0.35
44.5	5.07	0.24
45.7	3.63	0.38
46.5	2.76	0.31
47.3	2.09	0.24
47.7	2.47	0.13
47.9	1.56	0.085
48.5	1.26	0.15
49.3	0.852	0.079
50.5	0.523	0.0033
51.5	0.328	0.029
51.6	0.289	0.004
52.5	0.154	0.006
53.3	0.106	0.0006
54.3	0.0669	0.0075
55.6	0.0266	0.0026
56.1	0.017	0.0016
57.0	0.0095	0.00096
58.0	0.0059	0.0006

nucleation rate is much less than the substrate completion rate, crystallization occurs in Regime I. If the two rates are of the same order of magnitude, Regime II crystallization is found, and if i > g, Regime III crystallization is found.

The Lauritzen-Z test is used to determine if crystallization is in Regime I or II. It is based on a dimensionless parameter, Z, which compares the relative magnitudes of *i* to *g*,[7]

$$Z = \frac{iL^2}{4g} \tag{63}$$

where L is the substrate length. If crystallization is in Regime I, $Z < 0.01$, and if it is in Regime II, $Z > 1$. The value of Z can be approximated with the following equation[7]

$$Z \approx 10^3 \left(\frac{L}{2a}\right)^2 \exp\left[\frac{-X}{T\Delta T}\right] \tag{64}$$

where $X = K_g$ for Regime I and $2K_g$ for Regime II. The appropriate value of Z and X for each regime is placed in the equation, and the substrate length, L, is calculated. Generally, one value of L is reasonable and the other is unreasonable. The regime is taken to be the one where the calculated substrate length is reasonable.

The inequalities used to calculate the substrate length are the following (Table 8).

$$L \le 2a \left[\frac{0.01}{\exp\left(\frac{-X}{T\Delta T}\right)10^3}\right]^{1/2} \qquad \text{for Regime I} \tag{65}$$

Table 8: Z-test Results

Crystallization Temperature, °C	L(Regime I), Angströms	L (Regime II), Angströms
41	44.2	680000
46	99.5	3500000
55	860	2.59 E 8

$$L \geq 2a\left[\frac{1}{\exp\left(\frac{-X}{T\Delta T}\right)10^3}\right]^{1/2} \qquad \text{for Regime II} \qquad (66)$$

The value used for K_g was found from the slope of the line of $\ln G + U^*/[R(T_x - T_\infty)]$ (Figure 26). For the case of poly(ε–caprolactone), the calculated inequalities of L for the lowest, mid-range and highest crystallization temperatures for Regime II are unreasonable, and the lowest and middle crystallization temperatures for Regime I are also unreasonable. This indicates the polymer is definitely not crystallizing in Regime II, and probably not in Regime I. This suggests the polymer is crystallizing in Regime III. Note that the nucleation constant is defined identically for Regimes I and III, so the values obtained from analysis of the nucleation constant for these two Regimes will be the same.

Knowledge of the crystallization regime and the equilibrium melting temperature allows the nucleation constant to be calculated using equation 30. In order to analyze the data with this method, the free energy of crystallization , Δf, must be found as a function of temperature.

$$\Delta f(T_x) = \Delta h_f(T_x) - T\Delta s_f(T_x) \qquad (67)$$

where the enthalpy (Δh_f) and entropy of fusion(Δs_f) are found with the following relations.

$$\Delta h_f(T_x) = \Delta h_f(T_m) - \int_{T_x}^{T_m} \Delta C_p dT \qquad (68)$$

$$\Delta s_f(T_x) = \Delta s_f(T_m) - \int_{T_x}^{T_m} \frac{\Delta C_p}{T} dT = \frac{\Delta h_f}{T_m} - \int_{T_x}^{T_m} \frac{\Delta C_p}{T} dT \tag{69}$$

The change in heat capacity between the liquid and the solid is ΔC_p. This was calculated from group vibrations given at different temperatures.[59,60]

$$C_{p,(PCL)} = 5C_p^{CH_2} + C_p^{COO} \tag{70}$$

An equation for the temperature dependence of the heat capacity of the liquid and solid was determined for PCL using equation (70). Using the above equations, an expression for the change in heat capacity had the following form.

$$\Delta C_p = C_{p,liquid} - C_{p,solid} = (a_l - a_s) + (b_l - b_s) \cdot T \tag{71}$$

The above equation (71) was then integrated in equations (68) and (69) to determine the temperature dependence of the enthalpy and entropy in the crystallization range. The expression for the temperature dependence of the free energy of crystallization was found using equation (67). A comparison of the free energy of fusion using the empirical formula (equation 27) and Gibbs free energy equation shows the difference between the methods is small (Figure 25).

The product of the surface free energies is found with equation (30). This nonlinear equation was solved with Table Curve 2D software. This software is needed because the equation can not be solved by a single step solution. It must be solved in an iterative fashion. The software uses a Levenburg-Marquardt algorithm to fit the nonlinear equation such that it has the smallest value of the sum of squares due to error, SSE.

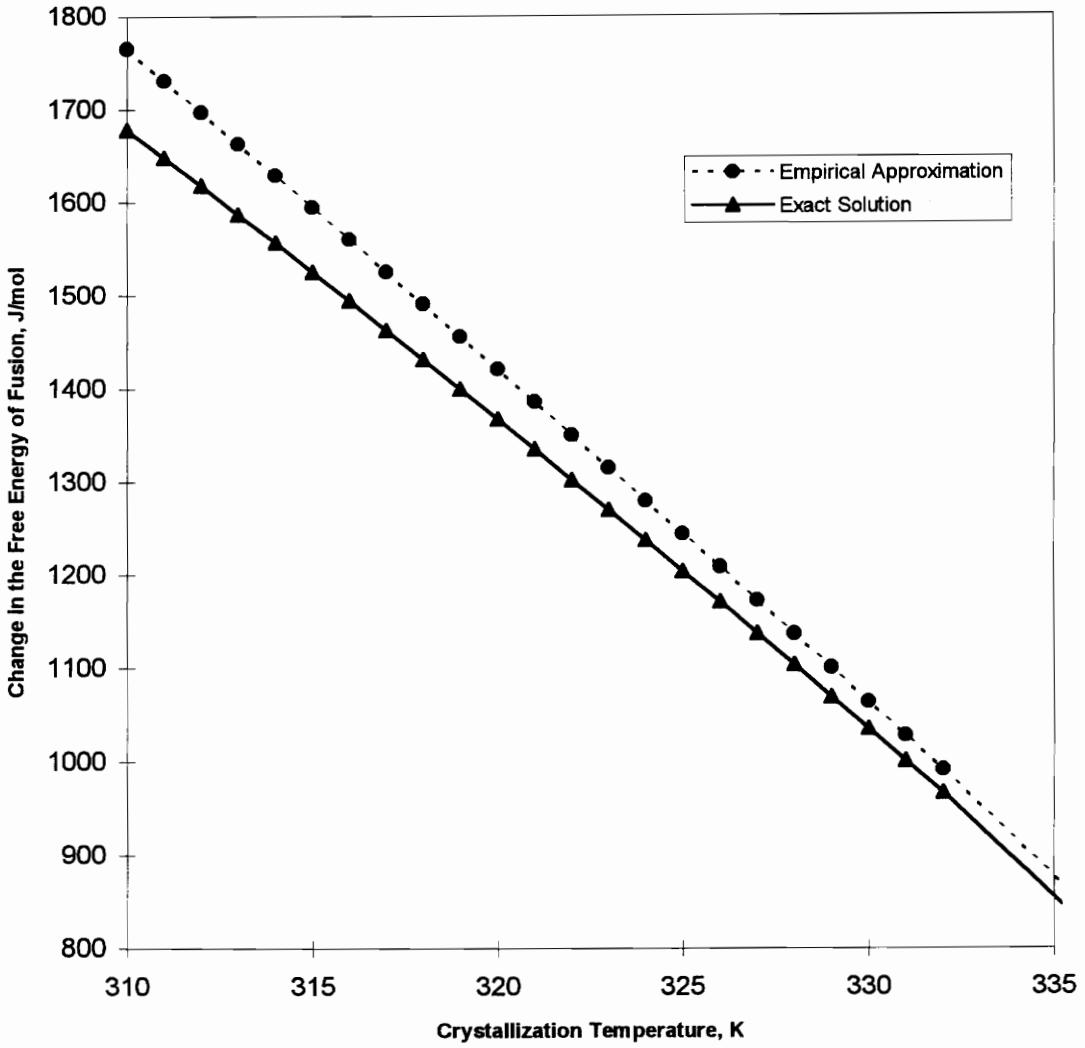

Figure 25. Temperature Dependence of the Free Energy of Fusion.

Analysis gives a value of 7.9 X 10^{11} K*erg/cm^2 for the nucleation constant, which corresponds to a value of 662 erg^2/cm^4 for the product of the surface energies. This value is larger than that of 583.3 erg^2/cm^4 reported by Phillips *et al*, which is to be expected because the equilibrium melting temperature that was used in their analysis was 10°C lower. A comparison of the value of $\sigma\sigma_e$ found using the modified Lauritzen-Hoffman growth rate equation with other forms of the equation (Table 9) shows that the value for $\sigma\sigma_e$ is the lowest using the analysis method in this thesis. There are even differences in the values obtained by the solving the same equation linearly or nonlinearly. These differences could be due to the fact that it is generally better to analyze data in the form that the experimental data was obtained. When the natural logarithm of the experimental data is taken, it involves manipulation and can make the parameters derived from the analysis less reliable. Additionally, the data was weighted by the experimental uncertainty in the non-linear analysis. The plots from which the nucleation constant were determined for the linear analysis are shown in Figures 26,27.

The value of $\sigma\sigma_e$ from growth rate measurements is divided by the value of σ_e from the Gibbs-Thomson-Tammann method to calculate a value for the lateral surface energy, σ. This method gives a value of 10.3 ± 1.3 erg/cm^2 for the lateral surface free energy of poly(ε−caprolactone). This value is larger than that reported by Phillip *et al* [6] (σ= 6.7erg/cm^2). These authors determined the lateral surface free energy, σ, using the Thomas-Staveley relation.

$$\sigma = \Delta h_f (a_o b_o)^{1/2} \alpha \qquad (72)$$

Generally, α is taken to be 0.1. Recent work has shown that α is not always equal to 0.1, but approximately 0.2 for the case of rigid polyesters[22]. Using the experimentally

Table 9: Calculated Values of $\sigma\sigma_e$, σ, and C_∞ using Various Growth Rate Equations.

Equation	**Linear Fit**	**Non-Linear Fit**
$G = G_o \exp\left(\frac{-U^*}{R(T_x - T_\infty)}\right) \cdot \exp\left(\frac{-K'_g}{T_x \Delta T}\right)$	$\sigma\sigma_e$ = 850 erg^2/cm^4 σ = 13.3 erg/cm^2 C_∞ = 3.3	$\sigma\sigma_e$ = 700 erg^2/cm^4 σ = 10.9 erg/cm^2 C_∞ = 4.0
$G = G_o \exp\left(\frac{-U^*}{R(T_x - T_\infty)}\right) \cdot \exp\left(\frac{-K_g}{T_x \Delta f}\right)$	$\sigma\sigma_e$ = 881 erg^2/cm^4 σ = 13.7 erg/cm^2 C_∞ = 3.2	$\sigma\sigma_e$ = 740 erg^2/cm^4 σ = 11.6 erg/cm^2 C_∞ = 3.8
$G = G_o \exp\left(\frac{-U^*}{R(T_x - T_\infty)}\right) \cdot \exp\left(\frac{-K'_g}{T_x \Delta T}\right) \exp\left(\frac{q}{kT}\right)$		$\sigma\sigma_e$ = 695 erg^2/cm^4 σ = 10.8 erg/cm^2 C_∞ = 4.1
$G = G_o \exp\left(\frac{-U^*}{R(T_x - T_\infty)}\right) \cdot \exp\left(\frac{-K_g}{T_x \Delta f}\right) \exp\left(\frac{q}{kT}\right)$		$\sigma\sigma_e$ = 662 erg^2/cm^4 σ = 10.3 erg/cm^2 C_∞ = 4.3

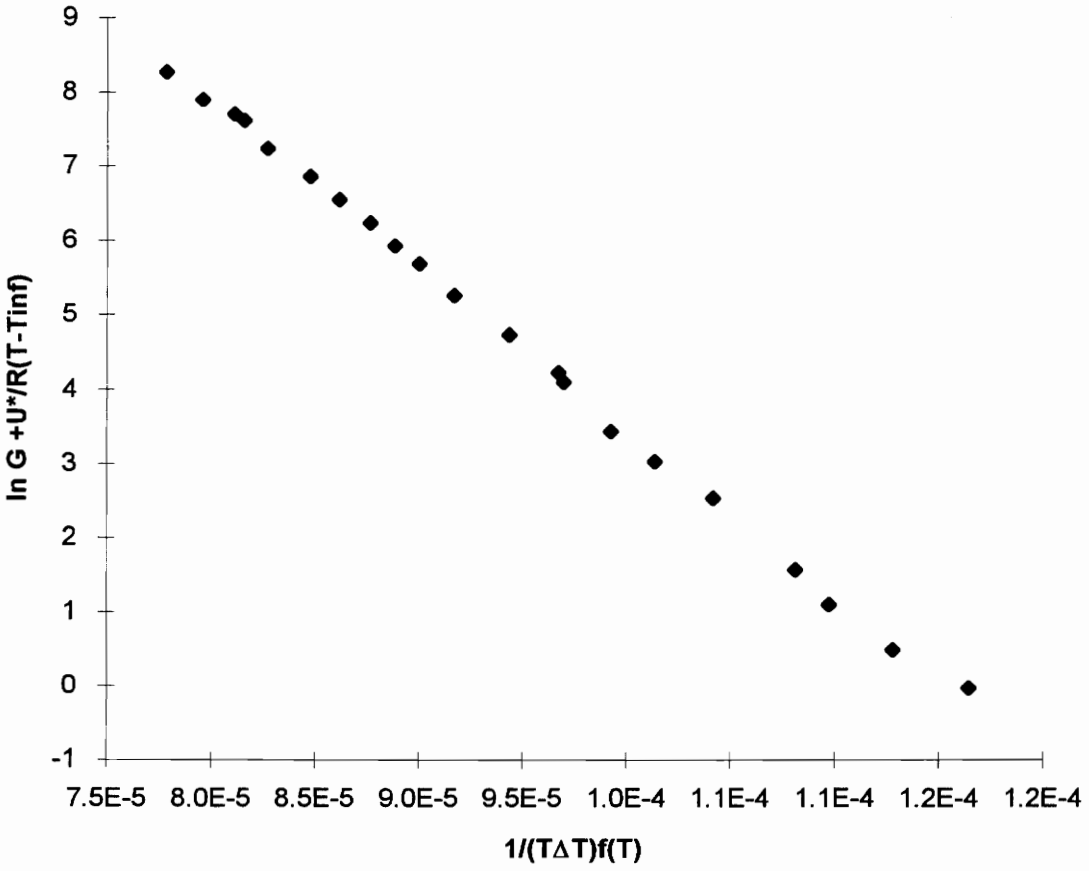

Figure 26. Determination of the Nucleation Constant for pure PCL, using equation (28).

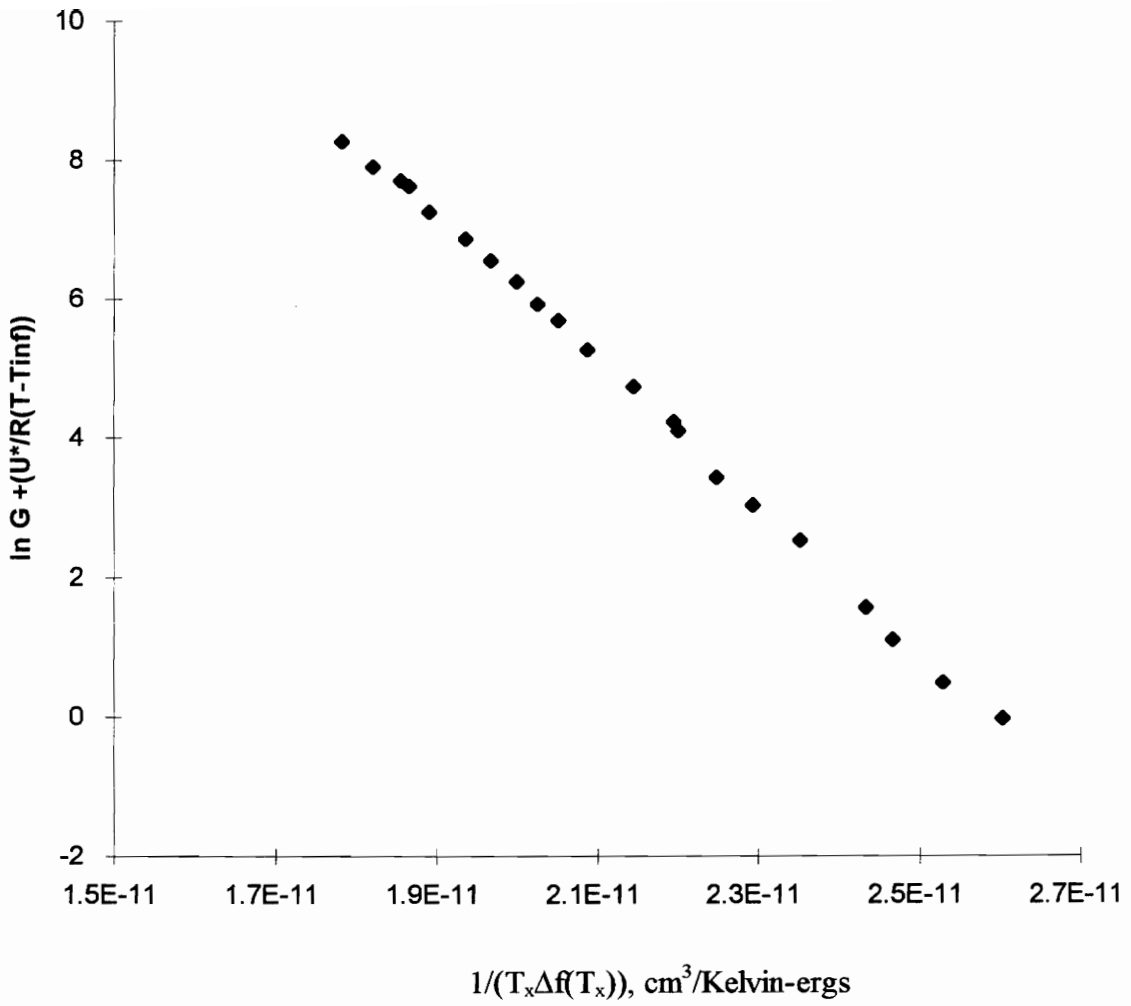

Figure 27. Determination of the Revised Nucleation Constant for poly(ε-caprolactone), using equation (25).

Table 10. Values used in Calculations.

Variable	Value	Reference
a_0	4.508 E -8 cm	1
b_0	4.13 E-8 cm	1
l_u	1.28 E -8 cm	1
σ	10.3 erg/cm^2	This Work
T_∞	183 K	19
U*	1500 cal/mol	19
T_m	85 °C	This Work
$\sigma\sigma_e$	661 erg^2/cm^4	This Work
σ_e	64 erg/cm^2	This Work
Δh_f	1.63 E 9 erg/cm^2	19
Regime I or III	n =4	This Work

determined value of σ, a value of 0.15 is found for α, which is intermediate between the two values.

The above analysis was carried out using a value for U^* of 1500 cal/mol, and the value of T_∞ was taken as 30 °C less than the glass transition temperature. Suzuki and Kovaks[69] determined a universal value of U^* from work on isotactic poly(stryrene). Recent work indicates that this value may be incorrect because it was obtained through analysis using the traditional LH growth rate equation (25), and a value for the equilibrium melting temperature that has been shown to be too low. Additionally, evidence has been presented which suggest the value of T_∞ is 50°C rather than 30° C less than the glass transition temperature.[70]

For this reason, the values of U^* and T_∞ were varied to see how this would effect the value of the nucleation constant, K_g, determined (Table10). Analysis was carried out using the modified growth rate equation (30). Calculations show that an increase in the value of U* and decrease in T_∞ both cause a small increase in the values of the nucleation constant and product of the surface energies calculated.

4.4 Proposed σ-C_∞ Relation

Once an experimental value of the lateral surface free energy, σ, has been determined, it is used in the relation proposed by Hoffman *et al*[1] to determine a value for

Table 10: Effect of the Values of U* and T_∞ on Parameters Obtained from Growth Rate Analysis.

U^*, cal/mol	$T_\infty = T_g$-30	$T_\infty = T_g$-50
1000	K_g= 7.5 E 11 erg•Kelvin/cm^3 $\sigma\sigma_e$= 628 erg^2/cm^4 σ = 9.8 erg/cm^2 C_∞ = 4.5	K_g= 7.3 E 11 erg•Kelvin/cm^3 $\sigma\sigma_e$= 612 erg^2/cm^4 σ = 9.4 erg/cm^2 C_∞ = 4.6
1500	K_g= 7.9 E 11 erg•Kelvin/cm^3 $\sigma\sigma_e$= 662 erg^2/cm^4 σ = 10.3 erg/cm^2 C_∞ = 4.3	K_g= 7.6 E 11 erg•Kelvin/cm^3 $\sigma\sigma_e$= 636 erg^2/cm^4 σ = 9.9 erg/cm^2 C_∞ = 4.4
2000	K_g= 8.3 E 11 erg•Kelvin/cm3 $\sigma\sigma_e$= 695 erg^2/cm^4 σ = 10.8 erg/cm^2 C_∞ = 4.1	K_g= 7.9 E 11 erg•Kelvin/cm^3 $\sigma\sigma_e$= 661 erg^2/cm^4 σ = 10.3 erg/cm^2 C_∞ = 4.3

the characteristic ratio from the melt

$$C_\infty \cong \Delta h_f \left(\frac{a_0}{2}\right)\left(\frac{l_b}{l_u}\right)\left(\frac{1}{\sigma}\right) \tag{73}$$

This relationship gives a value of 4.3 ± 1.3 for C_∞. Measurements of the characteristic ratio in solution have been made by Jones *et al* (5.9 ± 0.3)[26] and Knecht *et al* (5.6 ± 0.4).[68] The calculated value using the proposed relationship is within a 20 % margin of error for the C_∞ determined by solution measurements. Thus, the value of σ determined by the σ-C_∞ and from the LH growth rate equation are qualitatively consistent with one another. This conclusion seems to provide further support of the claim by Hoffman *et al*[1]. that the value of σ derived from the temperature dependence of the crystal growth rate is physically meaningful and can be related to the chain structure of the polymer of interest.

Chapter 5. Melting Behavior of (ε–caprolactone) in the Homopolymer and Triblock Copolymer

The melting behavior of poly(ε–caprolactone) in the homopolymer and triblock copolymer will be compared and contrasted. The similarities, differences, and origins of multiple endothermic behavior in both will be discussed.

5.1 Melting Behavior of Poly(ε–caprolactone)

The endotherms for samples of poly(ε-caprolactone) isothermally crystallized for long times (3-7 days) at a series of crystallization temperatures are compared in Figure 28. All the scan rates for the DSC scans shown are 10°C/min unless otherwise specified. It is seen that the endotherms for samples crystallized at lower temperatures have broad shoulders just before the melting peak. Samples crystallized at intermediate temperatures (46 °C) show the hints of a second endothermic peak that appears more definitively at higher crystallization temperatures (52 ° C). Samples crystallized at temperatures greater than 52 °C clearly exhibit double endothermic behavior. An examination of the maximum of the shoulder or lower endotherm prior to the melting peak shows that it increases with the crystallization temperature (Figure 29). Additionally, the temperature at which the lower endotherm or broad shoulder appears is centered around the crystallization temperature of the sample.

One of the explanations for double endothermic behavior is that the polymer melts and recrystallizes during the DSC heating scan. Slower heating rates will give the polymer more time to melt and recrystallize during the heating scan. Higher heating rates should not give the polymer enough time for reorganization.[15]

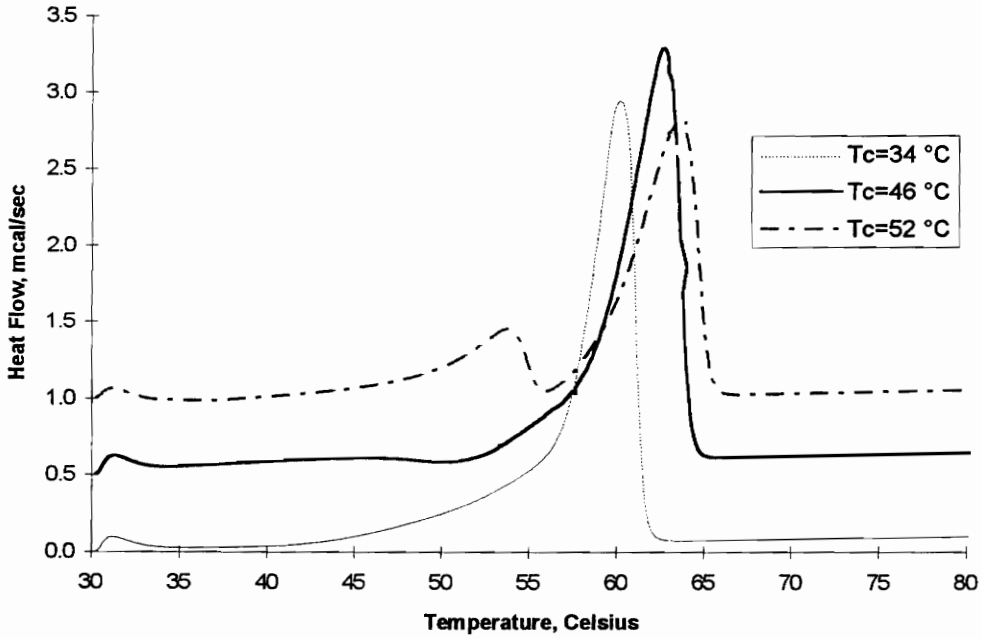

Figure 28. Crystallization Temperature Dependence on the Endotherm for Poly(ε–caprolactone).

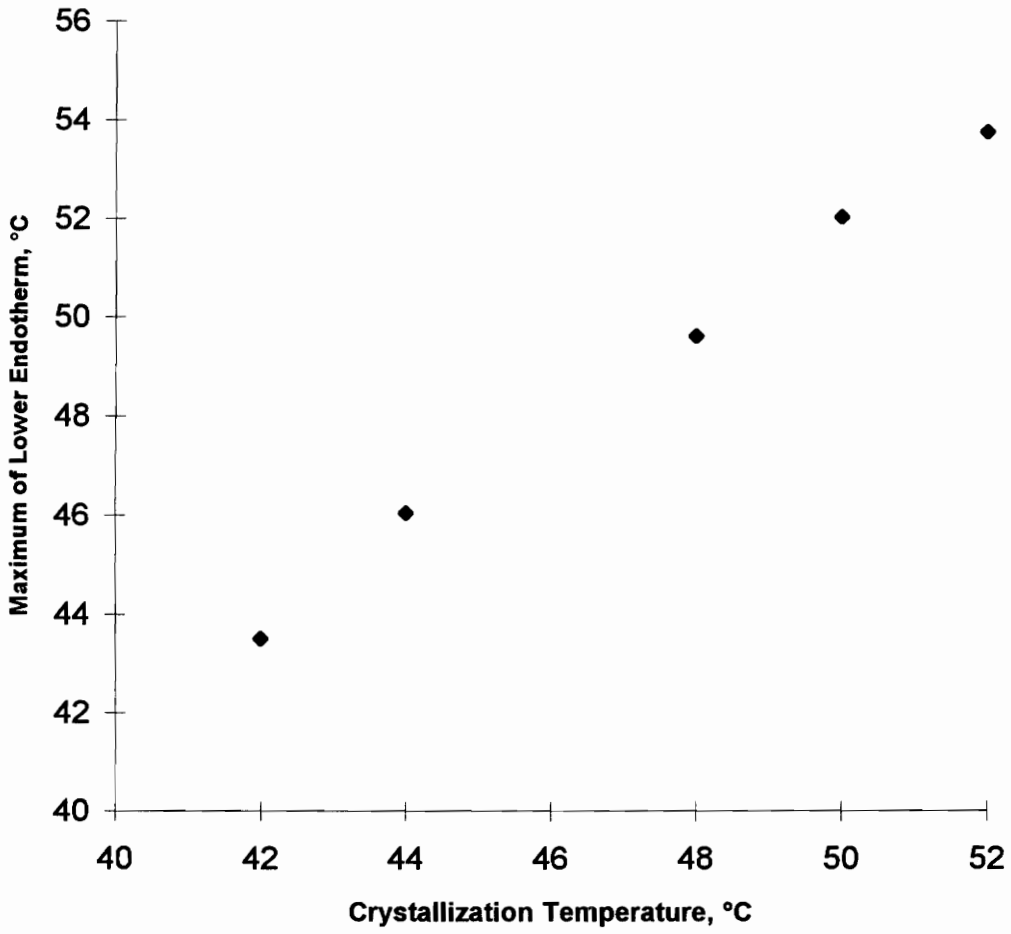

Figure 29. The Maximum of the Lower Endotherm as a Function of the Crystallization Temperature for Poly(ε–caprolactone).

During slow heating rate scans, a relatively large amount of the original lamellae (Figure 30c) has time to melt (M) and recrystallize (C). This recrystallized material will melt at a higher temperature (Mr). As the heating rate is increased, the crystals will have less time to reorganize, and C and Mr will decrease in magnitude. Thus, the magnitude of the second endotherm will decrease if the polymer does not have time to recrystallize at higher heating rates.[15]

An examination of the effect of heating rate on the shape of the endotherm (Figure 31) does not support the melting and recrystallization concept. There is no change in the relative magnitudes of first and second endotherms. The increase in the observed melting temperature with heating rate in the endotherms is due to thermal lag. The samples used were cut to identical size and weight so the increase in the endotherm area is only from the effects of the heating rate. The area under the endotherm should double when the heating rate is doubled. This is due to the fact that the calorimeter measures the heat flow rate, dH/dt, and not directly the heat capacity, Cp. These two quantities are related to one another through the heating rate, dT/dt.

$$\frac{dH}{dt} = \frac{dH}{dT} \cdot \frac{dT}{dt} = C_p \frac{dT}{dt} \tag{74}$$

Another explanation for double endothermic behavior is that if the polymer does not completely crystallize at the crystallization temperature, it could crystallize when it is cooled down to room temperature. This possibility was examined for the case of poly(ε-caprolactone) crystallized at 52 °C. Samples were isothermally crystallized at 52°C for various times, and then held at room temperature for a half-hour. The melting temperature and heat of fusion of each endotherm were compared for various

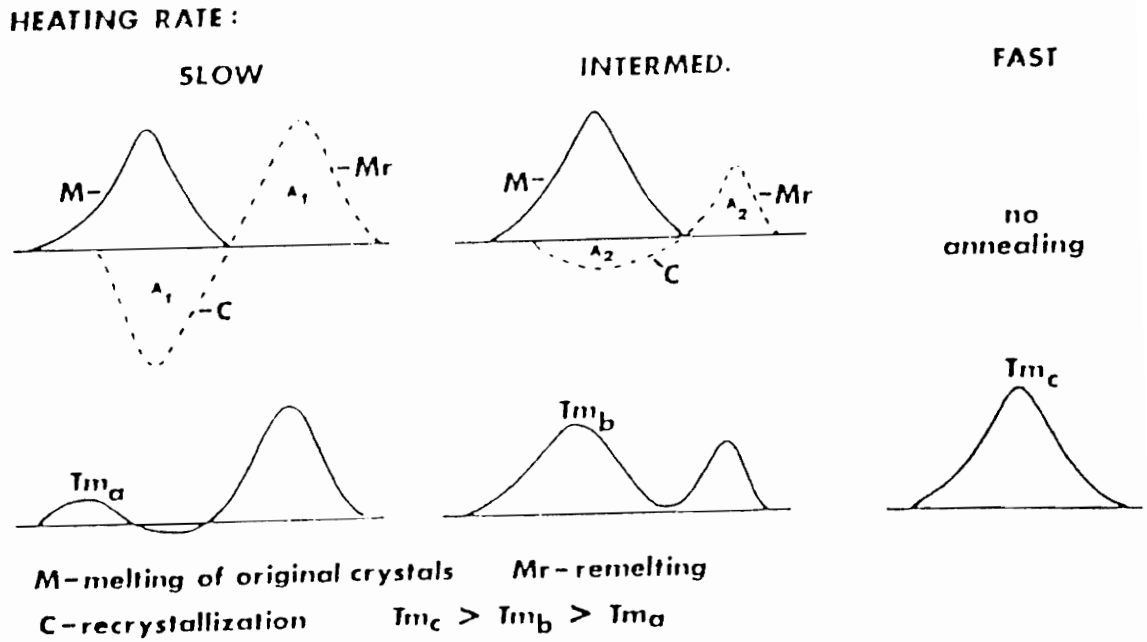

Figure 30. Effect of the Heating Rate on the Shape of the DSC Endotherm when Melting and Recrystallization Occurs. (from reference 15)

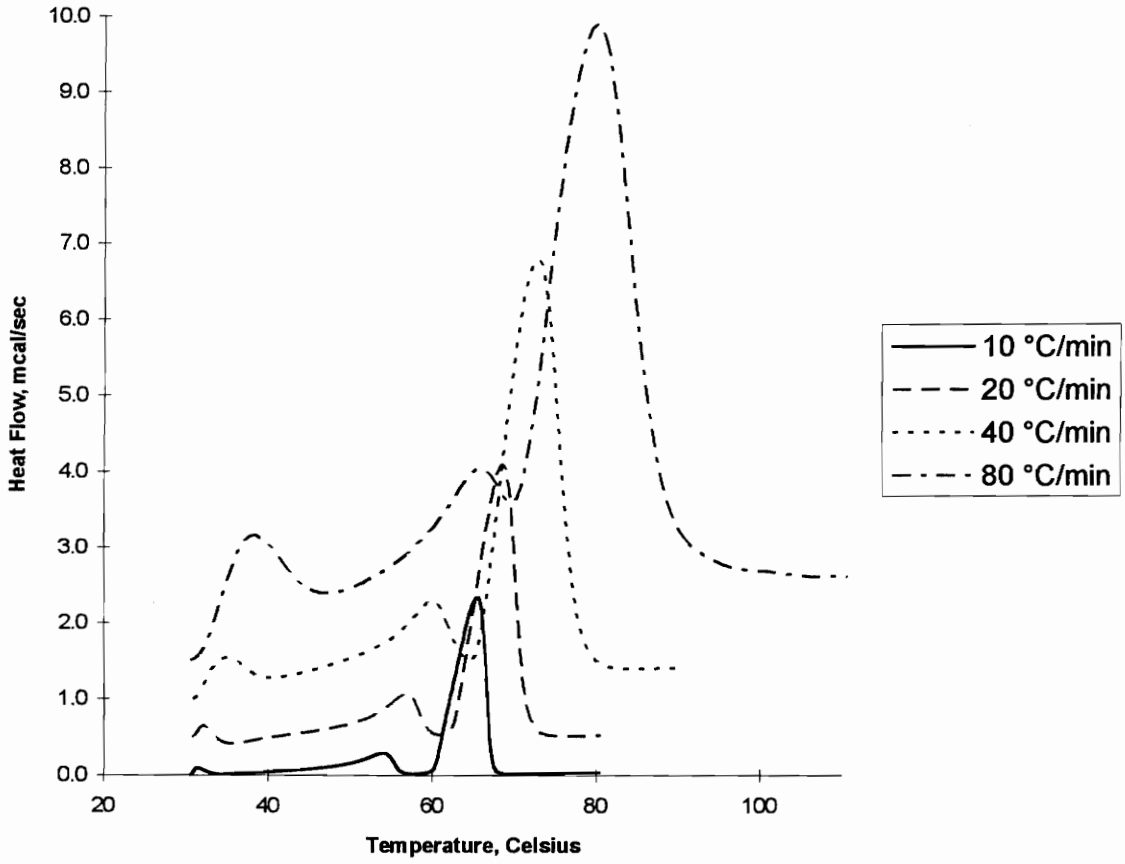

Figure 31. Effect of the Heating Rate on the Shape of the Endotherm for Poly(ε–caprolactone; T_c = 52 °C.

crystallization times (Table 11, Figure 32).

As the sample is crystallized for longer periods of time, the heat of fusion of the second endotherm increases, and that of the lower endotherm decreases. The increase in the second endotherm suggests that as the sample is crystallized for longer times, it becomes more crystalline, and the amount of amorphous material in the sample decreases with increasing isothermal crystallization time. Thus, when the sample is cooled to room temperature there is less material to crystallize. Due to the fact there is less amorphous material to crystallize, the magnitude of lower endotherm decreases.

The melting temperature of the upper endotherm increases with crystallization time, which is to be expected due to lamellar thickening. However, the melting temperature of the lower endotherm decreases with increasing crystallization time. This also supports the idea of uncrystallized material crystallizing when the sample is cooled to room temperature. Due to the fact that the lamellar thickness of the polymer increases with crystallization time, the regions of uncrystallized material decreases in size. Thus, the melting temperature of the lower endotherm would also decrease because of the lower lamellar thickness of the crystals that form in these regions.

The temperature dependence of the lower endotherm shows that with increasing crystallization temperature, the lower endotherm moves from a broad shoulder to a clearly defined peak. This supports the idea that the lower endotherm is from material which did not crystallize at the isothermal crystallization temperature, but crystallized as the sample was cooled to room temperature. The crystallization rate of a polymer is temperature

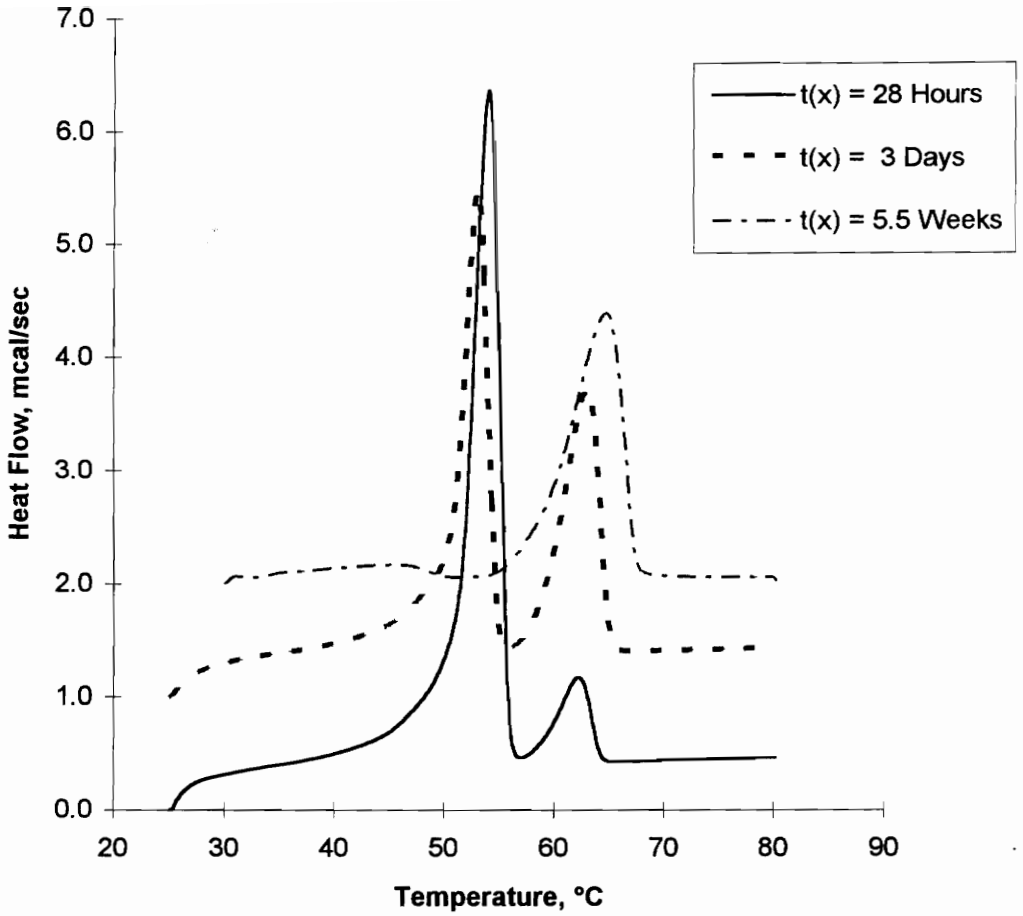

Figure 32. Effect of the Crystallization Time on the Shape of the Endotherm for Poly(ε–caprolactone; $T_c = 52°C$.

Table 12. Effect of the Crystallization Time on the Observed Melting Temperature and Heat of Fusion for Poly(ε–caprolactone).

	Observed Melting Temperature, °C		Heat of Fusion, cal/gm	
Crystallization Time	**Lower Endotherm**	**Upper Endotherm**	**Lower Endotherm**	**Upper Endotherm**
0 Hour	54.8	-	21.8	-
28.25 Hours	54.7	62.9	18.5	2.1
3 Days	54.3	64.2	12.8	7.8
5 Days	53.4	65.1	7.2	14.5
5.5 Weeks	46.9	66.4	1.8	23.9

dependent. For temperatures well above the glass transition temperature, the growth rate will decrease with increasing temperature. Thus, samples crystallized at higher crystallization temperatures, for approximately the same time as samples at the lower crystallization temperature, will not have crystallized as completely. They will have more amorphous material which can crystallize as the sample is cooled to room temperature. The fact that the lower endotherm becomes more clearly defined with increasing crystallization temperature shows that the samples crystallized at higher crystallization temperature had a larger fraction of amorphous phase to crystallize when the sample was cooled to room temperature.

Due to the fact that the molecular weight of the polymer is relatively low, the material which did not crystallize at the crystallization temperature could be due to lower molecular weight fractions that were rejected during crystallization. These fractions may be of low enough molecular weight to be in the region where the equilibrium melting temperature is highly dependent on the molecular weight. If this were the case, the lower molecular weight fraction would have a reduced growth rate due to a reduced undercooling, ΔT. This material would not crystallize completely at the crystallization temperature due to a reduced growth rate, and would be available for crystallization as the sample was cooled to room temperature.

5.2 Melting Behavior of Poly (ε-caprolactone-*b*-propylene oxide-*b*-ε-caprolactone)

The endotherms for samples of the triblock copolymer isothermally crystallized for long times at a series of crystallization temperatures are compared in Figures 33a-d . It is seen that the trend is similar to that of the pure homopolymer. A broad shoulder appears before the melting endotherm for low crystallization temperatures (36 °C). This shoulder becomes more defined at intermediate crystallization temperatures (40 °C). Samples crystallized at even higher crystallization temperatures (47°C) show a clearly defined lower endotherm as well as the beginning of a third endothermic shoulder prior to the shoulder before the melting peak. An examination of the temperature maximum of the intermediate endotherm show they increase with increasing crystallization temperature (Figure 34).

A difference between the homopolymer and triblock copolymer is that in the case of the triblock copolymer, three distinct endotherms are present. The lowest endotherm is centered around the crystallization temperature, while the intermediate endotherm is above the crystallization temperature. This is in contrast to the case of the homopolymer where only two endotherms are present and the lower endotherm is centered around the crystallization temperature of the sample. The position and origin of the lowest endotherm in the triblock copolymer are similar to those of the lower endotherm of the pure homopolymer.

The effect of crystallization time on the endothermic behavior of the triblock copolymer was studied for two different cases: I) the sample was crystallized for various times, cooled to room temperature for a half hour, and then heated, and II) the sample was crystallized for various times, and then heated. The reason the samples were cooled to

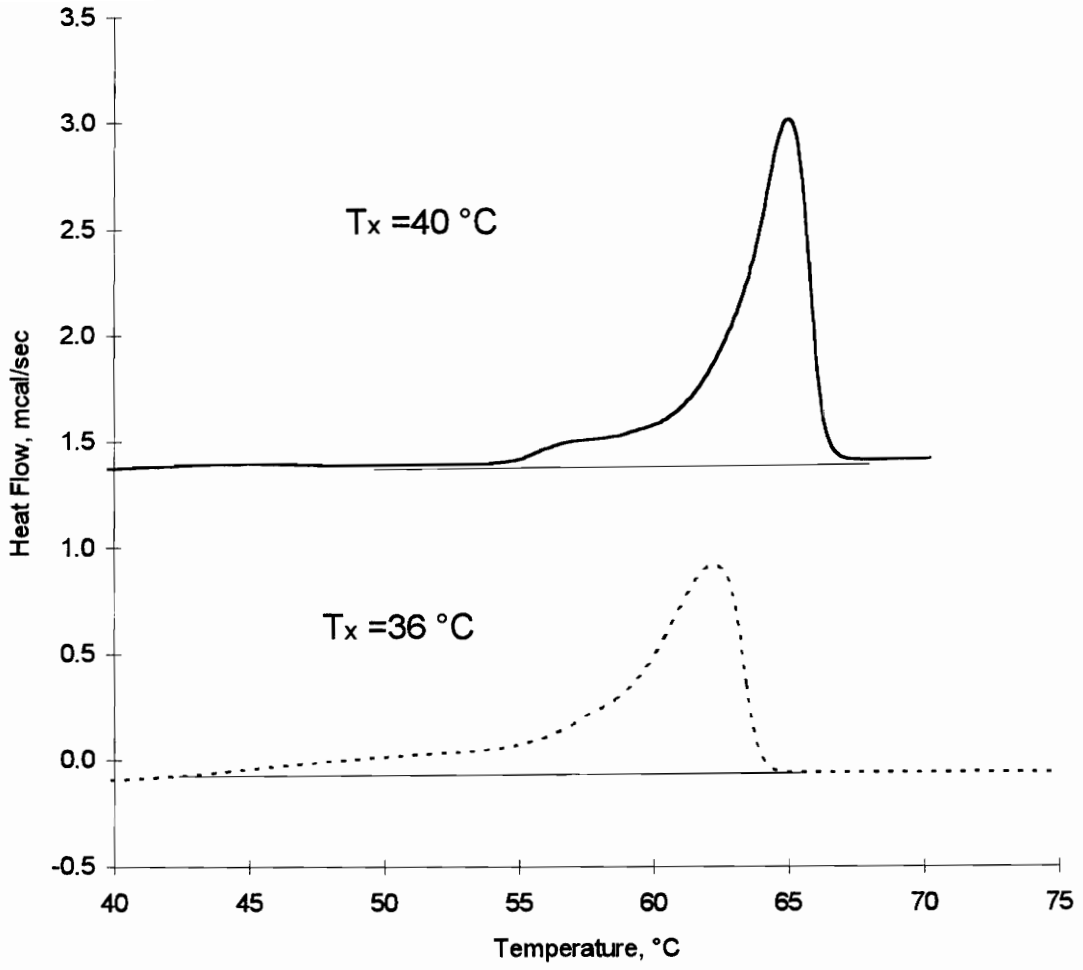

Figure 33. Crystallization Temperature Dependence of DSC Endotherm for Triblock Copolymer

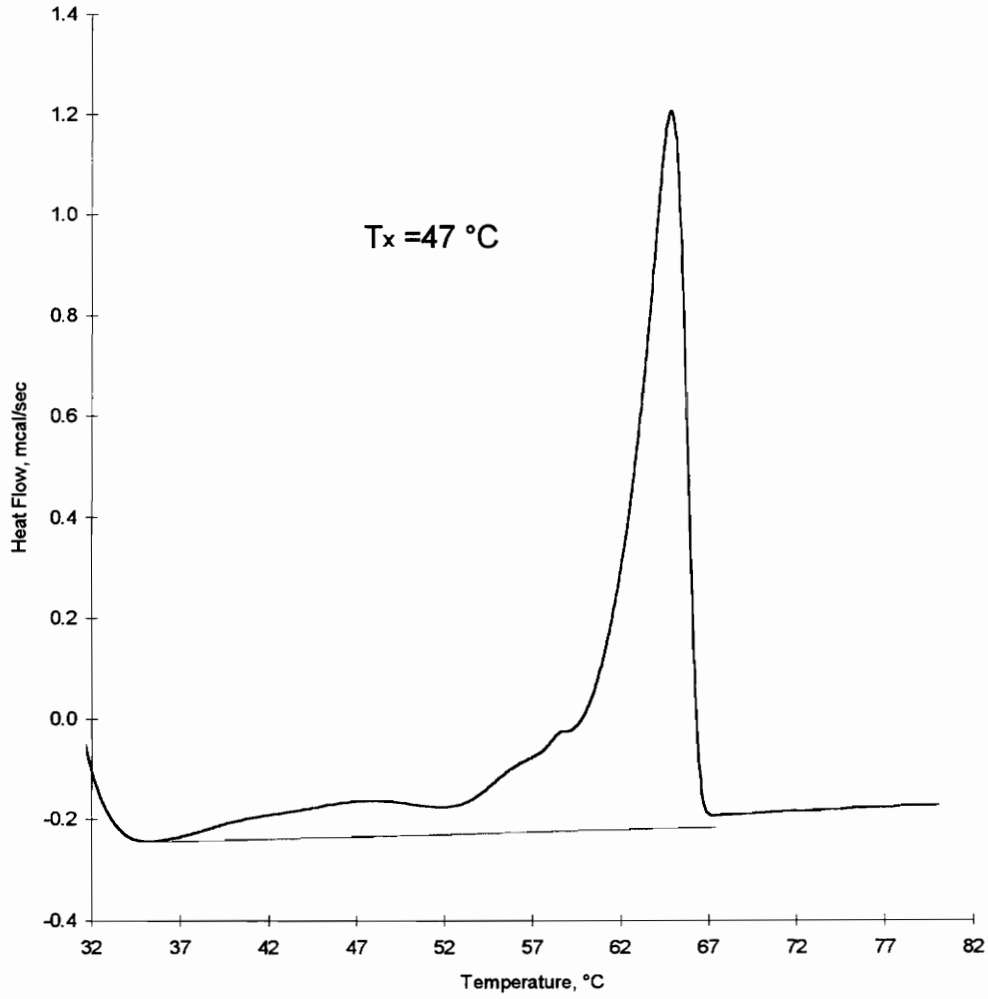

Figure 33. Crystallization Temperature Dependence of the DSC Endotherm for the Triblock Copolymer

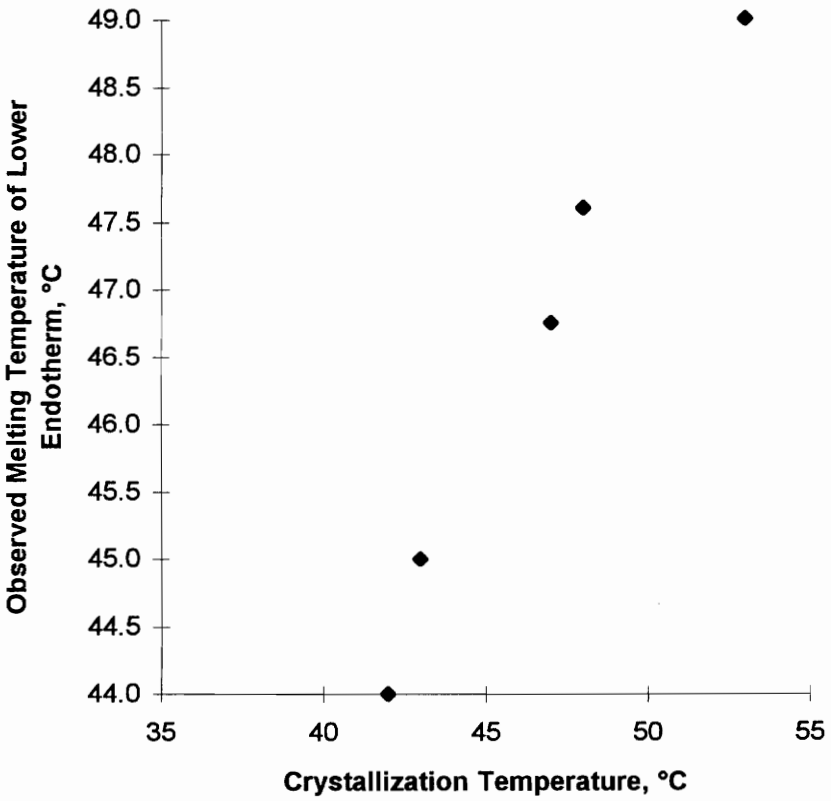

Figure 34. The Maximum of the Intermediate Endotherm as a Function of Crystallization Temperature for the Triblock Copolymer.

room temperature was to compare them to the homopolymer case, and to determine if crystallization occurred when the samples were cooled to room temperature

The effect of crystallization time on the lowest endotherm of the triblock copolymer were examined at the crystallization temperature of 45°C. It is seen that as the crystallization time is increased, the heat of fusion and the maximum temperature of the lowest endotherm decreases (Table 12). This is similar to the behavior of the lower endotherm in poly(ε-caprolactone). This behavior combined with the fact that the relative position of the lowest endotherm is centered around the crystallization temperature indicates that the origin of this endotherm is the same as that of the lower endotherm in the pure homopolymer. Both are due to material which did not crystallize at the crystallization temperature, but as the sample cooled down to room temperature.

Next, the effect of crystallization time on the endothermic behavior of the triblock copolymer was studied for samples which were not cooled to room temperature. This was carried out for three different crystallization temperatures; 41, 45, and 50 °C. At each temperature, no shoulder or intermediate endotherm is observed for the shortest crystallization time. For increasing crystallization times, a shoulder begins to develop prior to the melting endotherm (Figure 35). This shoulder becomes more defined and larger with longer crystallization times . The temperature of the maximum of the shoulder increases with crystallization time (Figure 36) .

This data shows the development of the intermediate endotherm for the triblock copolymer is not due to crystallization of the amorphous material when the sample is cooled to room temperature. The above samples were isothermally crystallized, and then the heating scan was run, starting from the crystallization temperature. The sample was never allowed to cool to room temperature, and the intermediate endotherm is clearly present.

Table 13. Effect of the Crystallization Time on the Observed Melting Temperature and Heat of Fusion on the Lowest Endotherm of the Triblock Copolymer; T_c =45°C.

Crystallization Time, Hours	Heat of Fusion, cal/gm	Observed Melting Temp, °C
0	14.4	56.1
2	1.1	43.5
11	0.8	43.2

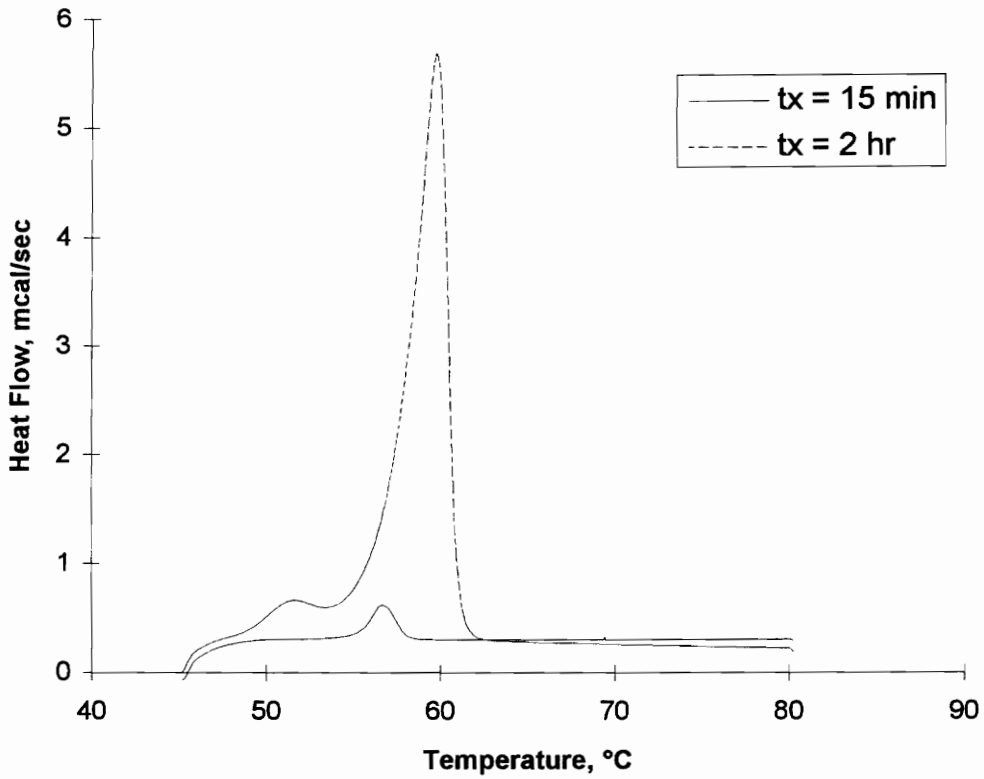

Figure 35. Effect of the Crystallization Time on the Intermediate Endotherm of the Triblock Copolymer; Tc= 45°C.

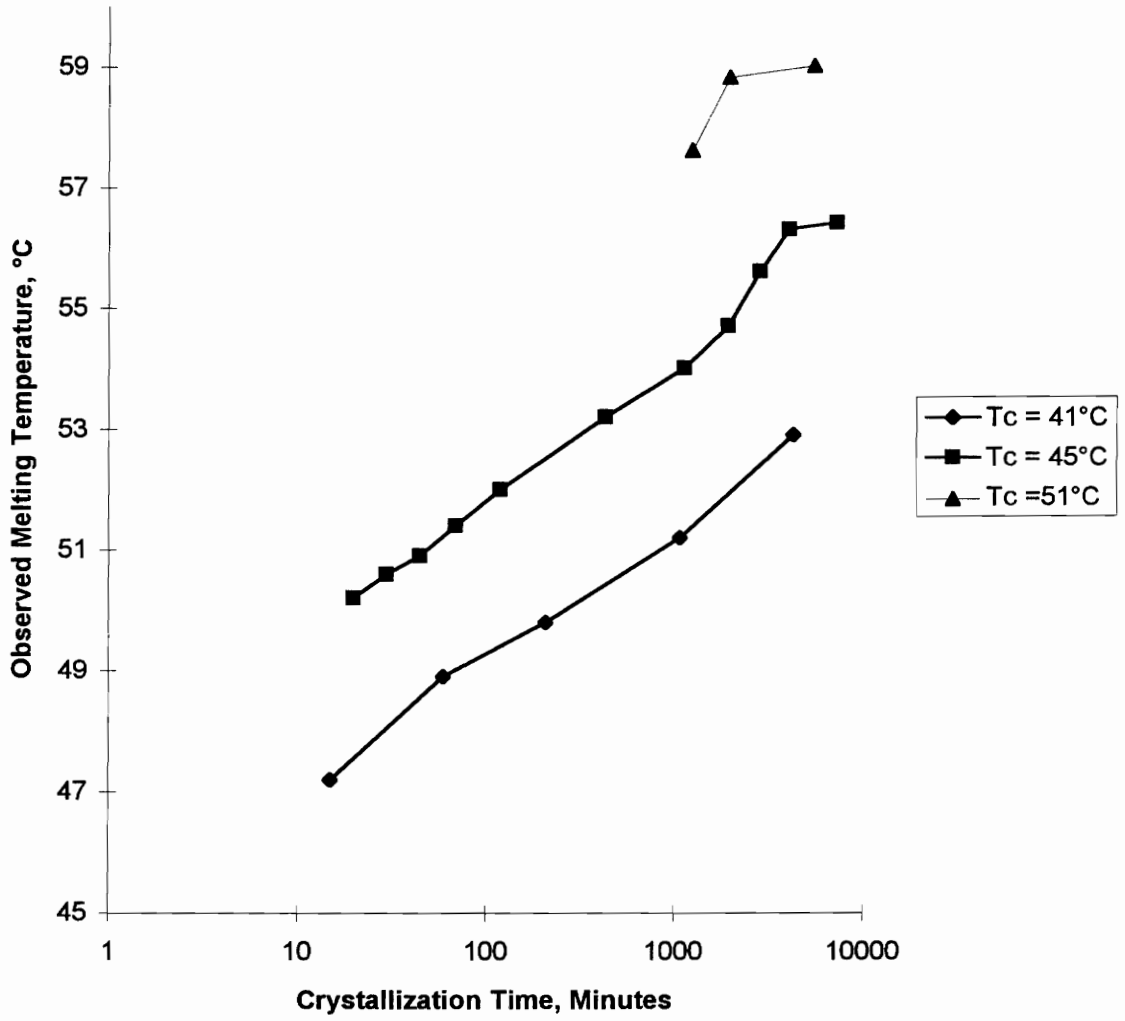

Figure 36. Effect of the Crystallization Time on the Observed Melting Temperature of the Intermediate Endotherm of the Triblock Copolymer.

Different crystal structures have been responsible for multiple endotherms in other polymers. An examination of the wide angle x-ray diffraction of the triblock copolymer shows that the peak positions coincide with those of the pure homopolymer (Figure 37). Thus, the lower endotherm can not be due to a different crystal structure. Similarly, the crystal structure of PCL did not change when it was crystallized from a triblock copolymer which had poly(dimethylsiloxane) as the midblock.[32]

The increase in the melting temperature associated with the intermediate endotherm (Figure 35) is similar to the behavior exhibited by it-PS, PET, PBT, PPS, and PEEK.[71] For PEEK, this behavior has been attributed to the melting of stacks of secondary lamellae. Small angle x-ray scattering results (Section 6.4) suggest that the origin of the intermediate endotherm in the PCL triblock copolymer is similar to PEEK, and is due to the formation of thinner lamellae.[72]

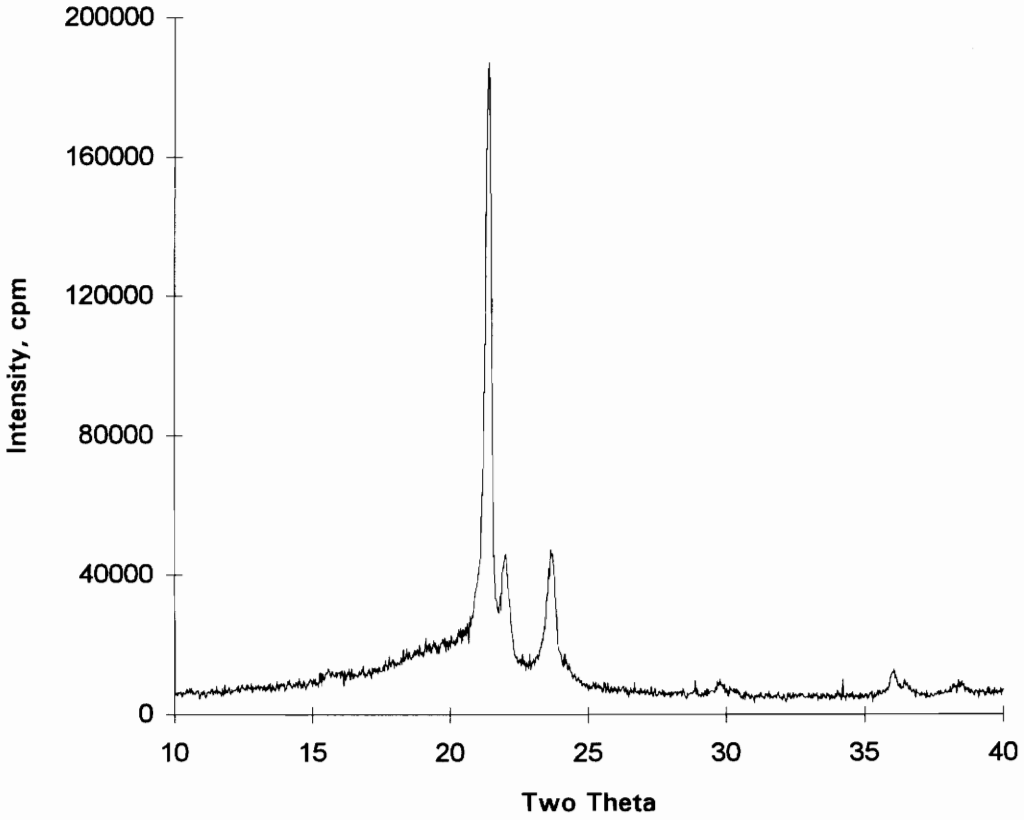

Figure 37. WAXD of the Triblock Copolymer; $T_c = 49°C$

Chapter 6. Crystallization Behavior of (ε-caprolactone) in the Triblock Copolymer

This chapter will compare and contrast the crystallization behavior of a triblock copolymer containing (ε-caprolactone) blocks with that of the pure poly(ε-caprolactone) homopolymer. First, the growth rate of the triblock copolymer is discussed. In order to analyze the growth rate data, a value for the equilibrium melting temperature is determined. This is followed with a discussion of whether the triblock copolymer melt is micro-phase separated. This information is needed in order to compare the crystallization behavior to block copolymer theory. Lastly, the isothermal SAXS data is compared and contrasted to the isothermal DSC crystallization discussed (Section 5.2) to elucidate the origins of the intermediate endotherm which is seen in the triblock copolymer, but not the homopolymer.

6.1 Polarized Optical Microscopy

A comparison of the growth rate of the poly(ε-caprolactone) homopolymer and poly(ε-caprolactone-*b*-propylene oxide-*b*-ε-caprolactone) determined by polarized optical microscopy shows the growth rate of the triblock copolymer is decreased with respect to the homopolymer for a given crystallization temperature (Figure 38, Table 13). This may be explained by the presence of the propylene oxide midblock which will decrease the proportion of crystallizable material in the melt. This decreased concentration of crystallizable chains near the growth front can decrease the growth rate. Additionally, the poly(propylene oxide) midblock may affect the transport term controlling the rate of diffusion of the polymer chain to the melt-crystal interface. The presence of the PPO

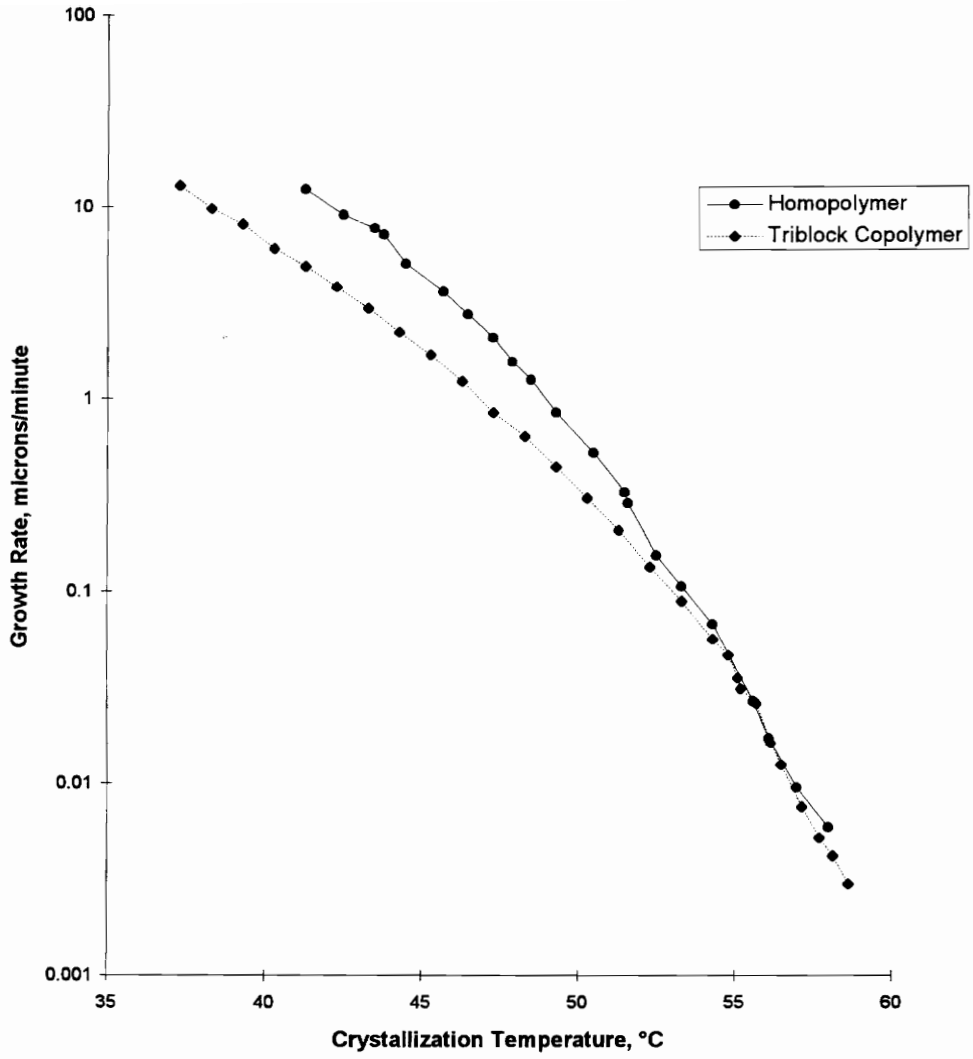

Figure 38. Comparison of the Growth Rate of Poly(ε–caprolactone) in the Homopolymer and Triblock Copolymer.

Table 14. Growth Rate for the Triblock Copolymer.

Crystallization Temperature,°C	Growth Rate, μm/min	Standard Deviation, μm/min
37.3	12.95	0.12
38.3	9.77	0.26
39.3	8.11	0.45
40.3	6.05	0.42
41.3	4.9	0.26
42.3	3.85	0.26
43.3	2.97	0.08
44.3	2.24	0.05
45.3	1.71	0.03
46.3	1.24	0.03
47.3	0.846	0.02
48.3	0.64	0.02
49.3	0.442	0.02
50.3	0.305	0.007
51.3	0.207	0.007
52.3	0.134	0.002
53.3	0.089	0.005
54.3	0.056	0.005
54.8	0.0464	0.005
55.1	0.0353	0.003
55.2	0.031	0.003
55.7	0.026	0.003
56.15	0.0162	0.0014
56.5	0.0125	0.0013
57.15	0.0075	0.0006
57.7	0.0052	0.0005
58.15	0.0042	0.0005
58.65	0.003	0.0004

block could impede the diffusion of the PCL segments to the growing crystal which would subsequently decrease the growth rate.

6.2 Equilibrium Melting Temperature

The equilibrium melting temperature is an important quantity in the analysis of growth rate data. It is the temperature at which an extended chain crystal will melt and crystallize simultaneously. The Hoffman-Weeks analysis (See Section 4.1.1) is used to obtain the equilibrium melting temperature for the triblock copolymer. It is seen that the Hoffman -Weeks plot for the triblock copolymer differs from the pure homopolymer (Figures 39, 18) in that there is no upswing at higher crystallization temperatures. This suggests that the thickening coefficient is constant in the temperature range in which the Hoffman-Weeks analysis was carried out. Perhaps the temperature independent thickening rate is due to constraints from the poly(propylene oxide) midblock.

Using the Hoffman-Weeks method, the extrapolated equilibrium melting temperature is found to be 85°C for the triblock copolymer. This is the same value found for the pure homopolymer using the Gibbs-Thomson-Tammann method. Another method which is used to obtain a value for the equilibrium melting temperature is to analyze the growth rate behavior of the triblock copolymer with the Lauritzen-Hoffman growth rate equation to determine the equilibrium melting temperature which best describes the growth rate data (See Section 4.1.3).[7] Use of the non-linear analysis method yields a value of 85 $\pm$ 8 °C , and linear analysis of the traditional equation yields a value of 84 °C for the equilibrium melting temperature of the triblock copolymer (Figure 40). All the estimations show that there is no equilibrium melting temperature depression due to the propylene oxide midblock in the triblock copolymer.

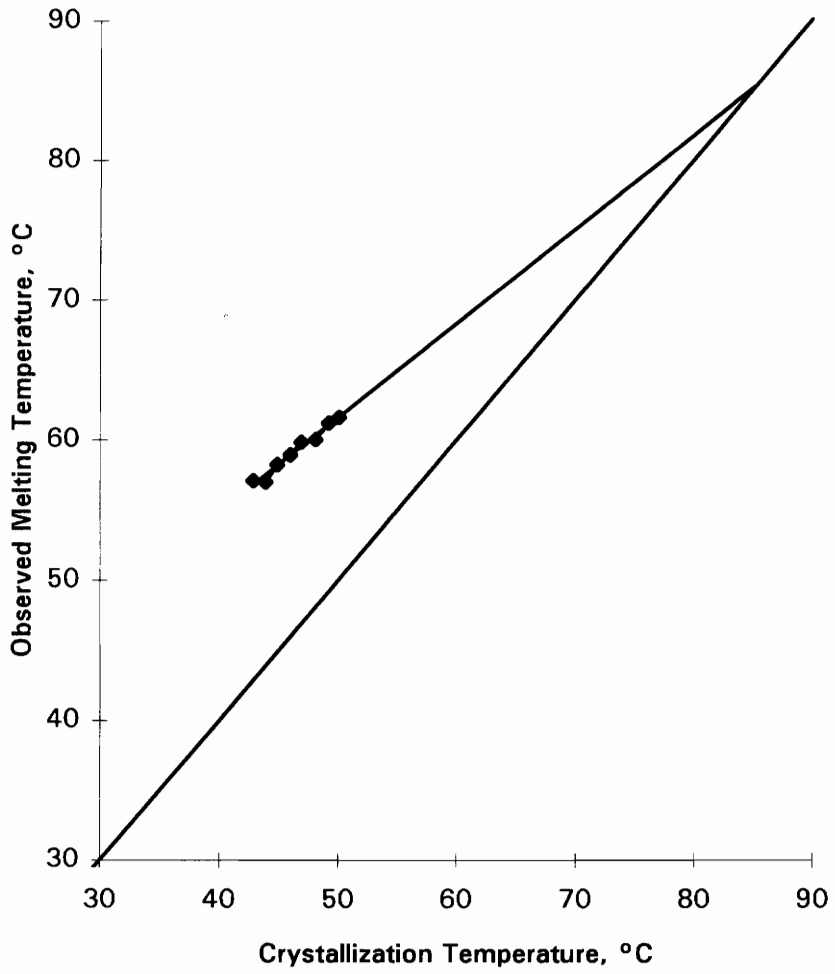

Figure 39. Hoffman-Weeks Plot for the Triblock Copolymer

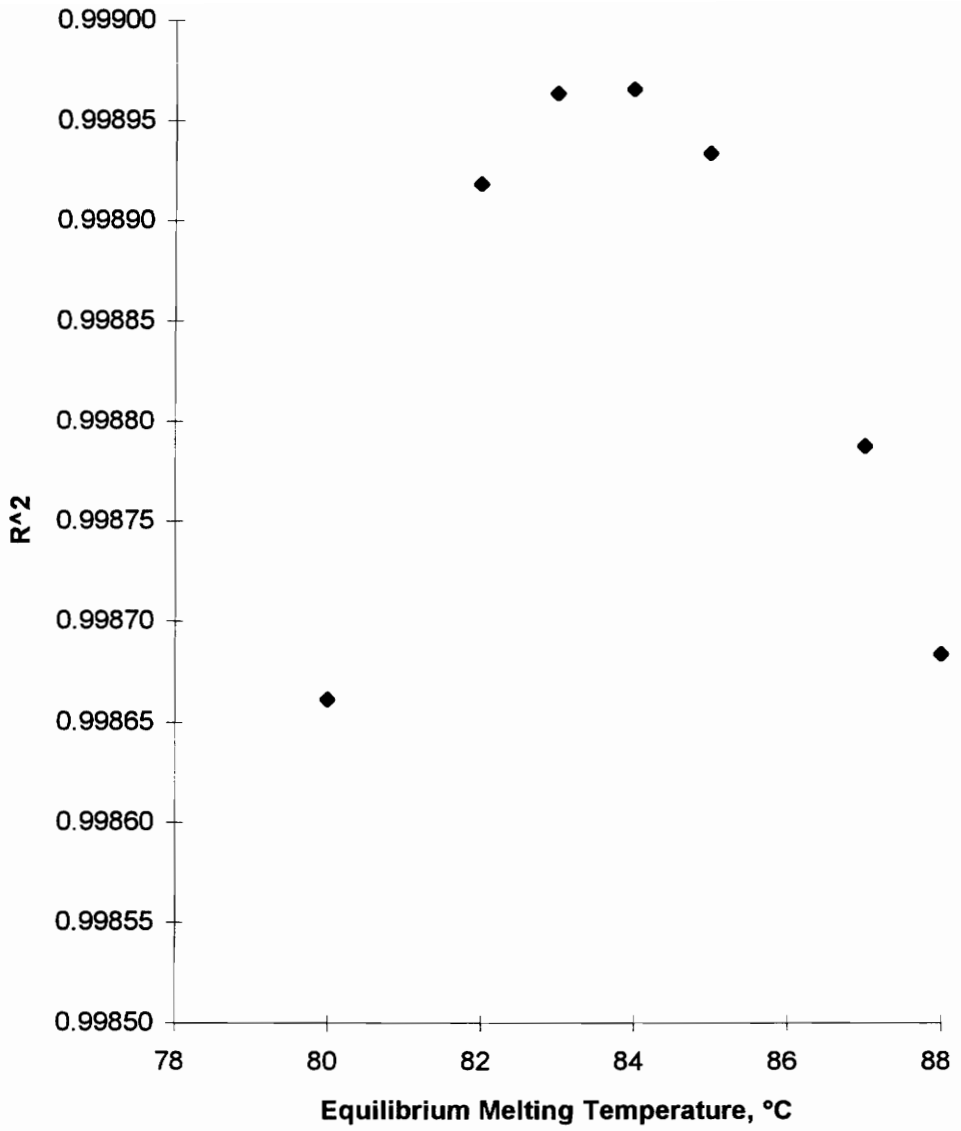

Figure 40. Determination of the Equilibrium Melting Temperature of the Triblock Copolymer by the Least Squares Method.

The traditional LH equation (28) was used to estimate a value for the product of the interfacial free energies, $\sigma\sigma_e$, because an independent value of σ_e is needed to analyze the data with the modified version of the equation. Using a value of 85°C for the equilibrium melting temperature, the product of the surface energies, $\sigma\sigma_e$, (754 erg/cm^2) , for the triblock copolymer was found to be slightly less than the homopolymer (881 erg/cm^2) analyzed with the same growth rate equation. This decrease could be due to either the fold, lateral surface free energy, or a combination of both. The poly(propylene oxide) midblock could change the fold surface of the polymer crystal or the characteristic ratio of the polymer in the melt.

The decrease in the growth rate at a given crystallization temperature for the triblock copolymer is not due to a decreased undercooling and must be from the connected nature of the blocks, decreased concentration of crystallizable material, or differences in the transport term. Normally, one would expect the propylene oxide midblock to lower the chemical potential of the melt and depress the equilibrium melting temperature. However, the poly(ε-caprolactone) blocks in the triblock copolymer have a greater number average molecular weight than the pure homopolymer. Perhaps the melting point depression due to the midblock is masked by the increase in the equilibrium melting temperature due to a higher number average molecular weight.[19]

Another possibility for the lack of melting point depression is that the blocks are micro-phase separated in the melt. If the blocks were micro-phase separated, the chemical potential of the PCL blocks would not be depressed by the poly (propylene oxide) block. In turn, the equilibrium melting temperature would not be decreased if the two block were not miscible, or if their interaction parameter was zero.

Miscibility of blocks can be determined by an examination of the glass transition temperature of the pure homopolymers of each block, and the triblock copolymer. In this

case both homopolymers and the triblock copolymers have glass transition temperatures in the range of -60° to -65°C (Figures 41-43). The miscibility of the blocks cannot be determined by the glass transition temperature because the range of values is too narrow.

A rough guide to polymer-polymer miscibility is the solubility parameter, δ. This parameter is based on the basic principle that "like dissolves like." The solubility parameter can be calculated for a solvent-solute pair where there are no specific interactions. An estimation of the solubility parameter is found through the following relation.

$$\delta = \frac{\left(\sum F\right)}{V} = \frac{\left(\sum F\right)\rho}{M_0} \qquad (75)$$

The molar attraction constant is F, the molar volume and mass of the repeat unit is V and M_0, the density of the polymer is ρ. Group contributions to F have been calculated by various workers (Table 14).[4]

Calculations of the solubility parameter are shown in Table 15. A rough, general rule of thumb for solubility is[48]

$$|\delta_1 - \delta_2| \leq 0.5 \quad \text{for solubility.}$$

An examination of the absolute value of the differences of the solubility parameters show the difference is less than 0.5 using Small's values. This indicates the two blocks in the copolymer should not be micro-phase separated in the melt.

Another indication that the melt is not weakly micro-phase separated came from a study of the effect of time in the melt on the SAXS profile. It was seen that the intensity

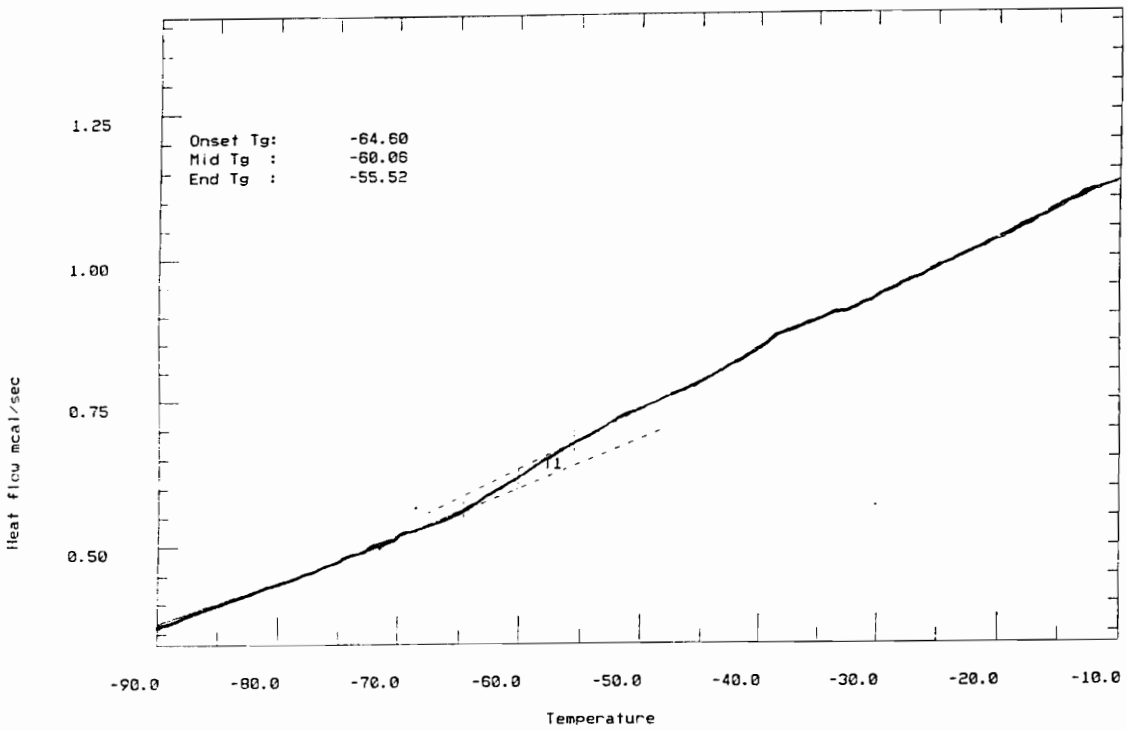

Figure 41. Glass Transition Temperature of Poly(ε–caprolactone).

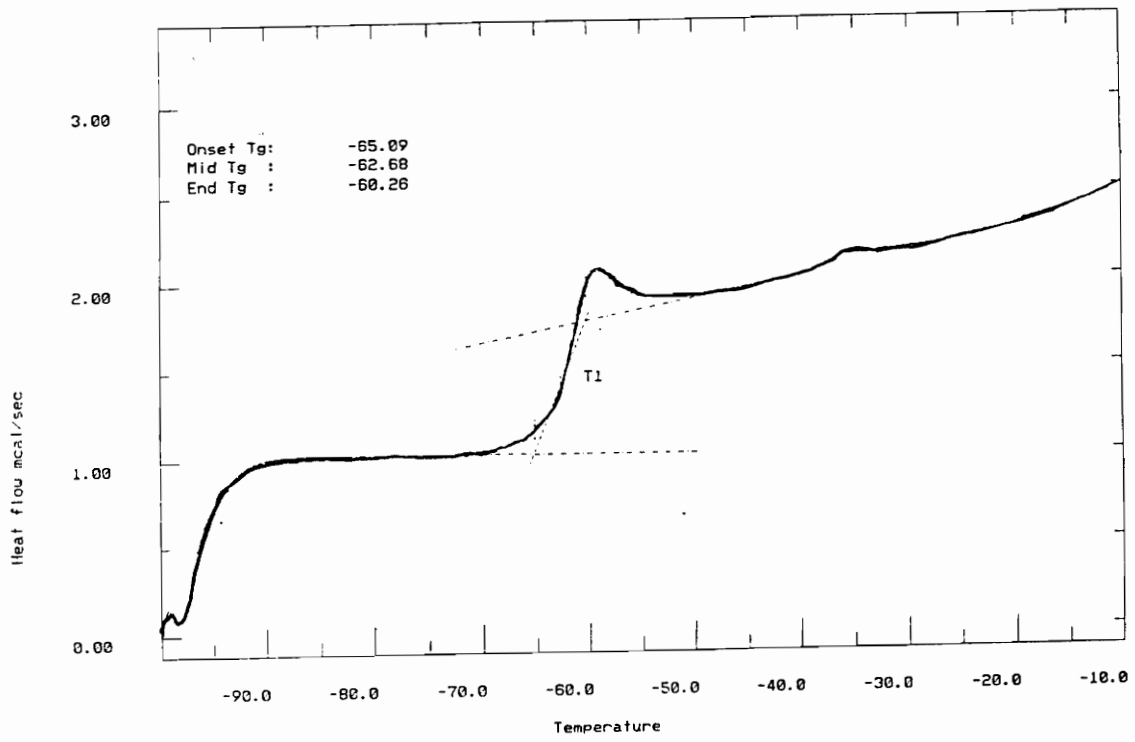

Figure 42. Glass Transition Temperature of Poly(propylene oxide).

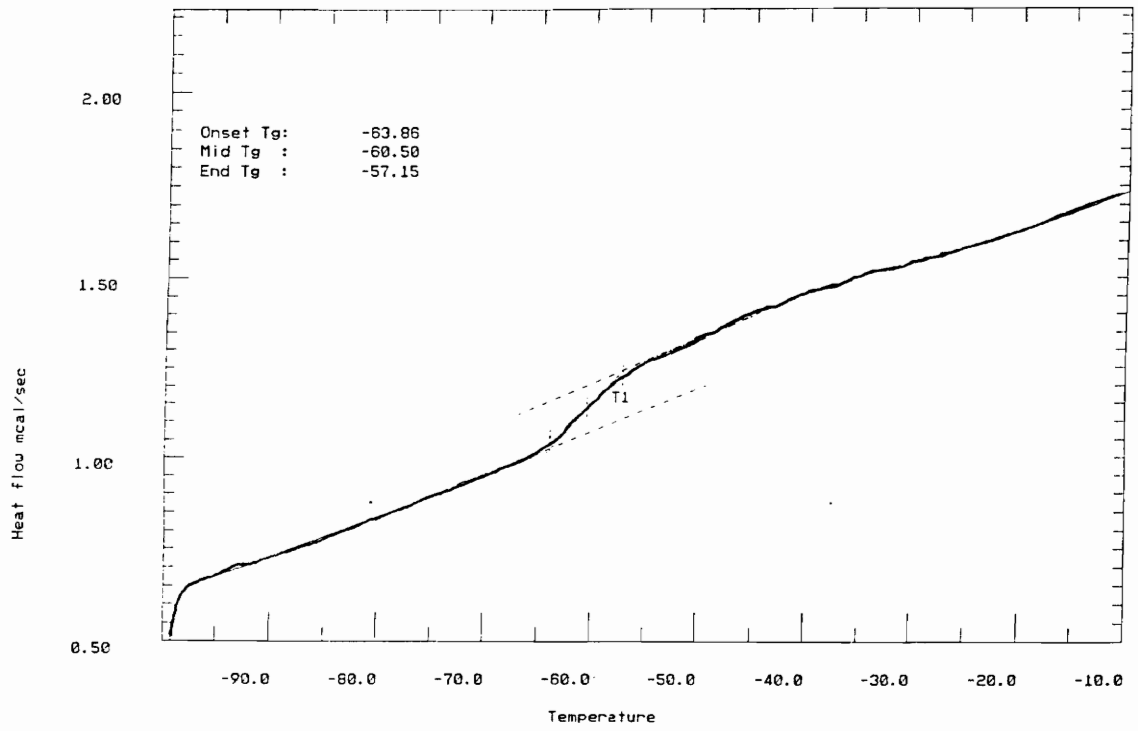

Figure 43. Glass Transition Temperature of Poly(ε–caprolactone-*b*-propylene oxide-*b*- ε–caprolactone).

Table 15: Application of Group Contribution Method to the Estimation of the Solubility Parameter

Group	Molar Atraction Constant,F, $[(MPa)^{1/2}cm^3mol^{-1}]$
$-CH_3$	438
-O-	143
$-CH_2$	272
-COO-	634

Table 16: Calculated Solubility Parameters for the Homopolymers in the Triblock Copolymer (from reference 47)

	Calculated Solubility Parameters,$(Jcm^{-3})^{1/2}$
Poly (propylene oxide)	19.1
Poly (ε-caprolactone)	19.2
$\lvert\delta_1-\delta_2\rvert$	0.1

of the SAXS profile stayed constant with time in the melt. This indicates the degree of micro-phase separation in the melt did not change with time, which would be expected for a homogenous melt.

6.3 Block Copolymer Crystallization Theory

The issue of whether of not the melt is homogenous is important in determining whether there could be an equilibrium melting temperature depression and in comparing the crystallization behavior of the triblock copolymer with theory. Theory on block copolymer crystallization predicts that a block copolymer crystallized from a strongly microphase-separated melt will be controlled by equilibrium considerations.[20,21] However, a homogenous melt can be treated as a crystallizable chain with a large defect in it. The growth rate and crystallization behavior will still be governed by kinetics.

Though the question of whether the melt is homogenous has not been definitively resolved, the crystallization behavior of the triblock copolymer shows it is governed by kinetic rather than equilibrium considerations. A homopolymer which is governed by kinetics will reduce the number of chain folds to become an extended chain crystal in the limit of infinite annealing times. In contrast, the diblock and triblock copolymers which are crystallized from a micro-phase separated melt will anneal to an equilibrium thickness. An extended chain crystal would not be in equilibrium for the block copolymer because the amorphous chain would also need to be fully extended. The fully extended chain is not the most favorable state for the amorphous chains because of the entropy gain that can be achieved in the random coil state. DSC studies on the effect of crystallization time on the melting temperature (which is an indirect measure of the lamellar thickness) show that the

melting temperatures of the lower and upper endotherms of the triblock copolymer increase with crystallization time (Figures 36, 46). Thus the polymer is reducing the number of chain folds to become closer to an extended chain crystal. If the crystallization of the block copolymer was controlled by equilibrium considerations, the melting temperature would not increase with the logarithm of the crystallization time. The melting temperature would level off once it has approached the equilibrium thickness.

The theoretical crystalline lamellar thickness, l_c, and the thickness of the amorphous region, l_a, have been calculated for diblock copolymers which are crystallized from a micro-phase separated melt.[21]

$$l_a = \frac{r_a^{2/3}\left(\sigma + \sigma_e \rho_c\right)^{1/3}}{\left(3kT\rho_a\right)^{1/3}} \tag{76}$$

$$l_c = \frac{r_a \rho_a^{2/3}\left(\sigma + \sigma_e \rho_a\right)^{1/3}}{\rho_c r_a^{1/3}\left(3kT\right)^{1/3}} \tag{77}$$

The molecular weight of the amorphous and crystalline forming portions are given by r_a and r_c, σ and σ_e are the interfacial free energies of the lateral and the fold surface, while ρ_c and ρ_a are the density of the crystalline and amorphous regions, respectively. These equations can be modified for the case of the triblock copolymer.

An important point these equations show is that both the crystalline and amorphous thicknesses are controlled by the molecular weight of the polymer. There is also a temperature dependence on the lamellar thickness. However, these equations predict that the lamellar thickness will decrease with increasing crystallization temperature.

This is in contrast to the kinetic theory which predicts the lamellar thickness will increase with crystallization temperature.

An examination of the effect of crystallization temperature on the long spacing of the triblock copolymer shows that the long spacing increases with crystallization temperature (Table 16). The long spacing is the sum of the amorphous and crystalline lamellar thickness. An **estimation** of the crystalline lamellar thickness, l_c, is obtained by multiplying the long spacing, L, by the volume percent crystallinity, φ_{cv}, obtained by DSC.

$$l_c = L\varphi_{c,v} \tag{78}$$

For a rigorous determination of the crystalline lamellar thickness, this equation can only be used if the non-crystalline component is in the interlamellar rather than interspherulitic region, and there are no pockets of amorphous material outside the lamellar stacks. The connected nature of the blocks in the triblock copolymer will not allow the amorphous poly(propylene oxide) block to be rejected into the interspherulitic region. However, the possibility of amorphous pockets within the sample exists. Thus, the following calculation provides only a rough estimate of the crystalline lamellar thickness, l_c.

The volume percent crystallinity is found by the following equation.

Table 17. Effect of the Crystallization Temperature on the Long Spacing and Lamellar Thickness of the Triblock Copolymer.

Tc, Celsius	*L, nm*	*l, nm*
36	14.9	6.5
43	16.3	6.9
45	17.0	7.9
47	18.3	8.6
53	18.8	8.7

$$\varphi_{c,v} = \frac{\left(\frac{\Delta h_f}{\Delta h_f^0}\right)\left(\frac{\rho_a}{\rho_c}\right)}{\left[1-\left(1-\left(\frac{\rho_a}{\rho_c}\right)\right)\left(\frac{\Delta h_f}{\Delta h_f^0}\right)\right]} \tag{79}$$

The heat of fusion of a perfect crystal is Δh_f^0, the heat of fusion of the sample is Δh_f, and the crystalline density of PCL is ρ_c. The first step to determine the amorphous density, ρ_a, is to calculate the weight of PCL, g_{PCL}, and PPO, g_{PPO}, in the original sample. This can be found because the composition of the triblock copolymer is 80 weight % PCL and 20 weight % PPO (See Section 3.1).

$$\begin{aligned} g_{PCL} &= (0.8)(g_{sample}) \\ g_{PPO} &= (0.2)(g_{sample}) \end{aligned} \tag{80}$$

The weight of PCL crystallized, $g_{PCL}^{Crystallized}$, can be determined from the weight percent crystallinity, $\varphi_{c,w}$.

$$g_{PCL}^{Crystallized} = g_{PCL}\varphi_{c,w} \tag{81}$$

This leaves the remaining amount of PCL in the amorphous phase, $g_{PCL}^{Amorphous}$. The volume fraction of each polymer in the amorphous phase is then found with the following.

$$\varphi_{PCL_{amorphous}} = \frac{\frac{g_{PCL}^{Amorphous}}{\rho_{a,PCL}}}{\frac{g_{PCL}^{Amorphous}}{\rho_{a,PCL}} + \frac{g_{PPO}}{\rho_{a,PPO}}} \tag{82}$$

$$\varphi_{PO} = \frac{\dfrac{g_{PPO}}{\rho_{a,PPO}}}{\dfrac{g_{PCL}^{Amorphous}}{\rho_{a,PCL}} + \dfrac{g_{PPO}}{\rho_{a,PPO}}} \tag{83}$$

The amorphous density of the sample, ρ_a, can be found by the following equation,

$$\rho_a = \left(\varphi_{PCL_{amorphous}}\right)\rho_{a,PCL} + (\varphi_{PPO})\rho_{a,PPO} \tag{84}$$

where $\rho_{a,PPO}$ is 0.998 g/cm^3[23]

The results show that the lamellar thickness increases with crystallization temperature. This would be expected if the crystallization was controlled by kinetics rather than by equilibrium considerations. Note that if there are pockets of amorphous material outside the lamellar stacks in the triblock copolymer sample, the calculated values would be underestimated. However, the general trend of increasing l_c with crystallization temperature should not change.

Another item which indicates that the melt can be considered homogenous with a large defect in it (*i.e.* the propylene oxide midblock) is the small angle x-ray scattering patterns. Samples of the pure homopolymer of poly(ε-caprolactone) and the triblock copolymer crystallized for long times at 46°C are shown in Figures 44-45. It can be seen that there are two maxima in the pure homopolymer, while there is only one maximum in the triblock copolymer SAXS profile. Analysis of the position of the two maximum in the homopolymer shows that the second peak appears at an angle approximately twice that of the first angle. This indicates the presence of long-range crystalline order. Thus, the long-range order in the homopolymer is greater than in the

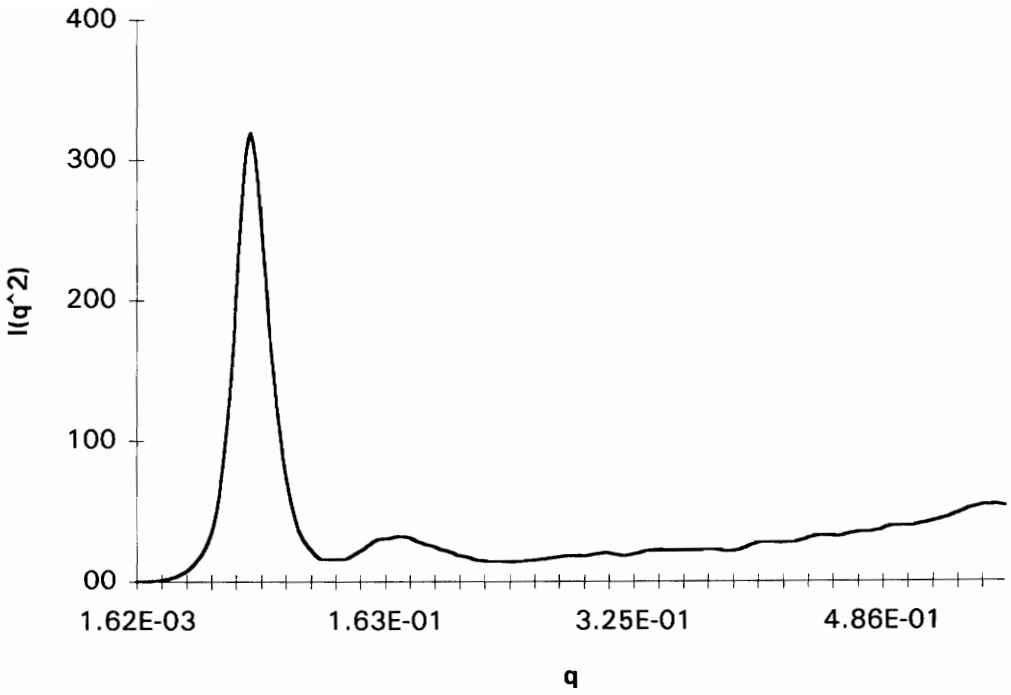

Figure 44. Small Angle X-ray Scattering Profile of Poly(ε-caprolactone); T_c =46°C

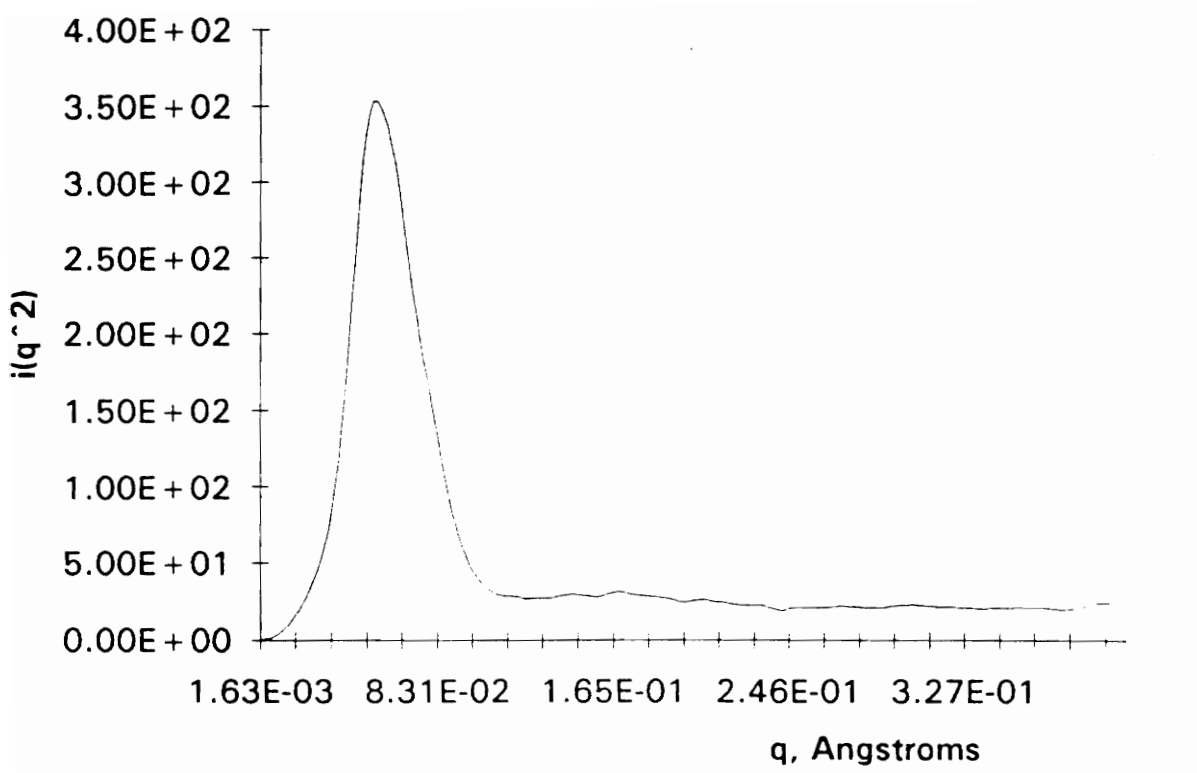

Figure 45. Small Angle X-ray Scattering of the Triblock Copolymer; T_c=46°C.

triblock copolymer. The poly(propylene oxide) midblock acts as a defect and reduces long range order in the triblock copolymer.

6.4 Small Angle X-ray Scattering

The isothermal crystallization behavior of the triblock copolymer was examined as a function of crystallization time with SAXS to elucidate the origins of the intermediate endotherm seen by differential scanning calorimetry in the triblock copolymer (See Section 5.2). DSC studies show that both the melting temperature and the heat of fusion of the triblock copolymer increase quickly at low crystallization times and then level off at long crystallization times for a crystallization temperature of 45°C (Figures 46, 47). These plots were compared to isothermal plots of the integrated intensity and relative invariant of the SAXS curve as a function of time at 45°C (Figure 48). It was seen that the integrated intensity of the SAXS curve leveled off at the same time as the heat of fusion and observed melting temperature for a given crystallization temperature.

The integrated intensity increases with crystallization time for the triblock copolymer at 45°C. A break in the slope of this curve occurs before the intensity levels off. A comparison with the DSC curves show that this break happens at approximately the same time as when the intermediate endotherm appears. Additionally, the long spacing was found from the position of the maximum of the SAXS curve with respect to crystallization time. It is seen that there is a small decrease in the long spacing at the same time the intermediate endotherm appears in the DSC scans (Figure 49).

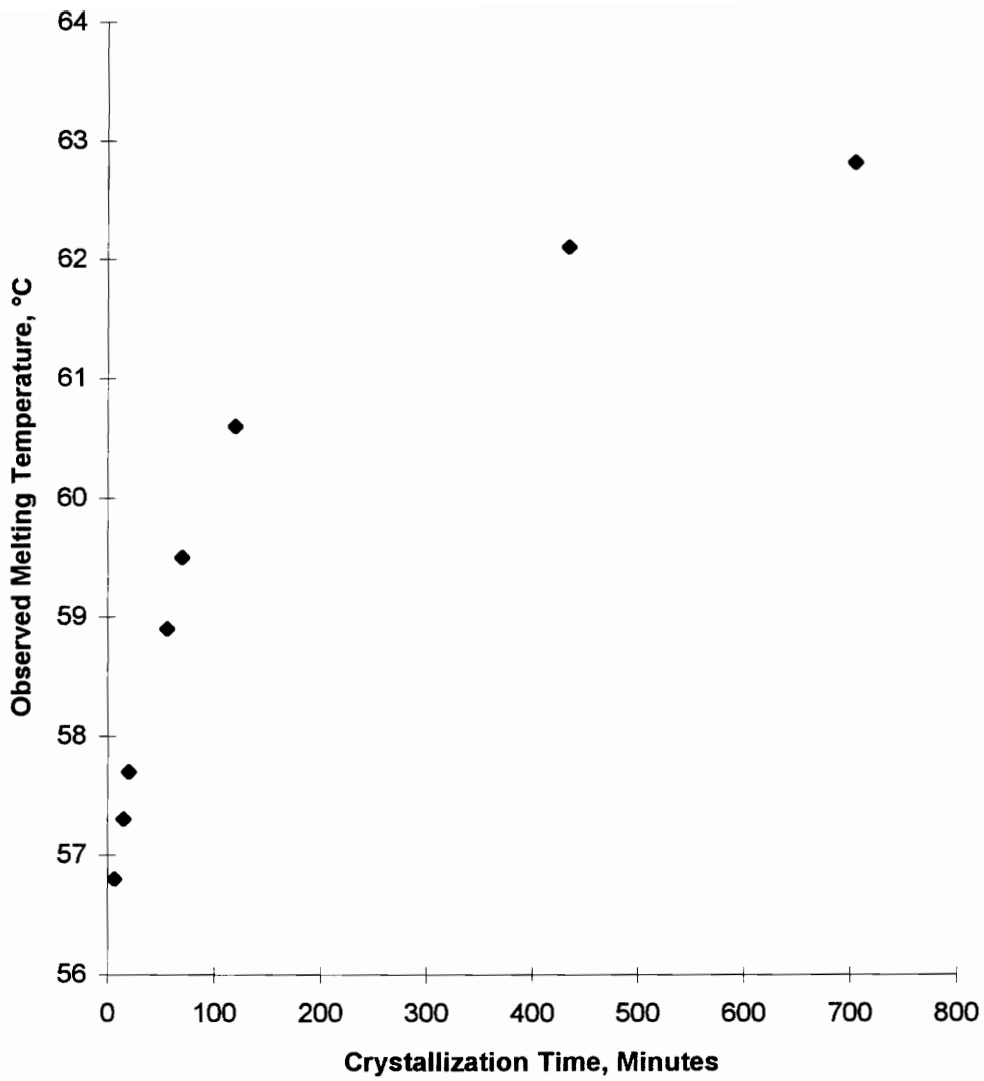

Figure 46. Effect of the Crystallization Time on the Observed Melting Temperature of the Triblock Copolymer; T_c = 45°C.

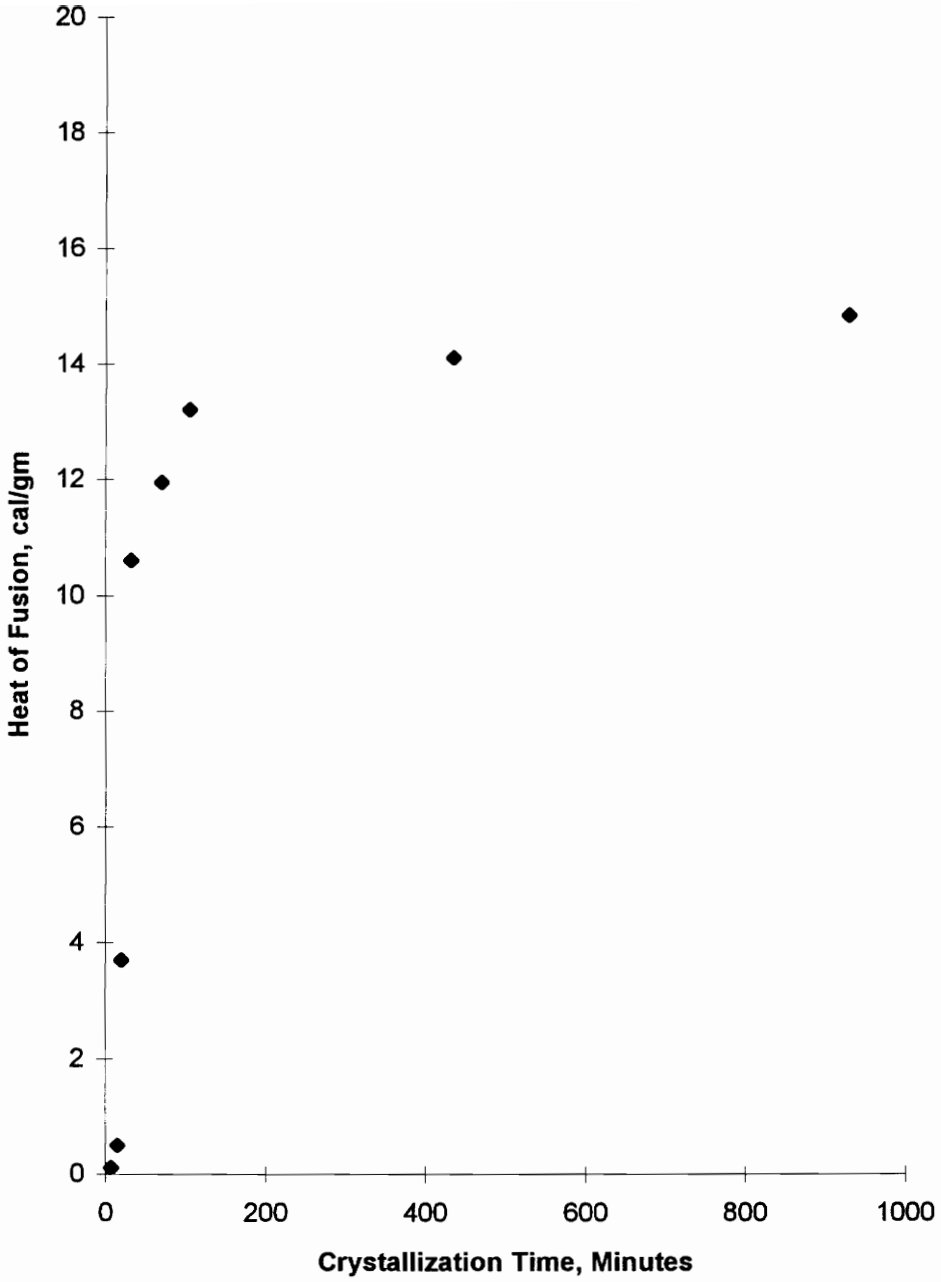

Figure 47. Effect of the Crystallization Time on the Heat of Fusion of the Triblock Copolymer; $T_c = 45°C$.

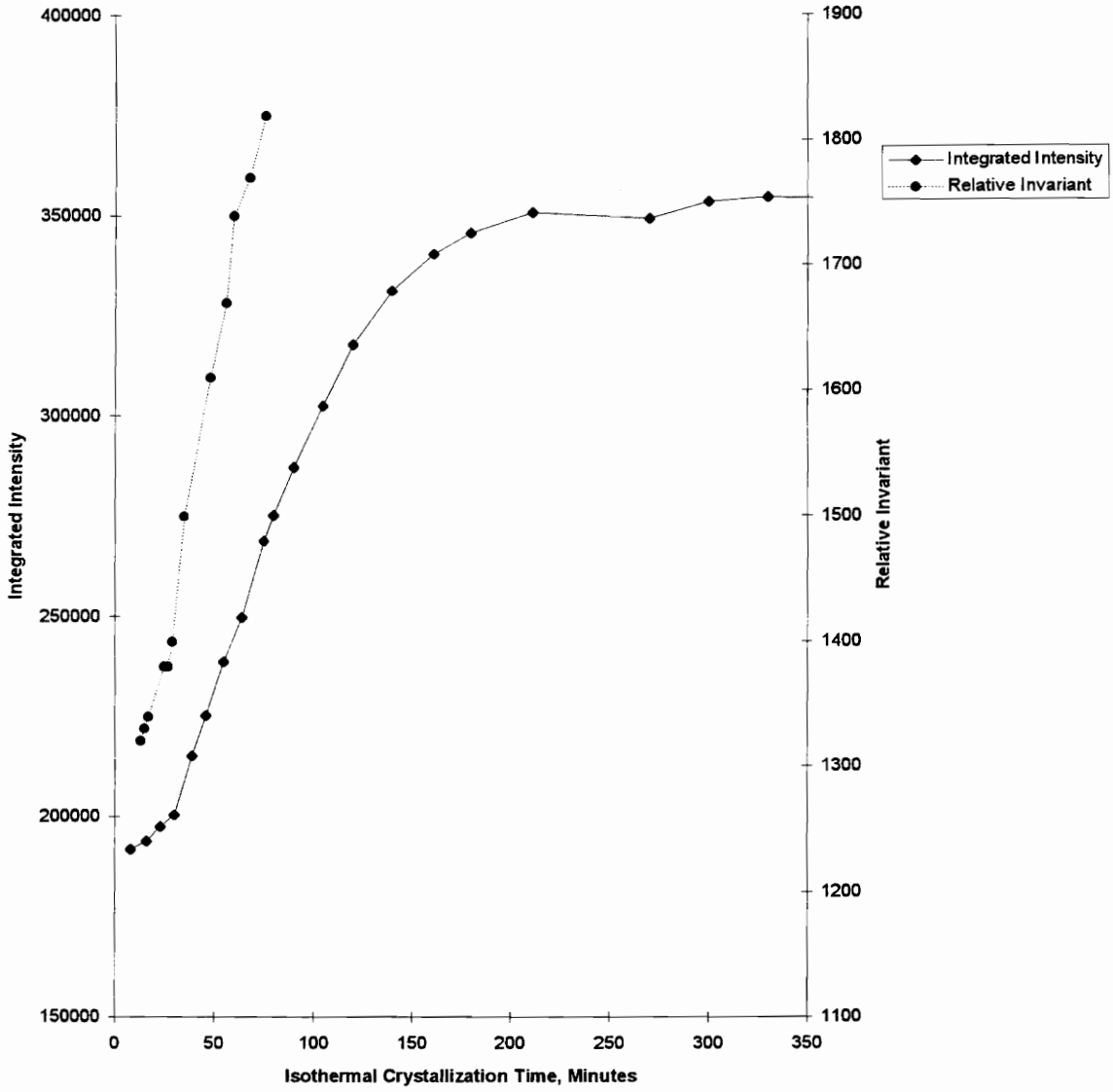

Figure 48. Effect of the Crystallization Time on the Integrated Intensity and Relative Invariant of the SAXS Curve for the Triblock Copolymer; $T_c = 45°C$.

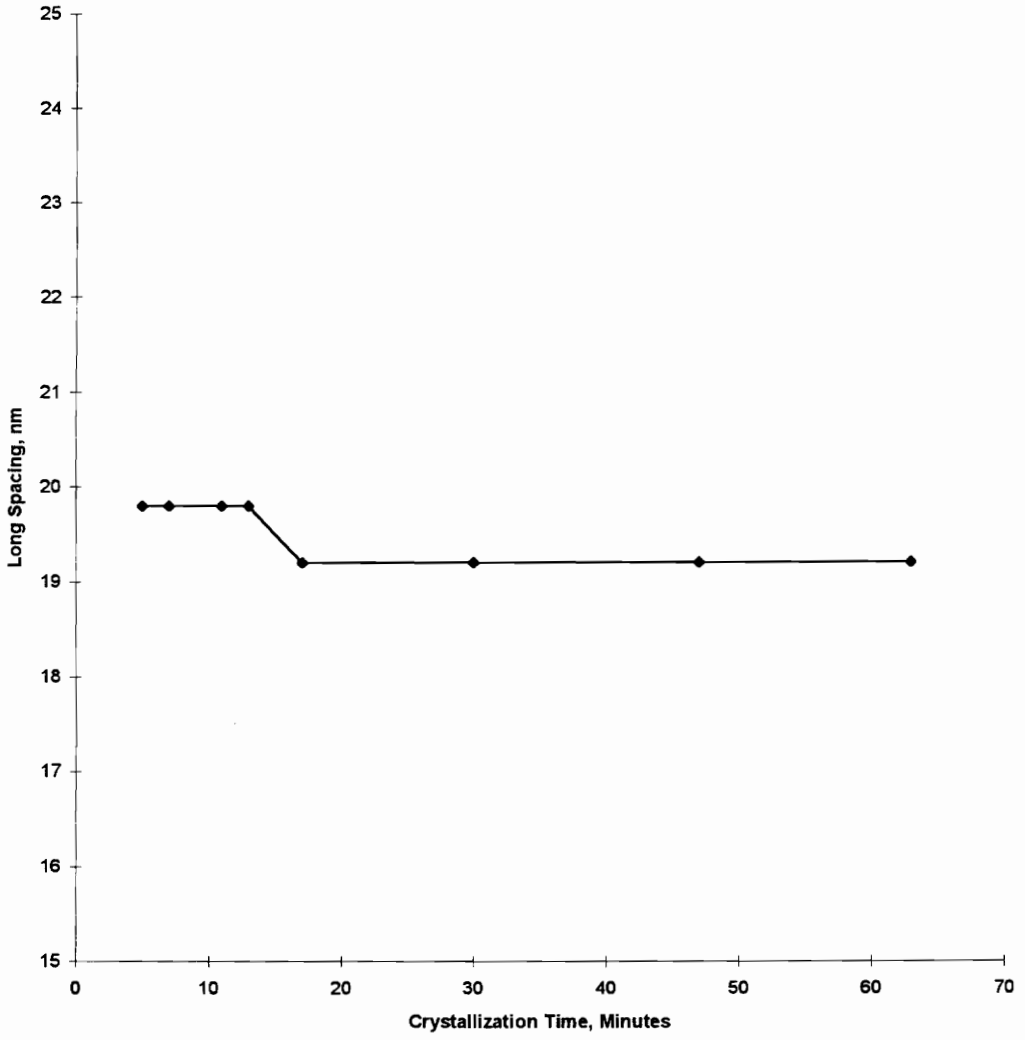

Figure 49. Effect of the Crystallization Time on the Long Spacing of the Triblock Copolymer; $T_c = 45°C$.

Previous studies on the crystallization behavior of blends of poly(ε-caprolactone) [28,39,43,47] have shown that the long spacing decreases for early crystallization times and then plateaus or slowly decreases with increasing crystallization times. An explanation that have been proposed for this behavior is the insertion of lamellar stacks in between the existing lamellar stacks[49].

In the case of the triblock copolymer used in this study, the fact that the long spacing decreases at about the same time a lower endotherm is seen in the DSC scan suggests that the decrease in long spacing is due to the formation of smaller lamellae. The smaller lamellae decrease the average long spacing and show up on the DSC scan as a shoulder prior to the main melting peak. The very small decrease in the long spacing is consistent with the fact that the area of the lower endotherm is very small. The long spacing is due to a weighted average over the entire sample and the small amount of thinner lamellae represented by the lower endotherm will not decrease the long spacing by a great amount. As the crystallization time proceeds, the lamellae thicken and melt at a higher temperature.

Another indication that the formation of thinner lamellae caused the appearance of the lower endotherm in the DSC scan was shown by a study of the effect of temperature on the long spacing of the triblock copolymer. A sample was crystallized at 45°C , and the long spacing was measured as the temperature was increased. This data was examined in light of the DSC endotherm of the triblock copolymer crystallized at 45°C (Figure 50). It was found that the long spacing increased when the sample was heated to a temperature

between the two endothermic peaks. This corresponds to the melting of stacks of smaller long spacing. Heating the sample above the main melting peak leads to a further decrease in SAXS intensity and the disappearance of a maximum in the SAXS curve. This indicates all the lamellae have melted.

A comparison of the isothermal crystallization behavior of the homopolymer with the triblock copolymer at 45°C using SAXS indicates a longer induction period for the homopolymer. When the integrated intensity starts to increase, it rises continuously until it levels off (Figure 51). The DSC study shows that only one endothermic peak occurs above the crystallization temperature even when the sample is crystallized for long periods of time.

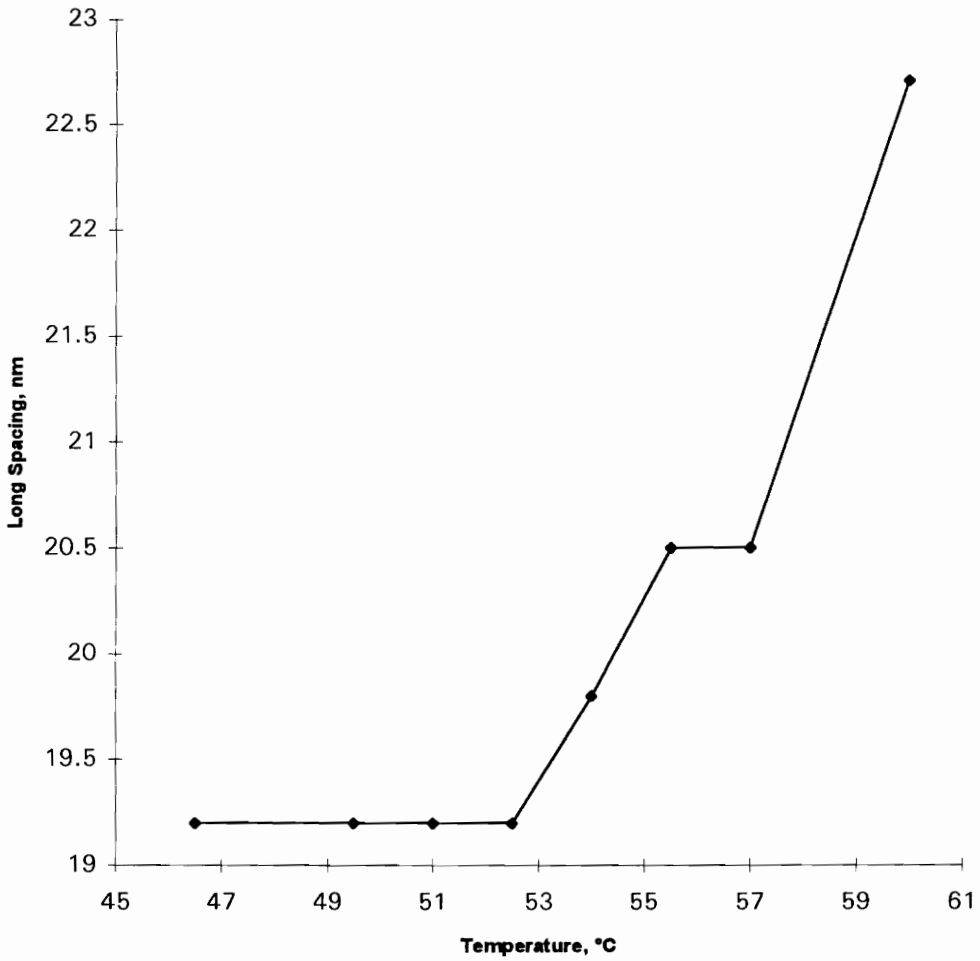

Figure 50. Effect of the Temperature on the Long Spacing of the Triblock Copolymer; $T_c = 45°C$.

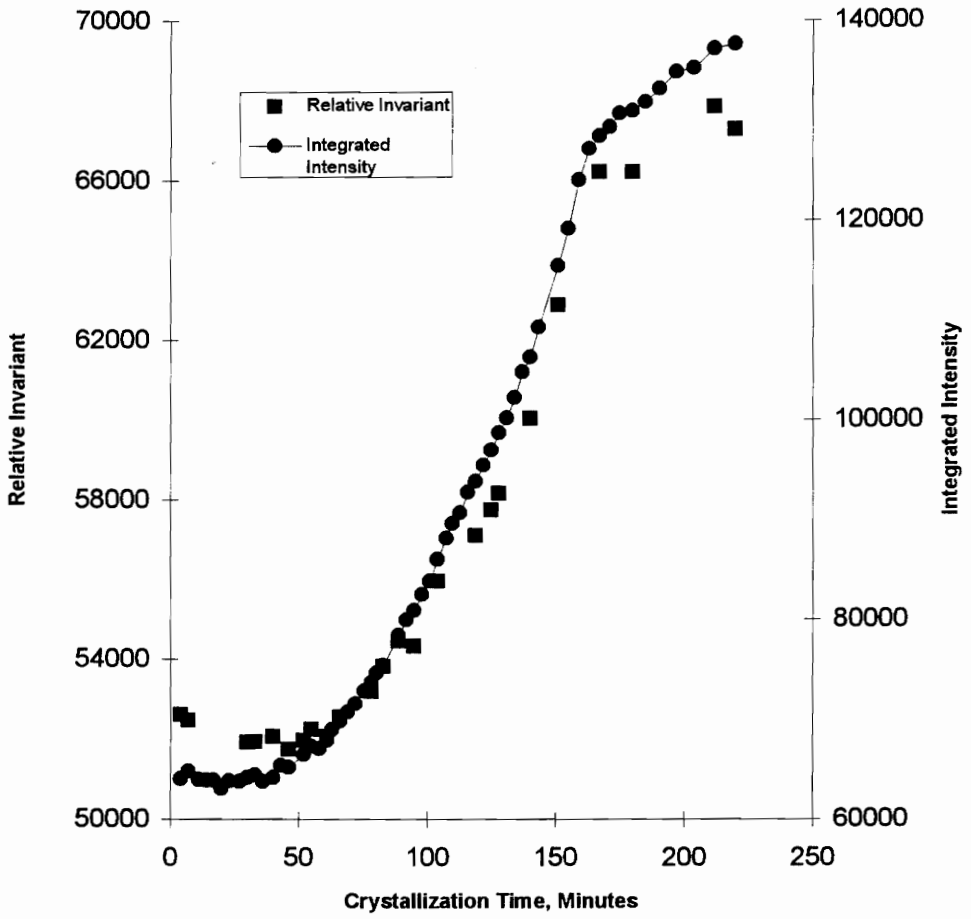

Figure 51. Effect of the Crystallization Time on the Integrated Intensity and Relative Invariant of the SAXS Curve for Poly(ε–Caprolactone); $T_c = 45°C$.

Chapter 7. Conclusions

This thesis has examined the crystallization and melting behavior of poly(ε–caprolactone) in the homopolymer and triblock copolymer. A careful determination of the equilibrium melting temperature of the poly(ε–caprolactone) homopolymer was carried out. The method used was based on the Gibbs-Thomson-Tammann analysis. The effect of thickening during the DSC scan and thermal lag for various heating rates was accounted for to calculate a value of 85 ± 4 °C for the equilibrium melting temperature. This value is approximately 10 -15 °C higher than previously reported values which did not take thickening and thermal lag effects into account. The fold lateral free energy was also found from the Gibbs-Thomson-Tamman analysis (σ_e = 64 ± 6 erg/cm^2), and was combined with the value of the product of the surface energies obtained from growth rate measurements to determine a value for the lateral surface free energy, σ. This gave a value of 10.3 ± 3.1 erg/cm^2, which was used in the proposed inverse relation between the characteristic ratio of a polymer chain and the lateral surface free energy of a melt crystallized polymer. A value of 4.5 ± 1.3 was found for the characteristic ratio, which is within the range of the characteristic ratio determined by solution measurements (5.9 ±0.3[26] and 5.6 ± 0.3[70]).

The multiple endothermic behavior of poly(ε–caprolactone) was examined for the case of the homopolymer and triblock copolymer. For the homopolymer, the lower endotherm appeared around the crystallization temperature. The maximum of this lower

endotherm increased with increasing crystallization temperature. Crystallization studies of the time dependence of the lower endotherm indicated it was due to crystallization during cooling after isothermal crystallization.

Three distinct endotherms were observed for the triblock copolymer. The lowest endotherm was centered around the crystallization temperature, the intermediate endotherm was located above the crystallization temperature, and the highest endotherm was due to the melting of the primary lamellae. The origin of the lowest endotherm is the same for the pure homopolymer; material which did not completely crystallize at the crystallization temperature but did crystallize as the material was cooled to room temperature.

In order to understand the origins of the intermediate endotherm, isothermal crystallization studies were carried out by DSC and SAXS. DSC results showed that at short crystallization times; only one endotherm was present. Time resolved, isothermal crystallization studies by SAXS suggest that the intermediate endotherm in the DSC scan is due to the formation of lamellar stacks of smaller long spacing.

A temperature dependence study of the long spacing gave another indication that the intermediate endotherm of the triblock copolymer is associated with the melting of thinner lamellae. It was seen that the long spacing increased as the sample was heated to a temperature between the two endotherms seen on the DSC scan. This is due to the melting of lamellar stacks of smaller long spacing. A further increase in long spacing was seen when the sample was heated to a temperature above the highest endotherm.

The crystallization behavior of poly(ε–caprolactone) in the homopolymer and triblock copolymer was compared and contrasted. It was seen that for a given crystallization temperature, the growth rate of PCL in the triblock copolymer is reduced with respect to the homopolymer. An examination of the equilibrium melting temperatures showed that this reduced growth rate was not due to an equilibrium melting temperature depression in the triblock copolymer.

The crystallization behavior of the triblock copolymer was considered in light of theories published on block copolymer crystallization theory. These theories are for block copolymers which crystallize from a micro-phase separated melt, and state that crystallization will be governed by equilibrium considerations. The glass transition temperatures of the two blocks in the copolymer are too close to one another to determine if the melt of the triblock copolymer is a single phase. Solubility parameter calculations and the SAXS pattern as a function of time in the melt both indicate the melt is not micro-phase separated. In addition, the melting behavior, SAXS patterns, and long spacing as a function of crystallization temperature of the triblock copolymer all show that the crystallization of the triblock copolymer is governed by kinetic factors. These factors indicate the triblock copolymer can be considered as a poly(ε–caprolactone) chain with a large defect crystallizing from a homogenous melt.

Chapter 8. Suggested Future Work

This thesis has compared and contrasted the crystallization and melting behavior of poly(ε–caprolactone) in the homopolymer and triblock copolymer. In order to better understand why an intermediate endotherm is seen in the (ε-caprolactone)-based triblock copolymer and not in the homopolymer, the effect chain architecture has on the melting behavior could be further investigated.

The melting studies done on the triblock copolymer could be extended by examining the effect of molecular weight. Both the molecular weight of the midblock and two poly(ε–caprolactone) endblocks could be varied. These experiments could help determine the effect of the molecular weight on the appearance of the lower endotherm of the triblock copolymer. There may be a molecular weight above or below which the lower endotherm does not appear. The relative magnitude of the lower endotherm in the total endotherm may also be a function of molecular weight. Similarly, melting studies could be done on the triblock copolymer where the relative percentage of each block is varied. Lastly, the chemical composition of the midblock could be changed. Differences in the chemical interactions between the blocks could change the crystallization and melting behavior. Additionally, the polymer topology could be changed by examining diblock and multiblock copolymers.

The block copolymer crystallization theories could be investigated for a block copolymer where the two blocks are strongly phase separated in the melt (assuming one block is crystallizable and the other is not). The effect of crystallization temperature and molecular weight of the crystallizable and amorphous blocks could be studied over a series

of block copolymers. It would be interesting to determine if crystallization as predicted by theory from a phase separated melt is indeed controlled by equilibrium considerations.

A Gibbs-Thomson-Tammann analysis on the triblock copolymer could be done to determine an accurate value of the equilibrium melting temperature and fold surface free energy. Once these values are known, the growth rate data can be analyzed to determine values for σ and σ_e. These values can be compared to those of the homopolymer to determine how the chain architecture affects the lateral and fold interfacial free energies. It would be interesting to determine whether the decrease in the product of the surface energies in the triblock copolymer is due to the fold, lateral surface, or combination of both.

References

1) J.D. Hoffman, R.L. Miller, H. Marand, and D. Roitman, *Macromolecules*, 1992, **25**, 2221.

2) R.J. Roe, "X-ray Diffraction," in *Encyclpd. Polym. Eng. Sci.*, 1989, **17**, 943.

3) D.C. Bassett, Principles of Polymer Morphology, Cambridge Univeristy Press, 1981, 18.

4) J.M.G. Cowie, Polymers: Chemistry and Physics of Modern Materials, 2nd Edition, New York, Thosom Litho Ltd, 1991, 243.

5) T. Lee, Virginia Polytechnic and State University, M.S. Thesis. February 1992.

6) F.J. Balta-Calleja, C.G. Vonk, X-ray Scattering of Synthetic Polymers, Polymer Science Library 8, Elsevier Science Publishers, 1989.

7) J.D. Hoffman, G.T. Davis, J. Lauritzen, Jr., In *Treatise on Solid State Chemistry*; Hannay, N.B. Ed., Plenum Press; New York, 1976, **3**, Chapter 7.

8) F. Khoury and E. Passaglia, "The Morphology of Crystalline Synthetic Polymers." In *Treatise on Solid State Chemistry*, 1976, **3**, p 468.

9) L. Marton, C. Marton; Methods of Experimental Physics: Polymers Part B: Crystal Structure and Morphology. Academic Press, New York, 1980.

10) H.S. Kaufman, and J.J. Falcetta, Editors; Introduction to Polymer Science and Technology, John Wiley and Sons, New York, 1977, 226.

11) H.D. Keith and F.J. Padden, Jr., *J. Appl. Phys.*, 1964, **35**, 1270.

12) L.E. Alexander, X-ray Diffraction Methods in Polymer Science; 1979; Robert E Krieger Publishing Company; Huntington, NY.

13) O.Glatter, *J Appl Cryst.* 1974, **7**, 147.

14) I. Hall, "Small-Angle X-ray Scattering from Crystalline Polymers," In Comprehensive Polymer Science, Pergamon Press, New York, 1991, 669.

15) P.B. Rim, J.P. Runt, *Macromolecules*, 1983, **16**, 762-768.

16) H. Zhang, R.E. Prud'homme, *J. Polym. Sci., Polym. Phys. Ed.*, 1987, **24**, 723.

17) J.D. Hoffman, *Polymer*, 1992, **33**, 2643.

18) J. Chiarng, K. Min, J.L. White, *Polym. Eng. Sci.*, 1988, **28**, 24, 1590.

19) P.J. Phillips, G.J. Rensch, and K.D. Taylor, *J. Polym. Sci., Polym. Phys. Ed.*, 1987, **25**, 1725.

20) T. Vilgis and A. Halperin, *Macromolecules*, 1991, **24**, p 2090.

21) E.A. DiMarzio, C.M. Guttman, and J.D. Hoffman, *Macromolecules*, 1980, **13(5)**, 1194.

22) H. Marand and J.D. Hoffman, *Macromolecules*, 1990, **23,** 3682.

23) J.P. Runt, "Crystallinity Determination," In Encyclpd. Polym. Sci. Eng.; 1986, **4**, John Wiley & Sons, New York, 487.

24) V. Crescenzi, G. Mancini, G. Calzolari, and C. Borni, *Eur. Polym. J.*, 1972, **8**, 449.

25) J.D. Hoffman, R.L. Miller; To be submitted.

26) A.A. Jones, W.H. Stockmayer, and R.J. Molinari, *J. Polym. Sci., Symp. #54*, 1976, 227.

27) M.D. Whitmore and J. Noolandi, *Macromolecules*, 1988, **21**, 1482-96.

28) S. Nojima, K. Kuto, S. Yamamoto, and T. Ashida, *Macromolecules*, 1992, **25**, 2237.

29) M. Gervais and B. Gallot, *Polymer*, 1981, **22**, 1129.

30) M. Gervais, B. Gallot, R. Jerome, and P. Teyssie, *Makromol. Chem*, 1981, **182**, 989.

31) S. Nojima, M. Ono, and T. Ashida, *Polym.*, **24,** 11, 1271.

32) A.J. Lovinger, B.J. Han, F.J. Padden, Jr, and D.A. Mirau, *J. Polym. Sci.,Polym. Phys.*, 1993, **31**, 115.

33) B. Monasse, J.M. Haudin, *Colloid Polylm Sci*, 1985**, 263**, 822.

34) J.D. Hoffman, *Polymer*, 1983, 24, 3.

35) F.A. Bovey, F.H. Winslow, Macromolecules: An Introduction for Polymer Science, Academic Press, 1979.

36) Y. Chatani, Y. Okita, H. Tadokoro, and Y. Yamashita, *Polym. J.*, 1970, **1**, 55.

37) H. Hu, D. Dorset, *Macromolecules*, 1990, **23**, 4604.

38) R. Perret and A. Skoulious, *Makromol. Chem.*, 1972, **156**, 157.

39) S. Nojima, H. Tsutsui, M. Urushihara, W. Kosaka, N. Kato, and T. Ashida; *Polym. J.*, 1986, **18**, 451.

40) J.V. Koleske and R.D. Lundberg, *J. Polym. Sci., Chem. Ed.*, 1969, **7** , 795.

41) M.K. Neo and S.H. Goh, *Eur. Polym. J.*, 1991, **27**, 927.

42) R. De Juana and M.Cortazar, *Macromolecules*, 1993, **26**, 1170.

43) S. Nojima, K. Kato, M. Ono, and T. Ashida, *Macromolecules*, 1992, **25**, 1922.

44) L. Goulet and R.E. Prud'homme, *J. Polym. Sci., Phys. Ed.*, 1990, **28**, 2329.

45) W. Li, R. Yan, X. Jing, B. Jiang, *J. Macromol. Sci., Phys*, 1992, **B31(2)**, 227

46) J.M. Jonza and R.S. Porter, *Macromolecules*, 1986, **19**, 1946.

47) S. Nojima, W. Kosaka, T. Ashida, Y. Muroga, T. Ueki, Y. Hiragi, M. Kataoka, Y. Izumi, H. Tagawa, and Y. Amemiya., *Polym. J.*, 1985, **77**, # 11, 1229.

48) S. Rosen, Fundamental Principles of Polymeric Materials, John Wiley & Sons, Inc, New York, 1982, p77.

49) Y. Cheung, R. Stein, B. Chu, G. Wi, *Macromolecules*, 1994, **27**, 3589.

50) B. Belorgey, R.E. Prud'homme; *J. Polym. Sci., Phys. Ed.*, 1982, **20**, 191.

51) W. Li and R.E. Prud'homme; *J. Polym. Sci., Phys, Ed.*, 1993, **31**, 719.

52) W.Y. Kim and D.S. Lee; *Polym. Bull.*, 1991, **26**, 701.

53) C. Nakafuku; *Polym. J.*, 1989, **21**, 781.

54) Y.W. Cheung, R.S. Stein, B. Chu, and G. Wu, *Macromolecules*, 1994, **27**, 3589.

55) P.C. Hiemenz, Polymer Chemistry, The Basic Concepts, Marcel Dekker, Inc., New York, 1984

56) B. Lebedev, A. Yevstropov, *Makromol. Chem.*, 1984, **185**, 1235.

57) A.E. Brink, K.E Weber, J.S. Riffle, and D.R. Paul; Private Communication.

58) J.M. Guenet, C. Picot, C; *Macromolecules*, 1981, **14**, 309.

59) U. Gaur, M. Cao, R.Ran, and B. Wunderlich, *J. Therm. Anal.*, 1986, **31**, 421.

60) R. Pan, M. Cao, and B. Wunderlich; *J. Therm. Anal.*, 1986, **31**, 1319.

61) A. Keller, G. Goldbeck-Wood; "Polymer Crystallization," To be submitted.

62) K. Armitstead, and G. Goldbeck-Wood;, "Polymer Crystallization Theories," in Macromolecules: Synthesis, Order and Advanced Properties; Springer-Verlag, 1992., 221.

63) L. Robeson, *J. Appl. Polym. Sci.*, 1973, **17**, 3607.

64) C.J. Ong, F.J Price, *J. Polym. Sci., Polym. Symp.*, 1978, **63**, 45.

65) C. Snyder, H.D. Iler, and H. Marand; To be submitted.

66) M. Whitmore, J. Noolandi, *Makromol. Chem., Macromol. Symp.*, 1988, **16**, 235.

67) J. Kressler, H.W. Kammer; *Polym. Bull.*, 1982, **191**, 283.

68) K.H. Storks, *J. Am. Chem. Soc.*, 1938, **60**, 1753.

69) T. Suzuki, A.J. Kovacs, *Polym J.*, 1970, **1**, 82.

70) H.D. Iler, Virginia Polytechnic and State University. Ph.D. Dissertation, August 1995

71) Work in progress

72) K.N. Kruger, H.G. Zachmann, *Macromolecules*, 1993, **26**, 5202.

Vita

Lisa Arnold was born on October 27th, 1968 in New London, Connecticut. After attending high school in her hometown, she went on to study chemistry at the University of Connecticut where she earned her Bachelor's degree in December of 1990. Following graduation, she married her husband, Robert Arnold, and moved to Virginia to begin her graduate studies. At Virginia Tech, she worked under the supervision of professor Hervè Marand in the area of the crystallization and melting behavior of polymers. After completing her Ph.D. requirements, she will move to Douglas, Georgia to begin teaching at South Georgia College.